MODELLING AND SIMULATION OF THE COMBUSTION OF BIO-DERIVED FUELS IN A PT6A-27 TURBOPROP ENGINE

By

Rodgers Bwalya Chisenga

A Dissertation submitted to

The University of Zambia in Partial Fulfilment of the Requirements for

The Degree of Master of Engineering in Thermal Fluids Engineering

The University of Zambia

Lusaka

2023

COPYRIGHT

DECLARATION

I Rodgers Bwalya Chisenga do hereby solemnly declare that this dissertation represents my own work, and that it has not previously been submitted for a degree at the University of Zambia or any other University.

Signature: …….

Date: ……

Supervisor

Name: ……

Signature: …….

Date: …….

CERTIFICATE OF APPROVAL

This dissertation by Rodgers Bwalya Chisenga is approved as fulfilling the partial requirements for the award of the degree of Master of Engineering in Thermofluids by the University of Zambia.

Name	**Signature**	**Date**
……..... Examiner 1	…….	……
……..... Examiner 2	…….	……
……..... Examiner 3	…….	……
……..... Dissertation Chairperson	…….	……
…….....	…….	……

ABSTRACT

The motivation for venturing in alternative jet fuels has partly been due to the elevated level and volatility of the price of Jet A (a kerosene-based aviation gas turbine fuel) and environmental impacts on global climate change and air quality.

The model of the annular combustor for the PT6A-27 engine was created using SOLIDWORKS and exported to ANSYS DESIGN MODELER for further conversion from a solid geometry into a fluid-based model. Creation of the computational mesh for the geometry using ANSYS MESHING was done in preparation for the setting up of the CFD simulation in ANSYS FLUENT. The simulation also included, setting material properties and boundary conditions for a non-premixed combustion problem, initiating the calculation with residual plotting, calculating the solution using the pressure-based solver and visually examining the flow and temperature fields using the post-processing in ANSYS FLUENT.

In the non-premixed combustion, the Standard k-ε 2 equation turbulence model was used.

The fuel blend from the range of 30% bioethanol and 70% biodiesel (BE30-BD70) to 70% bioethanol and 30% biodiesel (BE70-BD30) indicated a combustion characteristic consistency with that obtained from the combustion of Jet-A1. Further, from the comparisons of the blends in terms of performance and single biofuel combustion simulation the best blend combination was 40% bioethanol with 60% biodiesel (BE40-BD60) whose adiabatic flame temperature was about 2260 Kelvins. The single biofuel combustion simulation best pick was 100% biodiesel whose adiabatic flame temperature was about 2310 Kelvins.

The blend of 40% bioethanol to 60% biodiesel was observed to have a reduced Fuel NOx footprint. However, the rise in the calorific energy content of the fuel blend due to the presence of biodiesel in the mixture contributed to the increase in Thermal NOx production, albeit still less than that obtained from a pure hydrocarbon fuel of JetA-1. A pure JetA-1 hydrocarbon fuel had a production rate of Thermal NOx ranging from $0.002699526\ \text{Kgmol/m}^3\ \text{s}$ to $0.002705489\ \text{Kgmol/m}^3\ \text{s}$. The Prompt NOx rate for Jet fuel was observed to be $1.789729 \times 10^{-6}\text{Kgmol/m}^3\ \text{s}$. On the selected fuel blend of biofuels at the proportions of 40% bioethanol and 60% biodiesel, the observed production rate values of Thermal NOx and Prompt NOx were a range of $4.798448 \times 10^{-6}\text{Kgmol/m}^3\ \text{s}$ to $5.01322 \times 10^{-6}\text{Kgmol/m}^3\ \text{s}$ and $2.054488 \times 10^{-7}\text{Kgmol/m}^3\ \text{s}$ respectively. This was indicative of a reduction in both Thermal and Prompt NOx when the two groups of fuels (Jet-A against 40BE & 60BD blend) were compared.

These results showed that reduction of NOx emissions is achievable for a blend of 40% bioethanol and 60% biodiesel in a combustion reaction as a substitute for the hydrocarbon JetA in the PT6A-27 turboprop engine.

ACKNOWLEDGEMENTS

It is a great pleasure to acknowledge the people who contributed their support, time, and physical energy to this project. Foremost, I acknowledge the inestimable guidance, advice, and encouragement Dr. Edwin Luwaya. ceaselessly provided throughout this study.

I also acknowledge the help rendered by Professor Francis Yamba, for the expertise in combustion. Further, I render my gratitude to Brig. Gen Stephen Kabanda and Eng. Tanda Siyamunyangwa for their support. I also extend my gratitude to my friends and colleagues, with whom I shared many wonderful experiences and friendly diversions.

The financial aid, from the Zambia Air Force (ZAF) for the Tuition Fees is greatly appreciated.

All this work would have been neither possible nor meaningful without the understanding, patience, and unflagging support from my family. They tolerated amazingly well the time spent on the project for days on end, time that I could have spent with them.

TABLE OF CONTENTS

List of Tables

List of Figures

Definition of Terms

Adiabatic Flame Temperature (AFT)- The temperature attained when all the chemical reaction heat released heats combustion products.

Computational Fluid Dynamics (CFD)- The use of applied mathematics, physics, and computational software to visualize how a fluid flows as well as how the fluid interacts with objects as it flows.

Fluid- a substance that continuously flows or deforms under an applied shear stress or external force.

Combustion- A high temperature exothermic redox chemical reaction between a fuel and an oxidant.

Non-Premixed Combustion- Type of Combustion where the fuel and oxidizer streams are introduced separately, and combustion occurs after the fuel and oxidizer mix.

Turboprop Engine- A jet engine designed to produce thrust principally by means of a propeller driven by a turbine with additional thrust usually obtained in by a rearward discharge of hot exhaust gases.

Annular Combustor- Is a combustion chamber shaped in a ring form or cylindrical form and whole annulus between the compressor and the turbine is used for combustion.

CHAPTER 1: INTRODUCTION

1.1 Background

1.1.1 International push for alternative biofuels for aviation gas turbines

Throughout the history of aviation there has been a continuous improvement of fuel efficiency driven by the necessity to save weight and costs and increasingly by environmental concerns. The aviation sector currently accounts for around 2% of man-made global greenhouse gas emissions. Though this represents a relatively small share compared to other modes of transport such as road transport. However, aviation is the fastest growing transport mode and is projected to grow by around 4% to 5% annually by 2050, (Toop, 2014).

The motivation for venturing in alternative jet fuels has partly been due to the elevated level and volatility of the price of Jet A (a kerosene-based aviation gas turbine fuel) and environmental impacts on global climate change and air quality, (Hilleman, 2008).

In 2008 aviation industry was the first transport sector to set targets for cutting its carbon emissions. They set out their short, medium- and long-term goals. Sustainable alternative fuel will play a significant role in achieving the industry's long-term emissions reduction goal, (IATA, 2015).

The sustainable source of energy requirements in the aviation industry is key to developing the sector. Fossil fuels have for long been a source of concern both locally and globally due to pollution. The fossil fuels are a depleting resource and thus the need to use sustainable biofuels. However, replacing fossil fuels with biofuels requires investigation to ascertain compatibility to specific aircraft gas turbine engines.

The engine and commercial aircraft research and development communities have been investigating the practicality of using alternative fuels in near, mid, and far-term aircraft. Presently, it appears that an approach of using a "drop in" jet fuel replacement, which may consist of a kerosene and synthetic fuel blend, will be possible for use in existing and near-term aircraft. Future mid-term aircraft may use a bio-jet and synthetic fuel blend in ultra-efficient airplane

designs. Future, long-term engines and aircraft in the 50-plus year horizon, may be specifically designed to use a low or zero-carbon fuel, (Dagget, 2007).

This points to the fact that new engines would have to be designed to conform to the bio derived jet fuels. It is on this premise that studies in '*drop in'* fuels need to be conducted so that countries which are unable to develop new engines can operate the aviation gas turbines without modification.

1.1.2 Alternative aviation fuels

In the report on alternative fuels for aviation use in commercial aircraft Dagget et al (2007) acknowledged the fact that the synthetic fuels '*may*' reduce particulate exhaust emissions. This is an area that requires thorough investigation. It is important to point out that currently Sasol fuel in South Africa's Johannesburg airport is a blend with kerosene-based jet fuels. This fuel is used on specific aircraft engines. The question of whether synthetic fuels are interchangeable on different gas turbine engines would have to be answered by having the same fuel blend tested on other engines in determining the compatibility of the fuel with engine operations.

In the 2006 Technical Review of alternative jet fuels, Hemighaus *et al* (2006), highlighted that biomass was being increasingly considered as an alternative raw material of transportation fuels. The report further stated that ethanol and biodiesel had been used in recent years as blend components for gasoline and diesel fuel respectively, and this use was likely to continue to expand because of government mandates in many countries and a desire to diversify energy sources.

1.2 Problem Statement

There is an international effort in the aviation industry to push for the use of cleaner and sustainable biofuels in aviation gas turbine engines. However, countries like Zambia without the manufacturing capability of aviation gas turbine engines, need as a short-term goal, to carryout research in the area of drop in biofuels. Drop in fuels would be used as alternative fuels in available engines without any modifications done to the combustor and the fuel system. The cost implications for carrying out combustion tests on aircraft engines is high owing to the possibility of the engine failure if fuels are incompatible. The study in drop in biofuels should therefore be carried out using numerical methods. Upon review of the simulated results, future tests can be

carried out on the actual engines. This research will therefore involve modelling of the combustion chamber and carrying out simulation of the selected biofuels.

There is need to firstly carry out numerical simulations safely to ascertain among other things, compatibility of the bio derived fuels and the level of emissions.

1.3 Aim of Study

This research sought to model and simulate the combustion of bioethanol and biodiesel and compare the results with the performance of conventional hydrocarbon fuels. The potential for high compatibility of biofuels with some selected gas turbine engines exists. The purpose of this study is to determine if alternative biofuels can be used in the PT6A-27 turboprop engine without any modification done to the combustor and fuel system. This study will form as a basis for future practical tests of bio derived fuels in gas turbine engines under Zambia Air Force (ZAF).

1.4 General Objective

To determine engine performance characteristics if powered by bio derived fuels, without any modification to the PT6A-27 gas turbine engine combustor.

1.4.1 Specific objectives

- To model and simulate combustion properties of bio-derived fuels in a PT6A-27 annular combustor.
- To determine the adiabatic flame temperature and compare the performance of the simulated results to those obtained in practical situations.
- To determine the levels of NOx emissions from bioethanol, biodiesel and compare with emissions produced from Kerosene based jet fuels as obtained from similar literature results.

1.5 Research questions

1. What are the biofuel combustion properties?

2. What are the differences in combustion properties between simulated results against the those obtained in practical situations?

3. What are the differences in NOx emissions if conventional Jet fuels are substituted with biofuels?

1.6 Rationale

For the local aviation industry to move with the international community in exploring sustainable biofuels for aircraft, thorough research in combustion compatibility of biofuels need to be conducted. As a country, Zambia has no manufacturing capacity of gas turbines with modified combustion chambers and the fuel systems to accommodate biofuels. One government institution which has been operating aviation gas turbines in Zambia is the Zambia Air Force (ZAF). Zambia Air Force seeks to undertake research in sustainable aviation. Before practical tests can be carried out on actual aviation gas turbine engines, it would be safe and cheaper to start these studies with numerical simulations. Thus, this research will focus on a type of military transport aircraft engine to be assessed if it can run on biofuels, as well as meeting the power to weight ratio as that obtained when powered by Kerosene based Jet fuels. The research shall further seek to establish the levels of emissions produced.

1.7 Scope of Study

This research sought to model and simulate the combustion of biofuels in a PT6A-27 Annular Combustor using Computational Fluid Dynamics (CFD) software. The research was restricted to numerical simulations and no physical experiments were conducted. The research further made use of a fixed model and no modifications to the fuel systems in the geometry were included. The assumption of no phase separation in the blended biofuels was also considered.

1.8 Ethical Considerations

All real time data regarding the engine and aircraft performance had been gotten with clearance from the relevant authorities.

CHAPTER 2: LITERATURE REVIEW AND THEORY

2.1 Introduction

Rodionova *et al* (2016) defined the term "biofuels" as the energy enriched chemicals generated through the biological processes or derived from the biomass of living organisms, such as microalgae, plants, and bacteria. Turbine engine manufacturers, General Electric, Honeywell, Pratt & Whitney, and Rolls Royce presented a consensus position at the Aviation Alternative Fuel Workshop held in May 2006 and concluded that there where plausible alternatives to conventional jet fuel, but these new fuels cannot jeopardize safety and reliability of aircraft systems. Producers of these new fuels must also account for the lifecycle of the fuel and its total environmental impact along with health and toxicological effects (Hemighaus *et al*, 2006). This research also sought to determine the levels of emissions. The Turbine Engine Manufactures did acknowledge plausibility of alternative aviation fuels and this research was centered on the combustion of alternative aviation fuels in particular the bio derived fuels.

2.2 Feedstock Types and Biofuels Production

One of the main factors to be considered in biofuel production is the raw material, i.e., the feedstock used in the process. Not only is the final cost directly proportional to the price of available feedstock, but a huge part of the process is also related to different pretreatments required for different feedstock. This means that by choosing or adopting the right feedstock, advantages such as high efficiency and low production cost, sustainable processes, and lower environmental issues could be gained simultaneously. Here, feedstock is discussed as shown in table 2.1 from the viewpoint of different biofuel generations i.e., first, second and third generation biofuels (Rodionova, 2016).

Table 2. 1: Biofuel production, source: Challenges and opportunities, International Journal of Hydrogen Energy (2016).

Biofuels			
Primary	Secondary		
	First generation	Second generation	Third generation
Firewood, wood chips, pellets, animal waste, forest and crop residues, landfill gas.	Bioethanol or butanol by fermentation of starch (from wheat, barley, corn, potato) or sugars (from sugarance and sugar beet.) Biodiesel by transesterification of oil crops (rapeseed, soybeans, sunflower, palm, coconut, used cooking oil, and animal fats.)	Bioethanol and biodiesel produced from Conventional technologies but based on novel starch, oil and sugar crops such as *Jatropha*, cassava or *Miscanthus*; Bioethanol, biobutanol, syndiesel produced from lignocellulosic materials (e.g. straw, wood and grass)	Biodiesel from microalgae Bioethanol from microalgae and seaweeds Hydrogen from green microalgae and microbes

In contrast to first generation biofuels, second-generation biofuels from waste and renewable feedstocks could help bridge the gap and enable the airline industry to reach carbon-neutral growth in the medium-term, and even reduce CO2 emissions over the longer term. Up until 2015, three second-generation production processes have been certified for blends with petroleum-derived jet fuels, and many other processes are either expected to receive certification or are still being explored. Among the certified processes, only HEFA fuels are already being produced at industrial scale (Chuck, 2016).

Multiple policy targets, measures, and Research and Development (R&D) programs that affect aircraft manufacturers, airlines, and fuel producers directly or indirectly are already in place or about to be introduced. However, in many countries, energy policies supporting the deployment of biofuels have focused on road transportation via cellulosic ethanol and renewable diesel through mandatory production quotas and fiscal incentives. These policies consist of subsidies, mandatory production quotas, or other measures. Although comparatively abundant, competition for cellulosic feedstocks may ultimately arise between road and air transportation. However, once a level playing field exists that is, subsidies and regulations are applied equally to both sectors, the market will decide about the quantities consumed in each sector. Given the reduced degrees of freedom for fuel shifting in air transportation, this sector's willingness to pay for biofuels may be larger and thus attract a larger share (Chuck, 2016).

If biofuels were to meet the combustion requirements, they must have the characteristics similar if not exact with the fossil fuels. Chuck (2016) lists the following fundamental requirements aviation jet fuel of Aircraft:

- low weight per unit heat of combustion to increase the payload such as more people/goods.
- low volume per unit heat of combustion to allow fuel storage without compromising the aircraft size, weight, and performance.

With regards to fuel efficiency with full safety of aircraft operation he further outlines the following characteristics:

- Optimum distillation/volatile property: It is important for the mixture formation of air with fuel at a wide range of operating temperature conditions unlike ground vehicles.
- High ignition quality: Octane number for the aero piston engine and smoke point for the gas turbine aero engine.

It should be noted that both Synthetic Paraffinic Kerosene (SPK) are mixtures of pure hydrocarbons of almost all paraffinic nature. Fatty acid methyl esters (FAME), which are the major components in biodiesel, are considered as contaminants in jet fuel because of their degrading effect on jet fuel thermal stability. In light of the above concerns, it is clear that any biomass-based fuel should be first converted to pure hydrocarbon mixtures in order to be accepted as a jet fuel blending product. This limit, at least with the current technology, the potential biofuels for aviation to SPK obtained by the FT process from biomass and hydro processed esters and fatty acids (HEFA). HEFA is derived from animal and vegetable oils, but its composition is similar to SPK, that is, a mixture of pure paraffinic hydrocarbons. HEFA has also been approved to be blended with conventional jet fuel up to 50% by volume (ASTM International, 2011). This research blended only two biofuels in the combustion simulation in varying proportions, however the proposal at the ASTM conference in 2011 was to blend a biofuel with Jet A up to 50% ratio.

Since the first turbine engine, aviation fuel has evolved into a tightly regulated commodity, and its specifications have narrowed as engine technology and refining methods have advanced. As a result, aviation gas turbine engine fuels today are the most highly regulated transportation fuels with the most extensive set of specifications. Fuel specifications have material and manufacture requirements limiting the fuel feed stocks to petroleum crude oil, natural gas condensates, heavy crude oil, shale oil, and oil sands (i.e., hydrocarbons). Two major biofuels are present in the global fuel market: bioethanol, which is largely produced by the fermentation of sugars or starches, and

biodiesel, which is produced from the transesterification of vegetable oils such as rapeseed, soybean, or palm, as well as from animal fats. Ethanol and biodiesel are blended into gasoline and diesel fuels, respectively, in smaller percentages for ground transportation, (Zingg and Gülder, 2016).

Fossil fuels have been used as a main source of energy for many years; however, the usage of them is unsustainable and causes environmental issues related to fossil fuel combustion (Rodionova *et al*, 2016). Studies into the use of biofuel alternatives in gas turbines are ongoing and this research would contribute on the proposed blend between bioethanol and biodiesel in a combustion simulation as the first step prior to actual tests in the Zambia Air Force.

The overarching criterion in developing biofuels for aviation has been the development of drop-in fuels which can be used in the existing fleet without any modifications. Currently Synthetic Paraffinic Kerosene (SPK) produced by the Fischer-Tropsch (FT) process either from biomass sources or coal is allowed to be blended with conventional jet fuel.

2.3 Alternative aviation fuels

Dagget et al (2007), further stated that Synthetic jet fuels manufactured using a Fischer-Tropsch process, from coal, natural gas or other hydrocarbon feedstocks are very similar in performance to conventional jet fuel but have almost zero sulfur and aromatics. This may result in lower particulate exhaust emissions. In addition, synthetic fuels exhibit excellent low-temperature properties, maintaining a low viscosity at lower ambient temperatures. Thermal stability properties are also improved, resulting in less fuel system deposits. As synthetic fuels have very good performance and have already been in use for many years at Johannesburg airport (Sasol fuel) it will be easy to supplement current jet fuel supplies with synthetic derived fuel. If the additional CO_2 that is produced during the manufacturing process can be captured and permanently sequestered, synthetic fuel could be a good near-term supplement.

2.3.1 Aviation Kerosene

Aviation kerosene-type jet fuel is used by civil gas turbine-based engine aircraft. The different grades of jet fuels such as Jet A-1, Jet Ts-1, Jet RJ-1, Jet TH and Jet Fuel No. 3 are used in different countries. The fuel grades are classified mainly based on its fuel quality such as Sulphur, flash

point, freezing point, energy content and smoke point as shown in Table 2.2. Benzene and toluene have an aromatic structure. Naphthalene and anthracene are known as polycyclic aromatic hydrocarbon (PAHC). The aromatic content is higher in crude oil, which helps to increase the octane number. However, it is responsible for soot/smoke/PAHC emission formation during combustion. The soot deposits on turbine blades may lead to durability problems. Sulphur in fuel emits harmful emissions such as SOx, Sulphur acid and sulphate, which enhance the corrosion problem on blades and other components.

Table 2. 2: Jet Fuel Grades, Source: Biofuels for aviation Feedstocks, Technology and Implementation, 2016.

S. No.	Jet Fuel Properties	Jet A-1	Jet Ts-1	Jet RJ-1	Jet TH	Jet Fuel No. 3	Diesel
1.	Aromatics, % vol	19.5	15.2	19.5	16.5	16	
2.	Sulphur, % mass	0.02	0.04	0.02	0.01	0.02	50 (mg/kg)
3.	Initial boiling point, °C	156	138	140	142	153	
4.	T10, °C	167	160	154	155	168	
5.	Flash point, °C	42	31	35	40	39	35
6.	Freezing point, °C	–50	–64	–68	–53	–52	–40 to –34.4
7.	Energy content, MJ/kg	43.15	43.2	—	43.24	43.35	45.759
8.	Smoke point, mm	25	28	26	22	25	

2.3.2 Carbon-Neutral and Sustainable Fuels

Alcohol fuels such as methanol, ethanol and butanol, and biodiesel are carbon-neutral fuels as the carbon emitted from combustion engines is recycled through crop/plant. This means there is no new addition of CO_2 emission into the atmosphere. But alcohol fuels have the problem of lower energy density, which requires a larger wing and engines, resulting in the reduction of the aircraft's fuel efficiency (Table 3).

In case of biodiesel, it has poor cold flow properties and high unsaturated compounds. If hydrogen is produced from renewable resources, it is a sustainable fuel. Energy density, safety and storage are the major problems. Fischer-Tropsch. (F–T) diesel also known as gas to liquid fuel is produced when a gaseous fuel is converted to a liquid and refined to make diesel. F-T diesel is the only alternative fuel that has a good potential for an aero engine. This sustainable fuel needs to be explored for aircrafts. Crude oil-based aviation kerosene fuel will play a crucial role for at least another two decades. A summary of the qualitative comparison of alternative fuels for aircraft with base aviation jet fuel is presented in Table 2.3.

Table 2. 3: Summary of key properties of alternative fuels with a comparison of aviation kerosene, source; Biofuels for aviation Feedstocks, Technology, and Implementation, 2016.

Fuel Quality	CNG	Compressed Hydrogen	Liquid Hydrogen	Biodiesel	Fisher–Tropsch Diesel	Alcohol (Methanol, Ethanol)
Volumetric energy content (MJ/kg)	Very poor	Very poor	Moderate	Good	Excellent	Poor
Freezing point	Excellent	Excellent	Excellent	Poor	Excellent	Excellent
Infrastructure	To be built	To be built	To be built	Good for existing infrastructure	Good for existing infrastructure	Slight modification needed for existing infrastructure

2.3.3 Other Studies

Turbine engine manufacturers, General Electric, Honeywell, Pratt & Whitney and Rolls Royce presented a consensus position at the Aviation Alternative Fuel Workshop held in May 2006 (Hemighaus *et al*, 2006).

Some of their conclusions are summarized below.

- Kerosene based fuels are the preferred option.
- Biodiesel (FAME) presents major technical and logistical risks at present.
- The Fischer Tropsch (FT) process provides opportunity to produce aviation fuel from biomass at lower risk and shorter timescales.
- Liquefied gas options have non-gas-turbine-related barriers.
- All alternative fuel options require further study and whole life cycle analysis.
- New fuels will require certification of aircraft and engines.

These conclusions did not rule out the use of biofuels as an alternative. The FAME presented a major technical and logistical risk. This justifies the need to carry on with the research of alternative fuels.

2.4 Combustion of biofuels

Recent concerns over energy security and environmental considerations have highlighted the importance of finding alternative aviation fuels. It is expected that coal and biomass derived fuels

will fulfil a substantial part of these energy requirements. However, because of the physical and chemical difference in the composition of these fuels, there are potential problems associated with the efficiency and the emissions of the combustion process. Over the past 25 years Computational Fluid Dynamics (CFD) has become increasingly popular with the gas turbine industry as a design tool for establishing and optimising key parameters of systems prior to starting expensive trials (Uryga-Bugajska *et al*, 2008*).*

Biofuels, such as bioethanol, biobutanol, and biodiesel, are of increasing interest as alternatives to petroleum-based transportation fuels because they offer the long-term promise of fuel-source regenerability and reduced climatic impact. From the combustion perspective, the chemical decomposition and oxidation pathways of current and future biofuels are intimately coupled to the structure of the respective fuel molecule. Predicting the combustion behavior of these fuels, including ignition, extinction, heat release, and the formation of potential pollutants, requires the development of detailed combustion mechanisms. These must include all pertinent species, reactions, rate coefficients, and related thermochemical and transport parameters as functions of temperature and pressure. Combustion models which are validated with reliable experiments are used to examine all important aspects of the combustion performance and to transfer the results from the laboratory to the industrial process (Kohse *et al*, 2010). In this research the combustion simulation in ANSYS software considers, the different species transport as well as multi chemical species reaction.

In Ellis *et al* (2008) carried out an experiment on the Flameless Combustion of biodiesel in a Semi-Closed Cycle Gas Turbine. Biodiesel-derived from soy and palm oil feed stocks, including a B-20 (20% biodiesel and 80% petroleum diesel) soy blend, were compared to ultra-low sulfur fuel oil in a semi-closed cycle gas turbine. The behavior of the fuels related to soot production in the primary combustion zone and exhaust emission characteristics were investigated using two-color spectrometry and infrared absorption gas analysis. Results demonstrated soot production was reduced for biodiesels accompanied by a nominal increase in fuel rate. Unburned hydrocarbon emissions were low possibly due to lower Sulphur content of all fuels and lower aromatics in the case of biodiesel (Ellis *et al*, 2008). The CO and NO emissions were similar for all of the fuels tested. The test concluded that of the four fuels tested for exhaust emission and soot behavior in the Power gas turbine system at the University of Florida, no operability limitations were observed,

other than startup, for the fuels tested. Comparing B100 Soy, B100 Palm and B20 Soy biodiesel with ultra-low sulfur fuel oil, no significant difference in exhaust emissions among the fuels of unburned hydrocarbon as CH_4, CO or NO was measured. The NOx emissions increased with an increase in load for all the fuels, as expected (Ellis *et al*, 2008). This is a further illustration that at certain temperatures, NOx emissions are reduced and that biodiesel irrespective of the raw materials produces very low unburnt hydrocarbons. This study offers justification in conducting research on biodiesel due to their lower unburnt hydrocarbons.

Pierre-Alexandre *et al*, (2009) carried out a study using THERGAS software on Adiabatic Flame Temperature from biofuels and fossil fuels and derived effect on NOx emissions. While biodiesels reduce carbon containing pollutants, experimental data from diesel engines show a slight increase in NOx. The five FAMEs studied were Rapeseed Methyl Ester (RME), Soy Methyl Ester (SME) and methyl esters of sunflower, palm and tallow. The software THERGAS had been used to calculate the enthalpy and free energy properties of the fuels and GASEQ for the flame temperature, acknowledging the fact that "thermal NOx" represents the predominant form of NOx in gas turbines. The results showed that diesel fuels tend to generate the highest temperatures, natural gas the lowest and biodiesel lies in-between (Pierre-Alexandre *et al*, 2009). In this research determination of thermal NOx was one of the objectives using ANSYS software in Non-Premixed Combustion.

Spray characteristics and combustion performance of unheated and preheated liquid biofuels have been studied by Panchasara *et al* (2010). In their research, diesel, Vegetable Oil (VO), two types of biodiesels produced from VO and animal fat were investigated as potential fuels for gas turbines to generate power. Experiments were performed using a laboratory scale burner simulating gas turbine combustor operated at atmospheric pressure. A commercially available air blast (AB) atomizer was used to create the fuel spray. A parametric study of combustion performance (CO and NOx emissions) and spray characteristics (droplet diameter, drop size distribution, and mean and RMS axial velocities) was carried out by varying air to liquid mass ratio (ALR), and fuel inlet temperature in cold spray and spray flame with/without swirl air and without/with enclosure. Results showed that an increase in the fuel inlet temperature decreases NOx and CO emissions, which could be attributed to improved fuel atomization resulting from decreased kinematic

viscosity at higher fuel temperatures (Panchasara, 2010). However, in this research, the inlet temperatures of the biofuels are treated as a constant without varying it in the simulations.

As the push to make the use of biofuels more pervasive in the airline industry continues, it is important to understand their broader impact. Jonathan *et al* (2013) conducted engine performance simulations using the software Commercial Modular Aero-Propulsion System Simulation 40k (C-MAPSS40k). Engine performance simulations using C-MAPSS40k demonstrated the thermodynamic compatibility of biodiesel with existing engines. Biofuel engines will be able to produce equal amounts of thrust compared to conventionally powered engines with the same transient responses if the fuel flow controller is redesigned. From a system perspective, the most detrimental properties of certain biofuels are volume, weight, and freezing point. The volume and weight of certain biofuels will unavoidably reduce efficiency. Mixing standard fuel and biofuel would help reduce some of the issues. From a component perspective, biodiesel's higher viscosity could also lead to less desirable atomization characteristics, such as increased mean droplet size. Furthermore, ring sticking, injector coking, and injector deposit problems have all been known to lead to pump failure in biodiesel truck engines. A mix of biodiesel and standard fuel would optimize the properties while also alleviating fossil fuel dependency. Despite viscosity issues, it has been found that biodiesel actually causes less wear in ground vehicle diesel engines (Jonathan *et al*, 2013). This reseach included blends of biofuels and no modification to both the simplex and duplex nozzle diameters. This research will involve simulation of biofuel blends of bioethanol and biodiesel.

Altaher *et al* (2014), carried out a Study of biodiesel emissions and carbon mitigation in gas turbine combustor. The results obtained can be used to estimate pollutant emissions and carbon reductions by biodiesel in power generation industry and other sectors where gas turbine engines are used. Liquid fuels (B100, B50, B20 and Kerosene) were injected and premixed with incoming air in a premixed fuel injector with holes on centres of equal area. The air fuel ratio (equivalence ratio) was increased in small steps by increasing fuel flow rate and keeping air flow rate constant. Generally, pure biodiesel and blend fuels (B20&B50) had slightly lower UHC emissions than kerosene in all operating conditions. However, kerosene fuel had a higher UHC than biodiesel and biodiesel blend fuels in lean conditions ($\Phi < 0.6$) (Altaher *et al*, 2014).

Biodiesel is receiving increasing attention as an alternative fuel due to the ever-growing demand for energy. However, the inferior physiochemical properties of biodiesel render it incompatible for gas turbine application, which needs to meet the standard requirement of gas turbine fuel in accordance with ASTM D2880 (Saifuddin *et al*, 2017). Saifuddin *et al* (2017) studied the performance and emission characteristics of micro gas turbine (MGT) engine fueled with bioethanol-diesel-biodiesel blends. The research work was carried out to study experimentally the performance and exhaust emission characteristics of a 25kW micro gas turbine engine (Capstone Model C30) fueled with biodiesel-diesel-bioethanol blends. The assessment on the improved fuel properties of biodiesel by blending with bioethanol had shown more superior atomisation characteristics performance compared to unmodified biodiesel. Moreover, the performance test in the micro gas turbine was limited up to 20% blend of biofuel, which showed improved thermal efficiency during the test. Subsequently, the emission test carried out in this work also showed significant enhancement in emissions, except nitrogen oxides (NOx) which contributed to the higher formation in comparison with the distillate diesel. Finally, B80E20 (80:20 of biodiesel-bioethanol) was proposed to be selected as an ideal blended fuel ratio to be applied in micro gas turbine engine due to its adaptability to replace diesel fuel, while showed better performance and emission properties as compared to the pure petroleum diesel, (Saifuddin *et al*, 2017).

Maiorova *et al* (2017) analysed the atomization and burning of biofuels in the combustion chambers of gas turbine engines. The research analysed the effect of physical properties of liquid fuels with high viscosity (including biofuels) on the spray and burning characteristics. The study showed that the spray characteristics behind devices well atomized fuel oil, may significantly deteriorate when using biofuels, until the collapse of the fuel bubble. To avoid this phenomenon, it is necessary to carry out the calculation of the fuel film form when designing the nozzles. Several measures were recommended to modernize the conventional combustors when using biofuels in gas turbine engines. for carrying out of hot tests in aviation combustor mixed biofuel based on aviation kerosene (as most close relating to a turbine engine) has been chosen as alternative fuel. The combustion value of biofuels is significantly lower than that of fossil fuels. Furthermore, the viscosity of vegetable oils is ten times greater than the viscosity of the organic fuel. Therefore, for aircraft engines blend of biofuels with conventional aviation fuels is preferable than pure biofuels. Various versions of a percentage ratio of components of combustible mixtures based on plant oil

and ethanol have been investigated. In the capacity of the main component aviation kerosene TS 1 and gasoline have been chosen. The mix in a ratio of 40 % of kerosene TS 1, 20 % of castor oil, 40 % of ethanol has been chosen as the most homogeneous and well mixed without any precipitations and stratifications (Maiorova *et al*, 2017).

2.5 Improving Biofuels Properties for Combustion.

Hong (2011) carried out an experimental study of nanoadditives for biofuel combustion improvement**.** An experimental investigation of the combustion behavior of nano-aluminum (n-Al) and nano-aluminum oxide (n-$Al_2 0_3$) particles, stably suspended in biofuel ethanol as a secondary energy carrier was conducted. The heat of combustion (HoC) was studied using a modified static bomb calorimeter system. Combustion element composition and surface morphology were evaluated using a SEM/EDS system. N-Al and n-$Al_2 0_3$) particles of 50 nm and 36 nm diameters, respectively, were utilized in this investigation. Combustion experiments were performed with volume fractions of 1%, 3%, 5%, 7%, and 10% for n-Al, and 0.5 %, 1%, 3%, and 5% for n-$Al_2 0_3$). The results indicate that the amount of heat released from ethanol combustion increases almost linearly with n-Al concentration. N-Al volume fractions of 1% and 3% did not show enhancement in the average volumetric heat of combustion, but higher volume fractions of 5%, 7%, and 10% increased the volumetric heat of combustion by 5.82%, 8.65%, and 15.31%, respectively. N-Al2O3 and heavily passivated n-Al additives did not participate in combustion reactively, and there was no contribution from Al2O3 to the HoC in the tests (Li Calvin Hong, 2011).

Other tests in Combustion characteristics of improved biodiesel in diffusion burner by Kumaran *et al* in 2014, have shown that there is an improvement in the combustion of biofuels when the source of raw materials and other additives are incorporated. In the case of bio diesel SGB showed improved properties whereas bioethanol its heating value had increased by addition of nano-additives**.** these studies offer a possibility of the practicality of using pure biofuel blends for aviation gas turbines. The first steps which involve a much economical approach to such tests in developing countries like Zambia is CFD simulations in combustion of biofuels in gas turbines.

Kumaran *et al* (2014), evaluated the combustion characteristics of improved biodiesel or Second-Generation Biodiesel (SGB). In their work they addressed an alternative and inexpensive method

of performing combustion studies of such improved biodiesel. A diffusion burner which has similar combustion dynamics to a gas turbine combustor had been used to evaluate the combustion characteristics of improved biodiesel or Second-Generation Biodiesel. Biodiesel is considered as an alternative fuel for gas turbine application. However, the properties of biodiesel need further improvement to meet the combustion dynamics of a typical gas turbine (Kumaran *et al*, 2014). The combustion characteristics of the improved biodiesel have been evaluated in terms of fuel burning rate, flame length and emissions. Subsequently, the results were compared with biodiesel or First-Generation Biodiesel (FGB) and distillate diesel (DD). The results indicated improvement in physical properties; SGB and its blends possess better combustion characteristics in terms of flame length, mass of fuel flow rate and emissions compared to FGB and DD. They concluded that SGB can be considered as an alternative fuel for use in gas turbines and a 50% blend of SGB with DD had shown promising results compared to other blend ratios (Kumaran *et al,* 2014).

2.6 Modelling And Simulation of Biofuel Combustion

Bugajska *et al* (2008) assessed performance of alternative fuels in a Modern Airspray Combustor (MAC). In the paper titled "Assessment of Performance of Alternative Fuels in a MAC", the performance of a typical aviation fuel, kerosene, an alternative aviation fuel, biofuel and a blend had been examined using CFD modelling. The properties of a bio/aviation fuel had been investigated for a MAC using the recently developed detailed reaction mechanisms, AFRMv2.0, and a CFD simulation approach. The CFD predictions for kerosene were validated against experimental data from QinetiQ (Uryga-Bugajska et al, 2008). They concluded that the impact of using the blended fuel has been shown to be very similar in combustion performance to that of the 100% kerosene. The detailed reaction mechanism was validated against experimental data for kerosene and subsequently applied to blend and biofuel. The predicted temperature and NOx profile were in good agreement with the experimental values particularly at the exhaust. Although at the exhaust, the amount of NOx observed in the blended biofuel, was like that of kerosene, a substantially increased value was observed close to the injector. This phenomenon is primarily attributed to the increased oxygen content of the methyl ester molecule which effects changes to the combustion chemistry close to the injector (Uryga-Bugajska *et al*, 2008).

When using 100% biofuel there is a significant impact to the performance of the process. At the operating conditions considered in this work, 100% biofuel would result in a significant reduction

on combustion enthalpy. To improve the reliance on the theoretical work, it is essential to carryout experimental work using blend and biofuel for validation purpose (Uryga-Bugajska *et al,* 2008).

A primary interest for the CFD simulations was also to investigate the effect of fuel on NOx formation route and emission levels in the exhaust. The NOx profile in MAC combustor was computed with a partial equilibrium approach using the previously calculated temperature and species mixture fractions. Turbulence/chemistry interaction was modelled using a joint probability density function (pdf) approach using two statistically independent variables. It was observed that in both the kerosene and blend cases that, as dictated by the extended Zeldovich mechanism, most of the NOx formation occurs in the post/flame volume area where the gas temperature and OH/O concentration is high. The predicted NOx formation results show that the predominant source of NOx is from thermal, with prompt supplying less than 10%. The reactions used in the NOx post processor that are responsible for most of the NOx are taken from the extended Zeldovich mechanism (Uryga-Bugajska *et al,* 2008).

Laranchi *et al* (2013) conducted a CFD analysis of an annular micro gas turbine (MGT) combustion chamber fueled with liquid biofuels. A CFD numerical analysis was carried out to investigate the behavior of bioethanol as a fuel for an MGT with an annular combustion chamber. The computational model was developed in CD-ADAPCO STAR CCM+ environment. The analysis consisted of three simulations of bioethanol combustion, with different computational domains: original design, modified injector and modified injector with lower number of dilution air holes. A reduced combustion mechanism for ethanol combustion taken in literature was implemented in CHEMKIN format file and inserted in the hybrid kinetics-EBU non-premixed combustion model of the software. The results of the three simulations were compared with measured data and results of NG combustion. From comparison between natural gas (NG) and bioethanol simulations it appeared that the modifications of the geometry seemed to compensate adequately the variation in gas composition maintaining constant characteristics at the turbine inlet. In conclusion the modified injector and a dilution in the dilution air holes overall area were sufficient to achieve a comparable power and efficiency with respect to the NG case (Laranchi *et al*, 2013).

Maiorova *et al* (2017) analysed the effect of physical properties of liquid fuels with high viscosity (including biofuels) on the spray and burning characteristics. In their paper titled "the atomization and burning of biofuels in the combustion chambers of gas turbine engines" recommended that several measures should be taken to modernize the conventional combustors when using biofuels in gas turbine engines. The combustion value of biofuels is significantly lower than that of fossil fuels. They further concluded that for aircraft engines blend of biofuels with conventional aviation fuels is more preferable than pure biofuels. Various versions of a percentage ratio of components of combustible mixtures on the basis of plant oil and ethanol have been investigated in the capacity of the main component aviation kerosene TS 1 and gasoline have been chosen. The mix in a ratio of 40 % of kerosene TS 1, 20 % of castor oil, 40 % of ethanol has been chosen as the most homogeneous and well mixed without any precipitations and stratifications (Maiorova *et al*, 2017).

2.7 Conclusion on the combustion of biofuels

Jonathan *et al* (2013) simulated the use of alternative fuels in a turbofan engine. As the push to make the use of biofuels more pervasive in the airline industry continues, it is important to understand their broader impact, (Jonathan *et al*, 2013). A positive example of the engine performance simulations using C-MAPSS40k had demonstrated the thermodynamic compatibility of biodiesel with existing engines. Biofuel engines will be able to produce equal amounts of thrust compared to conventionally powered engines with the same transient responses if the fuel flow controller is redesigned (Jonathan *et al*, 2013). From a system perspective, the most detrimental properties of certain biofuels are volume, weight, and freezing point. Even with a fuel such as ethanol, which has significantly lower energy content than standard jet fuel, simple controller gain modifications were shown to completely recover the engine response, albeit with a higher fuel flow rate. Therefore, the simulation modified to accept tables representing the properties of a variety of alternative fuels, can be used to evaluate the impact of using these fuels on thrust specific fuel consumption, temperatures, and other variables, and these in turn can be used to evaluate the impact on aircraft weight and range (Jonathan *et al*, 2013). It is evident that most studies in the research area of biofuels for gas turbines have largely been from biodiesel, partly due to the higher heating value. The use of bioethanol in gas turbines has however not received the same attention. There is need to carry out research in bioethanol and its blends with biodiesel combustion through simulations to determine thermal compatibility in the PT6A-27 annular combustor.

CHAPTER 3: THEORETICAL FRAMEWORK

3.1 Introduction

Combustion modelling is the simulation of a physical process on a scale, or by a method, which enables combustion investigations to be carried out which would be difficult, if not impossible, to perform on the real combustor. The model mimics selected aspects of the real combustor processes and therefore predicts or simulates its characteristics and responses to certain design or operating changes.

3.2 Mathematical Models

This study uses mathematical modelling to simulate fluid flow and mixing, combustion and heat transfer phenomena. The steady state flow of gases and liquids plays a vital role in many kinds of engineering applications and devices. The problem of flow and heat transfer in furnaces and combustors are of a multidisciplinary nature, and hence, attention is focused on the general principles which govern the behaviour of the flow in complex configurations. The conservation equations of mass, momentum, species and energy are expressed through partial differential forms (Khalil, 1982).

These equations form the foundation and represent mathematical statements of the conservation laws of physics upon which all prediction procedures are based either directly or indirectly. The governing equations do not themselves provide complete specification of the mathematical problem, as additional information is required. This first information deals with the turbulent nature of the flow necessary to solve the set of momentum equations in turbulent flows and generally form turbulence models. The second type of information deals with reactive flows i.e., the specification of the rate of fuel consumption, heat release and flame properties including geometry of the reaction chamber. The various ways of preparation techniques of fuel and air result in diffusion, premixed and arbitrarily fired flames. These flames differ fundamentally from each other right from flame initialisation, development and stability. The difference become even more complex when these flames are analysed in turbulence regime. This information is important in understanding aspects of combustion modelling (Khalil, 1982).

Heat transfer to the workload in the chamber, in many situations, is the main requirement from the combustion process. This heat transfer is utilised to heat up the workload. Radiation and convective heat transfer models take care of this aspect. Radiation contribution to the energy balance is needed to complete the specification of the energy balance equation. To complete specification of the problem, details of thermodynamic properties are needed. To solve the equations, boundary and inlet conditions should be specified (Khalil, 1982).

3.3 Differential analysis of fluid flow

The differential equations of fluid motion, namely, conservation of mass (the continuity equation) and Newton's second law (the Navier–Stokes equation) are derived. These equations apply to every point in the flow field and thus enable us to solve for all details of the flow everywhere in the flow domain (Cengel and Chimbala, 2014).

3.3.1 Mass Conservation (Continuity)

Derivation of the Reynolds Transport Theorem-RTT as presented by Cengel and Chimbala (2014).

A mathematical derivation of the Reynolds transport theorem is done through use of the **Leibniz theorem.** Considering figure 3.1**,** the theorem allows one to differentiate an integral whose limits of integration are functions of the variable with which you need to differentiate.

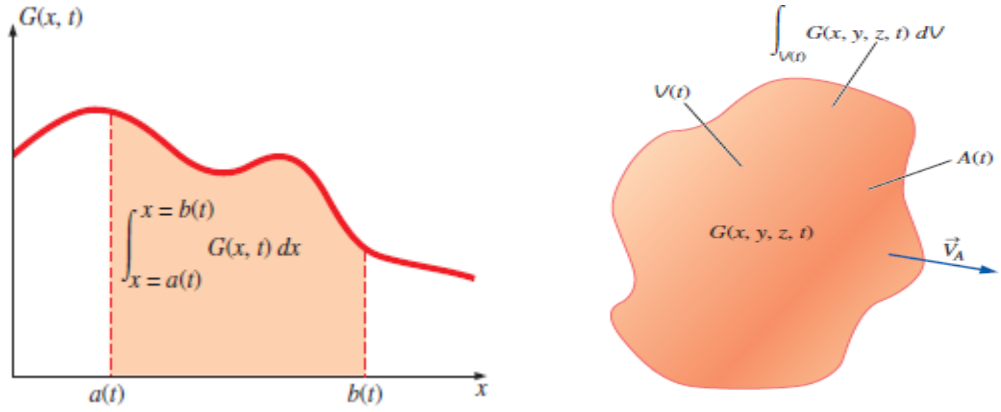

Figure 3. 1: One-Dimensional and Three-Dimensional Leibniz theorem. Source; Fluid mechanics fundamentals and applications

The *one-dimensional Leibniz theorem* is required when calculating the time derivative of an integral (with respect to *x*) for which the limits of the integral are functions of time. The *three-*

dimensional Leibniz theorem is required when calculating the time derivative of a volume integral for which the volume itself moves and/or deforms with time. It turns out that the three dimensional form of the Leibniz theorem can be used in an alternative derivation of the Reynolds transport theorem

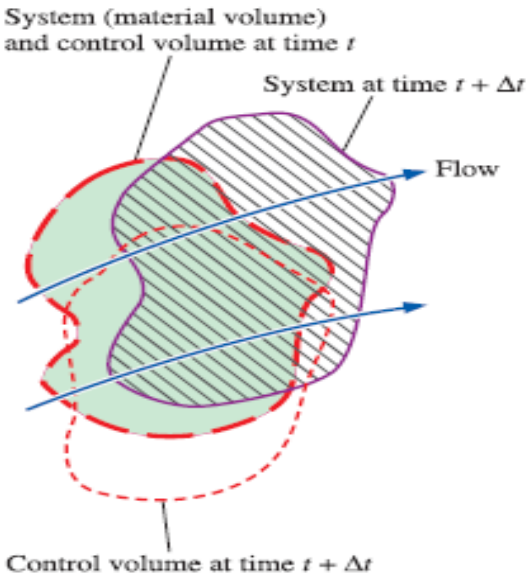

Figure 3. 2: Schematic drawing of control volume. Source; Fluid Mechanics fundamentals and applications

Considering figure 3.2, the material volume (system) and control volume occupy the same space at time *t* (the greenish shaded area) but move and deform differently. Later, they are *not* coincident.

One-Dimensional Leibniz theorem is given as.

$$\frac{d}{dt}\int_{x=a(t)}^{x=b(t)} G(x,t)dx = \int_a^b \frac{\partial G}{\partial t} + \frac{db}{dt}G(b,t) - \frac{da}{dt}G(a,t) \qquad Eq.\,1.0$$

The Three-Dimensional Leibniz theorem thus takes the form;

$$\frac{d}{dt}\int_{V(t)} G(x,y,z)dx = \int_{V(t)} \frac{\partial G}{\partial t} dV + \int G\overrightarrow{V_A}\ \overrightarrow{n}\ dA \qquad Eq.1.1$$

Where V (t) is a moving and/or deforming volume (a function of time), A (t) is its surface (boundary), and V_A is the absolute velocity of this (moving) surface (Fig. 2). Equation 1.1 is valid for *any* volume, moving and/or deforming arbitrarily in space and time. Setting integrand G to ρb for application to fluid flow,

Applying the above equation 2.1 to fluid flow.

$$\frac{d}{dt}\int_{V(t)} \rho b dV = \int_{V(t)} \frac{\partial}{\partial t}(\rho b) dV + \int_{A(t)} \rho b\vec{V}.\vec{n}\, dA \qquad Eq.1.2$$

Applying the Leibniz theorem to the special case of a **material volume** (a system of fixed identity moving with the fluid flow), then $\overrightarrow{VA} = V$ everywhere on the material surface since it moves *with* the fluid. Here $\vec{V}$ is the local fluid velocity, and Eq. 1.2 becomes.

$$\frac{d}{dt}\int_{V(t)} \rho b dV = \frac{dB_{sys}}{dt} = \int_{V(t)} \frac{\partial}{\partial t}(\rho b) dV + \int_{A(t)} \rho b\vec{V}.\vec{n}\, dA \qquad Eq.1.3$$

Equation 2.3 is valid at any instant in time t. We define our control volume such that at this time t, the control volume and the system occupy the same space; in other words, they are *coincident*. At some later time $t + \Delta t$, the system has moved and deformed with the flow, but the control volume may have moved and deformed differently (Fig. 2) above. The key, however, is that *at*

time t, the system (material volume) and control volume are one and the same. Thus, the volume integral on the right-hand side of Eq.1.3 can be evaluated over the *control volume* at time *t*, and the surface integral can be evaluated over the *control surface* at time *t*. Hence, general RTT, nonfixed CV:

$$\frac{dB_{sys}}{dt} = \int_{CV} \frac{\partial}{\partial t}(\rho b)dV + \int_{CS} \rho b\vec{V}\,.\,\vec{n}\,dA \qquad Eq.\,1.4$$

This expression is valid for an arbitrarily shaped, moving, and/or deforming control volume at time *t*.

Through application of the Reynolds transport theorem, we have the following general expression for conservation of mass as applied to a control volume: Eqn. 1.4 of unit mass reduces to eqn. 1.5 and is valid for both fixed and moving control volumes, provided that the velocity vector is the *absolute* velocity (as seen by a fixed observer).

$$0 = \int_{CV} \frac{\partial \rho}{\partial t} dV + \int_{CS} \rho\vec{V}\,.\,\vec{n}\,dA \qquad Eqn.\ 1.5$$

Applying the divergence theorem to Eq. 1.5

$$\oint_V \vec{\nabla}\,.\,\vec{G}\,dV = \oint_A \vec{G}\,.\,\vec{n}dA \qquad Eqn.\ 1.6$$

Eqn. 2.6 applies to any volume, so choosing the control volume of Eq. 1.5. We also let $\vec{G} = \rho\vec{V}$ since $\vec{G}$ can be any vector. Substitution of Eqn. 1.6 into Eq. 1.5 converts the area integral into a volume integral,

$$0 = \int_{CV} \frac{\partial \rho}{\partial t} dV + \int_{CV} \vec{\nabla}.(\rho\vec{V}) dV$$

Combining the two volume integrals into one

$$\int_{CV} \left[\frac{\partial \rho}{\partial t} + \vec{\nabla}.(\rho\vec{V})\right] = 0 \qquad \text{Eqn. 1.7}$$

Equation above implies the integrand equals zero. Therefore, the continuity equation is expressed as.

$$\boldsymbol{\frac{\partial \rho}{\partial t} + \vec{\nabla}.(\rho\vec{V}) = 0} \qquad Eqn. 1.8$$

The above equation is the compressible form of the continuity equation. Alternatively, the continuity equation can be expressed in the following form.

$\boldsymbol{\frac{\partial \rho}{\partial t} + \vec{\nabla}.(\rho\vec{V}) = \frac{\partial \rho}{\partial t} + \vec{V}.\vec{\nabla}\rho + \rho\vec{\nabla}.\vec{V}}$. Where $\boldsymbol{\frac{\partial \rho}{\partial t} + \vec{V}.\vec{\nabla}\rho}$ is the Material Derivative of density ($\boldsymbol{\rho}$)**.** Dividing through by($\boldsymbol{\rho}$) reduces to**.**

$$\frac{\mathbf{1}}{\boldsymbol{\rho}}\frac{\boldsymbol{D\rho}}{\boldsymbol{Dt}} + \vec{\boldsymbol{\nabla}}.\vec{\boldsymbol{V}} = \mathbf{0} \qquad Eqn\ 1.8.1$$

The continuity equation in Cartesian coordinates is expressed as.

$$\frac{\partial \rho}{\partial t} + \frac{\partial(\rho u)}{\partial x} + \frac{\partial(\rho v)}{\partial y} + \frac{\partial(\rho w)}{\partial z} = 0 \qquad Eqn\ 1.8.2$$

Special cases of the continuity equation:

If the flow is compressible but steady, $^{\partial}/_{\partial t}$ of any variable is equal to zero eqn. 1.8 reduces to:

$$\vec{\boldsymbol{\nabla}}.\left(\boldsymbol{\rho}\vec{\boldsymbol{V}}\right) = \mathbf{0}$$

In Cartesian coordinates it becomes:

$$\frac{\partial(\rho u)}{\partial x} + \frac{\partial(\rho v)}{\partial y} + \frac{\partial(\rho w)}{\partial z} = 0 \qquad Eqn\ 1.8.3$$

If flow is estimated as incompressible, the density is not a function of time and space. Thus, $^{\partial \rho}/_{\partial t} \approx 0$. Equation therefore reduces to.

$$\vec{\boldsymbol{\nabla}}\,.\vec{\boldsymbol{V}} = \mathbf{0}$$

In Cartesian coordinates equation is expressed as:

$$\frac{\partial u}{\partial x} + \frac{\partial v}{\partial y} + \frac{\partial w}{\partial z} = 0 \qquad Eqn\ 1.8.4$$

3.3.2 Momentum Conservation

Positive components of the stress tensor in Cartesian coordinates on the positive (right, top, and front) faces of an infinitesimal rectangular control volume as shown in figure 3.3. Positive components on the negative (left, bottom, and back) faces are in the opposite direction of those shown here.

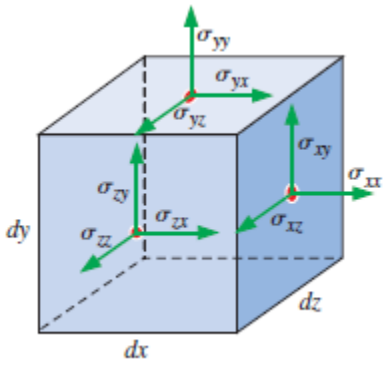

Figure 3. 3: Infinitesimal rectangular control volume-source; Fluid Mechanics Fundamentals and Applications

Through application of the Reynolds transport theorem, we have the general expression for the linear momentum equation as applied to a control volume,

$$\sum \vec{F} = \int_{CV} \rho \vec{g}\, dV + \int_{CS} \sigma_{ij} . \vec{n} dA = \int_{CV} \frac{\partial}{\partial t}(\rho \vec{V}) dV + \int_{CS} (\rho\, \vec{V})\, \vec{V} . \vec{n}\, dA \qquad Eq.1.9$$

The above equation applies to both fixed and moving control volumes provided, the velocity is absolute velocity. For the cases of well-defined inlets and outlets, the equation reduces to.

$$\sum \vec{F} = \sum \vec{F}_{body} + \sum \vec{F}_{surface} = \int_{CV} \frac{\partial}{\partial t}(\rho \vec{V}) dV + \sum_{out} \beta \dot{m} \vec{V} - \sum_{in} \beta \dot{m} \vec{V} \qquad Eqn.1.9.1$$

The extended divergence theorem is expressed as below.

$$\int_V \vec{\nabla} . G_{ij} dV = \oint_A G_{ij} . \vec{n}\, dA$$

Replacing G_{ij} with the quantity $(\rho\,\vec{V})\vec{V}$, a second order tensor in the extended divergence theorem the last term in Eq. 1.9 becomes.

$$\int_{CS}(\rho\,\vec{V})\,\vec{V}.\vec{n}\,dA = \int_{CV}\vec{\nabla}(\rho\,\vec{V}\vec{V})\;dV$$

Similarly, replacing G_{ij} in the extended divergence theorem equation by the stress tensor σ_{ij} , the second term on the left-hand side of Eq. 1.9 becomes

$$\int_{CS}\sigma_{ij}\,.\vec{n}dA = \oint_{CV}\vec{\nabla}.\sigma_{ij}\,dV$$

The two surface integrals of Eq. 1.9 become volume integrals. Combining and rearranging Eq. 1.9, the result becomes.

$$\int_{CV}\left[\frac{\partial}{\partial t}\,(\rho\vec{V}) + \vec{\nabla}.(\rho\vec{V}\vec{V}) - \rho\vec{g} - \vec{\nabla}.\sigma_{ij}\right]dV = 0 \qquad Eq.\,1.9.2$$

Finally, arguing that Eq.1.9.2 must hold for *any* control volume regardless of its size or shape. This is possible only if the integrand (enclosed by square brackets) is identically zero. Hence a general differential equation for linear momentum, known as Cauchy's equation,

$$\frac{\partial}{\partial t}\,(\rho\vec{V}) + \vec{\nabla}.(\rho\vec{V}\vec{V}) - \rho\vec{g} - \vec{\nabla}.\sigma_{ij} = 0$$

$$\frac{\partial}{\partial t}\,(\rho\vec{V}) + \vec{\nabla}.(\rho\vec{V}\vec{V}) = \rho\vec{g} + \vec{\nabla}.\sigma_{ij} \qquad Eqn.\,2.0$$

Alternatively, the Cauchy equation can be expressed as.

$$\rho\left[\frac{\partial\vec{V}}{\partial t} + (\vec{\nabla}.\vec{\nabla})\vec{V}\right] = \rho\frac{D\vec{V}}{Dt} = \rho\vec{g} + \vec{\nabla}.\sigma_{ij}$$

In Cartesian coordinates, the three components of the Cauchy equation can therefore be expressed as.

X- component: $\rho\frac{Du}{Dt} = \rho g_x + \frac{\partial\sigma_{xx}}{\partial x} + \frac{\partial\sigma_{yx}}{\partial y} + \frac{\partial\sigma_{zx}}{\partial z}$

Y- component: $$\rho \frac{Dv}{Dt} = \rho g_y + \frac{\partial \sigma_{xy}}{\partial x} + \frac{\partial \sigma_{yy}}{\partial y} + \frac{\partial \sigma_{zy}}{\partial z}$$

Z- component: $$\rho \frac{Dw}{Dt} = \rho g_z + \frac{\partial \sigma_{xz}}{\partial x} + \frac{\partial \sigma_{yz}}{\partial y} + \frac{\partial \sigma_{zz}}{\partial z}$$

Cauchy's equation is not very useful as it is, because the stress tensor σ_{ij} contains nine components, six of which are independent (because of symmetry). Thus, in addition to density and the three velocity components, there are six additional unknowns, for a total of 10 unknowns. (In Cartesian coordinates the unknowns are r, *u*, *v*, *w*,σ_{xx} , σ_{xy}, σ_{xz} σ_{yy}, σ_{yz} and σ_{zz}). Meanwhile, there are only four equations namely continuity (one equation) and Cauchy's equation (three equations). Of course, to be mathematically solvable, the number of equations must equal the number of unknowns, and thus six more equations (constitutive equations) are needed. These equations aid in writing the components of the stress tensor in terms of the velocity field and pressure field. The first thing to do is to separate the pressure stresses and the viscous stresses. When a fluid is at rest, the only stress acting at *any* surface of *any* fluid element is the local hydrostatic pressure *P*, which always acts *inward* and *normal* to the surface.

3.3.3 Navier Stokes Equations

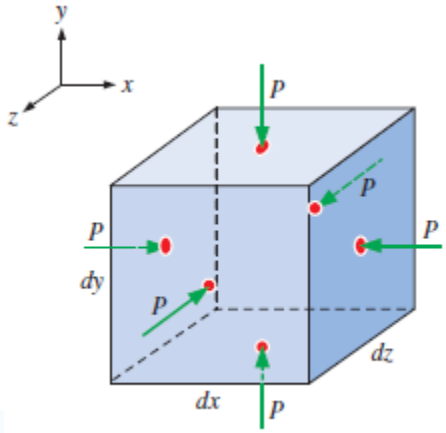

Figure 3. 4: Fluid element with hydrostatic pressure-source; Fluid Mechanics Fundamentals and Applications

For fluids at rest as depicted schematically in figure 3.4, the only stress on a fluid element is the hydrostatic pressure, which always acts inward and normal to any surface.

For a fluid at rest:

$$\sigma_{ij} = \begin{pmatrix} \sigma_{xx} & \sigma_{xy} & \sigma_{xz} \\ \sigma_{yx} & \sigma_{yy} & \sigma_{yz} \\ \sigma_{zx} & \sigma_{zy} & \sigma_{zz} \end{pmatrix} = \begin{pmatrix} -P & 0 & 0 \\ 0 & -P & 0 \\ 0 & 0 & -P \end{pmatrix} \qquad Eq.3.0$$

When a fluid is *moving*, pressure still acts inwardly normal, but viscous stresses may also exist. The above equation for moving fluids is generalized as:

$$\sigma_{ij} = \begin{pmatrix} \sigma_{xx} & \sigma_{xy} & \sigma_{xz} \\ \sigma_{yx} & \sigma_{yy} & \sigma_{yz} \\ \sigma_{zx} & \sigma_{zy} & \sigma_{zz} \end{pmatrix} = \begin{pmatrix} -P & 0 & 0 \\ 0 & -P & 0 \\ 0 & 0 & -P \end{pmatrix} = \begin{pmatrix} \tau_{xx} & \tau_{xy} & \tau_{xz} \\ \tau_{yx} & \tau_{yy} & \tau_{yz} \\ \tau_{zx} & \tau_{zy} & \tau_{zz} \end{pmatrix} \qquad Eq.3.1$$

Viscous stress tensor for an incompressible Newtonian fluid with constant properties can be expressed as:

$$\tau_{ij} = 2\mu\varepsilon_{ij} \qquad Eq.3.2$$

Where ε_{ij} the strain rate tensor and Eq.3.2 shows that stress is linearly proportional to strain. In Cartesian coordinates, the nine components of the viscous stress tensor are listed, only six of which are independent due to symmetry:

$$\tau_{ij} = \begin{pmatrix} \tau_{xx} & \tau_{xy} & \tau_{xz} \\ \tau_{yx} & \tau_{yy} & \tau_{yz} \\ \tau_{zx} & \tau_{zy} & \tau_{zz} \end{pmatrix} = \begin{pmatrix} 2\mu\dfrac{\partial u}{\partial x} & \mu\left(\dfrac{\partial u}{\partial y} + \dfrac{\partial \vartheta}{\partial x}\right) & \mu\left(\dfrac{\partial u}{\partial z} + \dfrac{\partial w}{\partial x}\right) \\ \mu\left(\dfrac{\partial \vartheta}{\partial x} + \dfrac{\partial u}{\partial y}\right) & 2\mu\dfrac{\partial \vartheta}{\partial y} & \mu\left(\dfrac{\partial \vartheta}{\partial z} + \dfrac{\partial w}{\partial y}\right) \\ \mu\left(\dfrac{\partial w}{\partial x} + \dfrac{\partial u}{\partial z}\right) & \mu\left(\dfrac{\partial w}{\partial y} + \dfrac{\partial \vartheta}{\partial z}\right) & 2\mu\dfrac{\partial w}{\partial z} \end{pmatrix}$$

In Cartesian coordinates the stress tensor of Eq. 3.2 thus becomes

$$\tau_{ij} = \begin{pmatrix} -P & 0 & 0 \\ 0 & -P & 0 \\ 0 & 0 & -P \end{pmatrix} + \begin{pmatrix} 2\mu\dfrac{\partial u}{\partial x} & \mu\left(\dfrac{\partial u}{\partial y} + \dfrac{\partial \vartheta}{\partial x}\right) & \mu\left(\dfrac{\partial u}{\partial z} + \dfrac{\partial w}{\partial x}\right) \\ \mu\left(\dfrac{\partial \vartheta}{\partial x} + \dfrac{\partial u}{\partial y}\right) & 2\mu\dfrac{\partial \vartheta}{\partial y} & \mu\left(\dfrac{\partial \vartheta}{\partial z} + \dfrac{\partial w}{\partial y}\right) \\ \mu\left(\dfrac{\partial w}{\partial x} + \dfrac{\partial u}{\partial z}\right) & \mu\left(\dfrac{\partial w}{\partial y} + \dfrac{\partial \vartheta}{\partial z}\right) & 2\mu\dfrac{\partial w}{\partial z} \end{pmatrix} \qquad Eq.3.4$$

Now we substitute Eq. 3.4 into the three Cartesian components of Cauchy's equation. Let's consider the *x-component* first. Cauchy Equation becomes.

$$\rho\frac{Du}{Dt} = -\frac{\partial P}{\partial x} + \rho g_x + 2\mu\frac{\partial^2 u}{\partial x^2} + \mu\frac{\partial}{\partial y}\left(\frac{\partial \vartheta}{\partial x} + \frac{\partial u}{\partial y}\right) + \mu\frac{\partial}{\partial z}\left(\frac{\partial w}{\partial x} + \frac{\partial u}{\partial z}\right)$$

Rearranging viscous terms

$$\rho\frac{Du}{Dt} = -\frac{\partial P}{\partial x} + \rho g_x + \mu\left[\frac{\partial}{\partial x}\left(\frac{\partial u}{\partial x} + \frac{\partial \vartheta}{\partial y} + \frac{\partial w}{\partial z}\right) + \frac{\partial^2 u}{\partial x^2} + \frac{\partial^2 u}{\partial y^2} + \frac{\partial^2 u}{\partial z^2}\right]$$

Assuming incompressibility, the term in parenthesis equal zero; the last three terms are the Laplacian of velocity component *u* in Cartesian coordinates. Thus, the x,y and z-components of the momentum equation are written as

X- component: $\rho\frac{Du}{Dt} = -\frac{\partial P}{\partial x} + \rho g_x + \mu\nabla^2 u$

Y- component: $\rho\frac{D\vartheta}{Dt} = -\frac{\partial P}{\partial y} + \rho g_y + \mu\nabla^2 \vartheta$

Z- component: $\rho\frac{Dw}{Dt} = -\frac{\partial P}{\partial z} + \rho g_z + \mu\nabla^2 w$

Combining the three components into one vector equation; the result is the Navier–Stokes equation for incompressible flow with constant viscosity.

$$\rho\frac{D\vec{V}}{Dt} = -\vec{\nabla}P + \rho g + \mu\nabla^2\vec{V} \qquad Eq.3.5$$

3.3.4 Individual Species Conservation

As derived by Law Chung K, in the book "Combustion Physics": Consider an extensive fluid property Ψ whose magnitude depends on the size of the control volume *V*, and its corresponding intensive quantity ψ, which is the "density" of Ψ per unit volume of the fluid. The rate of change of Ψ is then given by the sum of the temporal change of Ψ within *V* and the loss/gain of Ψ through fluxes across the surface of *V*. The general equation describing the rate of change of Ψ is expressed as

$$\frac{\delta \Psi}{\delta t} = \int_V \left(\frac{\partial \psi}{\partial t} + \nabla . \psi V \right) dV \qquad Eq. 4.0$$

If **Ψ** is the mass m_i of the ith species, then $\boldsymbol{\psi}$ is its partial density ρ_i . The above equation then becomes.

$$\frac{\delta m_i}{\delta t} = \int_V \left(\frac{\partial \rho_i}{\partial t} + \nabla . \rho_i V \right) dV \qquad Eq. 4.1$$

There are two sources which can lead to a change in m_i. The first is volumetric in nature, caused by the presence of chemical reaction as represented by the rate of production of i per unit volume w_i. The second is a surface process, due to diffusion across the control surface when spatial nonuniformity exists in the concentration of i. This diffusive transport is affected through molecular collision and its magnitude is proportional to the mass flux $\rho_i V_i$ of the molecular random motion. Thus

$$\frac{\delta m_i}{\delta t} = \int_V w_i dV - \int_S (\rho_i V_i . n) dS = \int_V (w_i - \nabla . \rho_i V_i) dV .$$

Equating the two equations above, yields

$$\frac{\partial \rho_i}{\partial t} + \nabla . [\rho_i (V + V_i)] = w_i \qquad i = 1,2, \dots, N \qquad Eq. 4.2$$

Equation above is the conservation equation for the ith species.

3.4 Chemical Thermodynamics

Law (2006) defines chemical thermodynamics as branch concerned with the description of the equilibrium states of reacting multicomponent systems. Compared to single-component systems in which only thermal equilibrium is required. Since practical combustors are designed to ensure that fuel and air have sufficient residence time to mix, react, and attain thermodynamic equilibrium, global performance parameters such as the heat and power output can frequently be estimated by assuming thermodynamic equilibrium of the combustion products.

In the past several decades, combustion has evolved from a scientific discipline that was largely empirical to one that is quantitative and predictive. These advances are characterized by the

canonical formulation of the theoretical foundation; the strong interplay between theory, experiment, and computation; and the unified description of the roles of fluid mechanics and chemical kinetics (Law, 2006).

3.4.1 Practical Reactants

For most of the practical combustion devices generating heat and power, the oxidizer is simply the oxygen in air.

For practical calculations air can be considered to consist of 21 percent oxygen and 79 percent nitrogen in molar concentrations, implying that for every mole of oxygen there are 3.76 moles of nitrogen. Therefore, we can write.

Air = $0.21O_2$ + $0.79N_2$ or 4.76Air = O2 + $3.76N_2$

3.4.2 Stoichiometry

The combustion intensity between a fuel and an oxidizer depends on their relative concentrations. When their concentration ratio is chemically correct in that all the reactants can be totally consumed in the reaction, then the combustion intensity is close to the highest and we call this mode of burning stoichiometric combustion.

To measure the relative concentrations of fuel and oxidizer in a mixture, we define a fuel–oxidizer ratio, *F/O*, as the ratio of the mass of fuel to the mass of oxidizer in the mixture. Similarly, a fuel–air ratio, *F/A*, can also be defined. To indicate the deviation of a mixture's concentration from stoichiometry, an equivalence ratio $\emptyset$ is defined as

$$\emptyset = \frac{{}^{F}/_{O}}{\left({}^{F}/_{O}\right)_{st}} \qquad Eq.5.0$$

The definition of $\emptyset$ is asymmetrical relative to fuel-lean $(0 < \emptyset < 1)$ and fuel rich

$(1 < \emptyset < \infty)$ cases.

3.5 Chemical Equilibrium

3.5.1 First and Second Laws

The first law of thermodynamics states that for a closed system, which is one with a fixed mass, the heat δQ added to the system in an infinitesimal process is used to increase its internal energy by *dE* and to perform a certain amount of work, δW.

Thus

$$\delta Q = dE + \delta W \qquad Eq.5.1$$

Note that E is a property of the system, and hence, dE an exact differential of the process, whereas δQ and δW are path-dependent quantities. Since we are developing the thermodynamics of equilibrium chemical systems, we need consider only the pdV work done by volume change, where p is the pressure, and V is the total volume.

Thus, equation above can be written as

$$\delta Q = dE + pdV \qquad Eq.5.1.1$$

The second law of thermodynamics states that there exists a quantity *S*, called the entropy, which has the property that for an infinitesimal process in a closed system,

$$TdS \geq \delta Q \qquad Eq.5.2$$

Where *T* is the temperature. For all-natural processes the inequality holds. Equality holds only if the process is reversible.

Relations (5.1.1) and (5.2) then imply that.

$$dE \leq TdS - pdV \qquad Eq.5.3$$

3.5.2 Thermodynamic Functions

Based on the functional form of Eq.5.3, we can define a thermodynamic function *E* as follows. Since we have assumed that there is only one mode of reversible work, *pdV*, the state of a single-component thermodynamic system in equilibrium can be completely characterized by two

independent variables, say *S* and *V* as indicated in Eq.5.3. For a multicomponent system, the composition also needs to be specified, say by the number of moles of the *i*th species, *Ni*. The same species in different phases is treated as different thermodynamic species by considering phase transition as a chemical reaction. Therefore, we can write, in general, that.

$$E = E(S, V, Ni) \qquad Eq.5.3.1$$

Which can be differentiated to yield.

$$dE = \left(\frac{\partial E}{\partial S}\right)_{SN_i} dS + \left(\frac{\partial E}{\partial V}\right)_{SN_i} dV + \sum_{i=1}^{N} \left(\frac{\partial E}{\partial N_i}\right)_{S,V,N_{j(j\neq i)}} dN_i \qquad Eq.5.4$$

By comparing Eq. (1.2.5) with (1.2.4), the temperature *T* and the pressure *p* can be defined as

$T = \left(\frac{\partial E}{\partial S}\right)_{SN_i}$, $P = -\left(\frac{\partial E}{\partial V}\right)_{SN_i}$.

Further, defining chemical potential as $\bar{\mu}$

$$\bar{\mu} = \left(\frac{\partial E}{\partial N_i}\right)_{S,V,N_{j(j\neq i)}}$$

Then Eq.5.4 can be written as

$$dE = TdS - pdV + \sum_{i=1}^{N} \bar{\mu}_i \, dN_i \qquad Eq.5.5$$

Where the overbar indicates a partial molar quantity. The corresponding symbol without the overbar indicates the same quantity based on per unit mass. Using Eq.5.5 analogous forms of energy can be obtained for the enthalpy.

H = *E* + *pV*, Helmholtz function *A*= *E* − *TS*, and Gibbs function *G* = *H* − *TS* as

$$dH = TdS + Vdp + \sum_{i=1}^{N} \bar{\mu}_i \, dN_i \qquad Eq.5.5.1$$

$$dA = -SdT + pdV + \sum_{i=1}^{N} \bar{\mu}_i \, dN_i \qquad Eq.5.5.2$$

$$dG = -SdT + Vdp + \sum_{i=1}^{N} \bar{\mu}_i \, dN_i \qquad Eq.5.5.3$$

where,

$$\bar{\mu} = \left(\frac{\partial H}{\partial N_i}\right)_{S,p,N_{j(j\neq i)}} = \left(\frac{\partial A}{\partial N_i}\right)_{T,V,N_{j(j\neq i)}} = \left(\frac{\partial G}{\partial N_i}\right)_{T,p,N_{j(j\neq i)}}$$

3.6 Energy Conservation

During reactions, exchanges in chemical and thermal energy take place. Typically, we are given a cold combustible mixture consisting of reactants and inerts. During the subsequent reaction sequence with net exothermicity, chemical energy is released as the reactant molecules are transformed into the product molecules. This chemical heat release is used to heat the product mixture to the final, adiabatic flame temperature. Since the total energy of the system is conserved, the difference between the initial and final states is simply a rearrangement of the different amounts of thermal and chemical energies in each state.

3.6.1 Energy Conservation in Adiabatic Chemical Systems

For a constant pressure process in a closed system, the total enthalpy per mole of species i, at temperature T, $\bar{h}_i(T;T^0)$, is the sum of its heat formulation at T^0, $\bar{h}_i^0(T)$, and the sensible heat at T relative to T^0, $\bar{h}_i^s(T;T^0)$,

$$\bar{h}_i(T;T^0) = \bar{h}_i^0(T^0) + \bar{h}_i^s(T;T^0) \qquad Eq\ 6.0$$

Therefore, energy conservation for a gas mixture before and after a chemical reaction, respectively designated by subscripts 1 and 2, is.

$$\sum_{i=1}^{N} N_{i,1} \, \bar{h}_i(T_1 : T^0) = \sum_{i=1}^{N} N_{i,2} \, \bar{h}_i(T_2 : T^0) \qquad Eq.6.1$$

Substituting Eq.6.0 into above equation

$$\sum_{i=1}^{N} N_{i,1}\ \bar{h}_i^0(T^0) - \sum_{i=1}^{N} N_{i,2}\ \bar{h}_i^0\ (T^0) = \sum_{i=1}^{N} N_{i,2}\ \bar{h}_i^S\ (T_2 : T^0) - \sum_{i=1}^{N} N_{i,1}\ \bar{h}_i^S(T_1 : T^0) \qquad Eq.6.2$$

The LHS side of Eq. 6.2 is the chemical heat release at the standard state, and the

RHS represents the difference between states 1 and 2 in the total sensible heat relative to T_0. Thus, for an initial composition $N_{i,1}$ and temperature T_1, the unknowns in Eq. 6.2 are the final composition $N_{i,2}$ and temperature T_2. T_2 is called the adiabatic flame temperature, designated by T_{ad}.

3.6.2 Adiabatic Flame Temperature and Equilibrium Composition

If a given uniform mixture with an initial temperature and composition is made to approach chemical equilibrium through an adiabatic, isobaric process at pressure *p*, then the final temperature is the adiabatic flame temperature, T_{ad} as shown in figure 3.5. This quantity is of importance in the study of combustion because it not only indicates the exothermicity and the maximum attainable temperature of this mixture when equilibrium is attained, it also directly affects the reactivity of the various chemical processes including those involving pollutant formation.

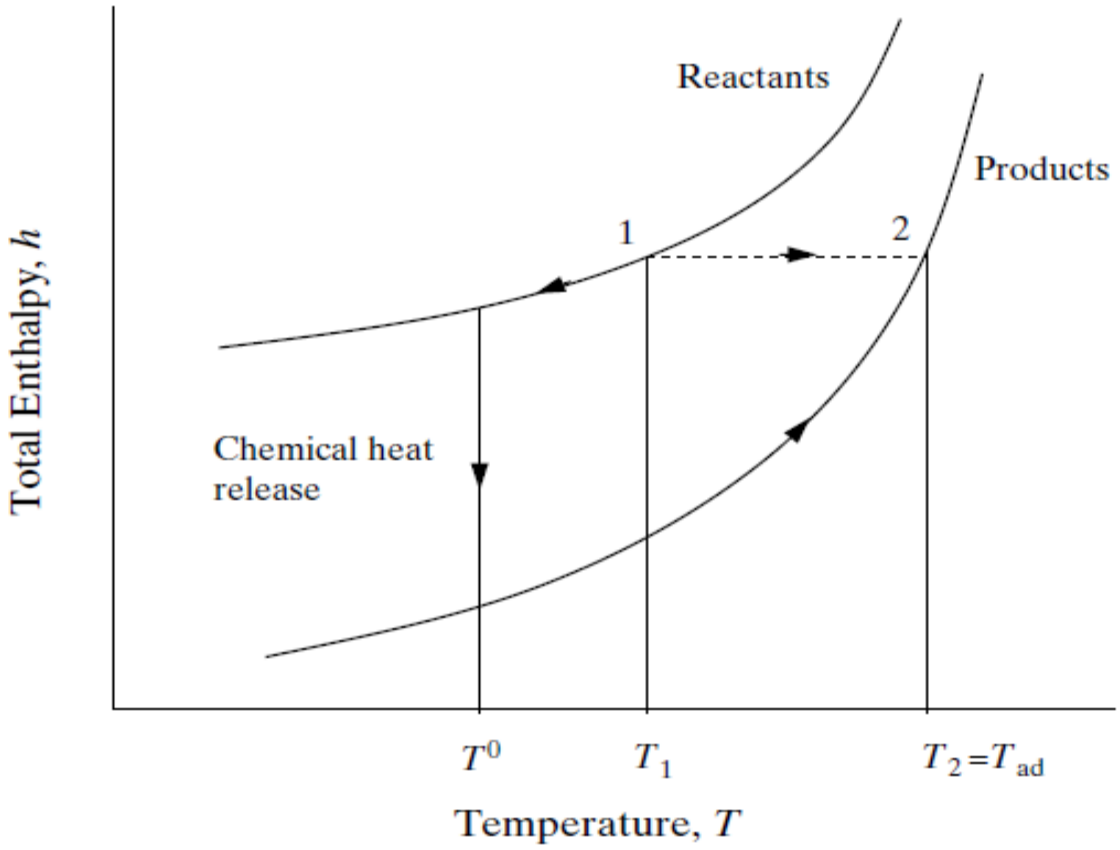

Figure 3. 5: The principle of energy conservation in the definition of adiabatic flame temperature

3.7 Combustion in Turbulent Flows

Most flows in practical combustion devices are turbulent, characterized by the presence of rapid, random fluctuations of the flow velocity and scalar properties at a given point in space. These fluctuations spread out in a manner similar to molecular diffusion as the flow evolves in time and/or proceeds downstream (Law, 2006).

Recognizing the importance of inertia and viscosity on flow stability, the relevant non-dimensional parameter characterizing the tendency for a flow to become unstable and subsequently turbulent is the Reynolds number, $Re = \rho UL/\mu$, which is the ratio of the inertial force to the viscous force in the flow, where U and L are respectively the characteristic velocity and dimension of the flow.

Consequently, the general structure of a turbulent flow is one that consists of large eddies created by abstracting energy from the mean flow motion. These eddies then continuously break up into smaller ones until a certain size range is reached over which viscous dissipation becomes effective.

There is a crucial difference when modeling the physical phenomena between laminar and turbulent flow. For the latter, the appearance of turbulence eddies occurs over a wide range of length scales. With the present-day computing power, the computing requirements for a direct numerical solution (DNS) of the time-dependent Navier-Stokes equations of fully turbulent flows at high Reynolds numbers are still truly phenomenal. Meanwhile, engineers require computational procedures that can supply adequate information about the turbulent processes but wish to avoid the need to predict all the effects associated with each and every eddy in the flow. This category of CFD users is almost always satisfied with information about the time-averaged properties of the flow (e.g., mean velocities, mean pressures, mean stresses, etc.). This process of obtaining mean quantities is applied on the incompressible, two-dimensional equations of continuity, and the *conservative* form of momentum and energy that produces the time averaged governing equations or more popularly known as the Reynolds-Averaged Navier-Stokes (RANS) (Tu, 2008).

3.8 Probabilistic Description

Although the Navier–Stokes equation and the conservation equations for energy and species are deterministic in that unique solutions should exist for properly specified boundary and initial conditions, for large Reynolds number flows the solutions are highly sensitive to conditions at points sufficiently away from the boundaries and/or at sufficiently early times. In other words, minute changes in these conditions can lead to huge changes in the solutions.

3.9 Turbulence Scales/models

A turbulent flow is often characterized by a spectrum of eddies. An eddy is a canonical structure represented by a vortical flow unit riding on the mean flow, for which the average rotational velocity and diameter characterize the relevant velocity and length scales (Law, 2006). Some of the available turbulence models in ANSYS Fluent include: Spalart-Allmaras Model Standard, RNG, and Realizable $k-\omega$ Models,

Standard and SST $k-\omega$ models, $k-kl-\omega$Transition Model, Transition SST Model Intermittency Transition Model, The V2F Model, Reynolds Stress Model (RSM), Scale-Adaptive Simulation (SAS) Model, Detached Eddy Simulation (DES), Large Eddy Simulation (LES) Model, Embedded Large Eddy Simulation (ELES), Near-Wall Treatments for Wall-Bounded Turbulent Flows, Curvature Correction for the Spalart-Allmaras and Two-Equation Models, Production Limiters for Two-Equation Models (ANSYS, Inc, 2013).

3.9.1 Underlying Principles of Turbulence Modeling

The underlying principles discussed hereunder for turbulence modeling include: The Reynolds (Ensemble) Averaging, Filtered Navier-Stokes Equations, Hybrid RANS-LES Formulations and the Boussinesq approach vs. the Reynolds Stress Transport Models, (ANSYS, Inc, 2013).

3.9.2 Reynolds (Ensemble) Averaging

In Reynolds averaging, the solution variables in the instantaneous (exact) Navier-Stokes equations are decomposed into the mean (ensemble-averaged or time-averaged) and fluctuating components. For the velocity components (ANSYS, Inc, 2013):

$$u_i = \bar{u}_i + u_i' \qquad Eq.7.0$$

Where $\bar{u}_i$ and u_i' are the are the mean and fluctuating velocity components

$i = (1,2,3..)$ Likewise, for pressure and other scalar quantities,

$$\emptyset_i = \overline{\emptyset}_i + \emptyset_i' \qquad Eq.7.1$$

Where $\emptyset$ denotes a scalar such as pressure, energy, or species concentration.

Substituting expressions of this form for the flow variables into the instantaneous continuity and momentum equations and taking a time (or ensemble) average (and dropping the overbar on the

mean velocity,$\bar{u}$) yields the ensemble-averaged momentum equations. They can be written in Cartesian tensor form as:

$$\frac{\partial \rho}{\partial t} + \frac{\partial}{\partial x_i}(\rho u_i) = 0 \qquad Eq.7.2$$

$$\frac{\partial \rho}{\partial t}(\rho u_i) + \frac{\partial}{\partial x_j}(\rho u_i u_j) = \frac{\partial}{\partial x_j}\left[\mu\left(\frac{\partial u_i}{\partial x_j} + \frac{\partial u_j}{\partial x_i} - \frac{2}{3}\delta_{ij}\frac{\partial u_l}{\partial x_l}\right)\right] + \frac{\partial}{\partial x_j}\left(-\rho\overline{u_i' u_j'}\right) \qquad Eq.7.3$$

Eq.7.2 and Eq. 7.3 are the Reynolds-averaged Navier-Stokes (RANS) equations. They have the same general form as the instantaneous Navier-Stokes equations, with the velocities and other solution variables now representing ensemble-averaged (or time-averaged) values. Additional terms now appear that represent the effects of turbulence. These Reynolds stresses,$\boldsymbol{\rho\overline{u_i' u_j'}}$,must be modeled in order to close Eq.7.3 (ANSYS, Inc, 2013).

For variable-density flows, Eq.7.2 and Eq.7.3 can be interpreted as Favre averaged Navier-Stokes equations, with the velocities representing mass-averaged values. As such, both equations can be applied to variable-density flows (ANSYS, Inc, 2013).

3.9.3 Filtered Navier-Stokes Equations

The governing equations employed for LES are obtained by filtering the time-dependent Navier-Stokes equations in either Fourier (wave-number) space or configuration (physical) space. The filtering process effectively filters out the eddies whose scales are smaller than the filter width or grid spacing used in the computations. The resulting equations therefore govern the dynamics of large eddies (ANSYS, Inc, 2013).

$$\overline{\emptyset}(x) = \int_D \emptyset(x')\, G(x, x')dx' \qquad Eq.7.4$$

Where **D** is the fluid domain, and **G** is the filter function that determines the scale of the resolved eddies. In ANSYS Fluent, the finite-volume discretization itself implicitly provides the filtering operation:

$$\overline{\emptyset}(x) = \frac{1}{V}\int_{D} \emptyset(x')\,dx'\,, x' \in v \qquad Eq.7.5$$

$$G(x,x') = \begin{cases} \frac{1}{V},\ x' \in v \\ 0,\ x'otherwise \end{cases} \qquad Eq.7.6$$

Filtering the continuity and momentum equations, yields.

$$\frac{\partial \rho}{\partial t} + \frac{\partial}{\partial x_i}(\rho \bar{u}_i) = 0 \qquad Eq.7.7$$

$$\frac{\partial \rho}{\partial t}(\rho u_i) + \frac{\partial}{\partial x_j}\left(\rho \bar{u}_i \bar{u}_j\right) = \frac{\partial}{\partial x_j}\left(\sigma_{ij}\right) - \frac{\partial \bar{P}}{\partial x_i} - \frac{\partial \tau_{ij}}{\partial x_j} \qquad Eq.7.8$$

Where σ_{ij} is the stress tensor due to molecular viscosity defined as;

$$\sigma_{ij} = \left[\mu\left(\frac{\partial \bar{u}_i}{\partial x_j} + \frac{\partial \bar{x}_j}{\partial x_i}\right) - {}^{2}/_{3}\,\mu \frac{\partial \bar{u}_l}{\partial x_i}\delta_{ij}\right] \qquad Eq.7.9$$

Where $\boldsymbol{\tau_{ij}}$ is the subgrid-scale stress defined by

$$\tau_{ij} = \rho\overline{u_i u_j} - \rho \bar{u}_i \bar{u}_j \qquad Eq.8.0$$

Filtering the energy equation, the equation below is obtained.

$$\frac{\partial \rho \bar{h}_s}{\partial t} + \frac{\partial \rho \bar{u}_i \bar{h}_s}{\partial x_i} - \frac{\partial \bar{P}}{\partial t} - \bar{u}_j \frac{\partial \bar{P}}{\partial x_i} - \frac{\partial}{\partial x_i}\left(\lambda \frac{\partial \bar{T}}{\partial x_i}\right) = \frac{\partial}{\partial x_i}\left[\rho\left(\overline{u_i h_s} - \bar{u}_i \bar{h}_s\right)\right] \qquad Eq.8.1$$

Where $\rho(\overline{u_i h_s} - \bar{u}_i \bar{h}_s)$ is the sub grid enthalpy flux and λ and h_s are the thermal conductivity and sensible enthalpy respectively.

The subgrid enthalpy flux term in the Eq.8.1 is approximated using the gradient hypothesis:

$$\rho\left(\overline{u_\iota h_s} - \bar{u}_i \bar{h}_s\right) = \frac{\mu_{SGS} C_p \partial \bar{T}}{Pr_{SGS} \partial x_j} \qquad Eq.8.2$$

Where μ_{SGS} is a subgrid viscosity, and Pr_{SGS} is a subgrid Prandtl number equal to 0.85.

3.9.4 Hybrid RANS-LES Formulations

At first, the concepts of Reynolds Averaging and Spatial Filtering seem incompatible, as they result in different additional terms in the momentum equations (Reynolds Stresses and sub-grid stresses). This would preclude hybrid models like Scale-Adaptive Simulation (SAS) or Detached Eddy Simulation (DES), which are based on one set of momentum equations throughout the RANS and LES portions of the domain. However, it is important to note that once a turbulence model is introduced into the momentum equations, they no longer carry any information concerning their derivation (averaging). Case in point is that the most popular models, both in RANS and LES, are eddy viscosity models that are used to substitute either the Reynolds- or the sub-grid stress tensor. After the introduction of an eddy viscosity (turbulent viscosity), both the RANS and LES momentum equations are formally identical. The difference lies exclusively in the size of the eddy-viscosity provided by the underlying turbulence model. This allows the formulation of turbulence models that can switch from RANS to LES mode, by lowering the eddy viscosity in the LES zone appropriately, without any formal change to the momentum equations (ANSYS, Inc, 2013)

3.9.5 Boussinesq Approach vs. Reynolds Stress Transport Models

The Reynolds-averaged approach to turbulence modeling requires that the Reynolds stresses in Eq.7.3 are appropriately modeled. A common method employs the Boussinesq hypothesis to relate the Reynolds stresses to the mean velocity gradients.

$$-\rho u_i' u_j' = \mu_t \left(\frac{\partial u_i}{\partial x_j} + \frac{\partial u_j}{\partial x_i}\right) - {}^2/_3 \left(\rho k + \mu \frac{\partial u_k}{\partial x_k}\right) \delta_{ij} \qquad Eq.8.3$$

The Boussinesq hypothesis is used in the Spalart-Allmaras model, the $k-\varepsilon$ models, and the $k-\omega$ models. The advantage of this approach is the relatively low computational cost associated with

the computation of the turbulent viscosity, μ_t. In the case of the Spalart-Allmaras model, only one additional transport equation (representing turbulent viscosity) is solved. In the case of the $k-\varepsilon$ and $k-\omega$ models, two additional transport equations (for the turbulence kinetic energy, k, and either the turbulence dissipation rate, ε, or the specific dissipation rate, ω) are solved, and μ_t is computed as a function of k and ε or k and ω. The disadvantage of the Boussinesq hypothesis as presented is that it assumes μ_t is an isotropic scalar quantity, which is not strictly true. However, the assumption of an isotropic turbulent viscosity typically works well for shear flows dominated by only one of the turbulent shear stresses. This covers many technical flows, such as wall boundary layers, mixing layers, jets, etc. The alternative approach, embodied in the RSM, is to solve transport equations for each of the terms in the Reynolds stress tensor. An additional scale-determining equation (normally for ε or ω) is also required. This means that five additional transport equations are required in 2D flows and seven additional transport equations must be solved in 3D.

In many cases, models based on the Boussinesq hypothesis perform very well, and the additional computational expense of the Reynolds stress model is not justified. However, the RSM is clearly superior in situations where the anisotropy of turbulence has a dominant effect on the mean flow. Such cases include highly swirling flows and stress-driven secondary flows (ANSYS, Inc, 2013).

3.10 Non-Premixed Combustion

In non-premixed combustion, fuel and oxidizer enter the reaction zone in distinct streams. This contrasts with premixed systems, in which reactants are mixed at the molecular level before burning. Examples of non-premixed combustion include pulverized coal furnaces, diesel internal-combustion engines and pool fires.

Non-premixed modeling involves the solution of transport equations for one or two conserved scalars (the mixture fractions). Equations for individual species are not solved. Instead, species concentrations are derived from the predicted mixture fraction fields. The thermochemistry calculations are preprocessed and then tabulated for look-up in ANSYS Fluent. Interaction of turbulence and chemistry is accounted for with an assumed-shape Probability Density Function (PDF). Non-premixed combustion and mixture fraction theory are analysed under the following:

Mixture Fraction Theory, Modeling of Turbulence-Chemistry Interaction, Non-Adiabatic Extensions of the Non-Premixed Model and Chemistry Tabulation.

Under certain assumptions, the thermochemistry can be reduced to a single parameter: the mixture fraction. The mixture fraction, denoted by $\boldsymbol{f}$, is the mass fraction that originated from the fuel stream. In other words, it is the local mass fraction of burnt and unburnt fuel stream elements $(C, H, CO_2\ , H_2O\ , O_2)$ and so on in all the species. The approach is elegant because atomic elements are conserved in chemical reactions. In turn, the mixture fraction is a conserved scalar quantity, and therefore its governing transport equation does not have a source term. Combustion is simplified to a mixing problem, and the difficulties associated with closing non-linear mean reaction rates are avoided. Once mixed, the chemistry can be modeled as being in chemical equilibrium with the Equilibrium model, being near chemical equilibrium with the Steady Diffusion Flamelet model, or significantly departing from chemical equilibrium with the Unsteady Diffusion Flamelet model.

3.11 Mixture Fraction Theory

The basis of the non-premixed modeling approach is that under a certain set of simplifying assumptions, the instantaneous thermochemical state of the fluid is related to a conserved scalar quantity known as the mixture fraction, $\boldsymbol{f}$ The mixture fraction can be written in terms of the atomic mass fraction as

$$f = \frac{Z_i - Z_{i,ox}}{Z_{i,fuel} - Z_{i,ox}} \qquad Eq.9.0$$

whereZ_i is the elemental mass fraction for element, i. The subscript ox denotes the value at the oxidizer stream inlet and the subscript fuel denotes the value at the fuel stream inlet. If the diffusion coefficients for all species are equal, then Eq.9.0 is identical for all elements, and the mixture fraction definition is unique. The mixture fraction is therefore the elemental mass fraction that originated from the fuel stream.

Under the assumption of equal diffusivities, the species equations can be reduced to a single equation for the mixture fraction, $\boldsymbol{f}$. The reaction source terms in the species equations cancel (since elements are conserved in chemical reactions), and therefore $\boldsymbol{f}$ is a conserved quantity.

While the assumption of equal diffusivities is problematic for laminar flows, it is generally acceptable for turbulent flows where turbulent convection overwhelms molecular diffusion. The Favre mean (density-averaged) mixture fraction equation is

$$\frac{\partial}{\partial t}\left(\rho\bar{f}\right) + \nabla.\left(\rho\vec{V}\bar{f}\right) = \nabla.\left(\frac{\mu_l + \mu_t}{\sigma_t}\nabla\bar{f}\right) + S_m + S_{user} \qquad Eq.9.1$$

Where μ_l is the laminar viscosity and μ_t is the turbulent viscosity. The source term S_m is due solely to transfer of mass into the gas phase from liquid fuel droplets or reacting particles (for example, coal). S_{user} is any user-defined source term.

3.12 Mixture Fraction vs. Equivalence Ratio

The mixture fraction definition can be understood in relation to common measures of reacting systems. Consider a simple combustion system involving a fuel stream (F), an oxidant stream (O), and a product stream (P) symbolically represented at stoichiometric conditions.

$$F + rO \xrightarrow{yields} (1 + r)P \qquad Eq.9.2$$

Where r is the air-to-fuel ratio on a mass basis. Denoting the equivalence ratio as ϕ,

$$\phi = \frac{(fuel/air)_{actual}}{(fuel/air)_{stoichiometry}} \qquad Eq.9.2.1$$

the reaction in Eq.9.2.1, under more general mixture conditions can be written as,

$$\phi F + rO \xrightarrow{yields} (\phi + r)P \qquad Eq.9.2.2$$

Looking at the left side of this equation, the mixture fraction for the system as a whole can then be deduced to be.

$$f = \frac{\phi}{\phi + r} \qquad Eq.9.3$$

Eq.9.3 allows the computation of the mixture fraction at stoichiometric conditions ($\phi = 1$) or at fuel-rich conditions ($\phi > 1$), or fuel-lean conditions ($\phi < 1$) (ANSYS, Inc, 2013).

3.13 Pollutant Formation

The theory behind the models available in ANSYS Fluent for modeling pollutant formation. These models include NOx Formation, SOx Formation, Soot Formation, and Decoupled Detailed Chemistry Model (ANSYS, Inc, 2013). This research however focused on the NOx Formation.

3.13.1 NOx Formation

NO_x emissions consist of mostly nitric oxide (NO), and to a lesser degree nitrogen dioxide (NO_2) and nitrous oxide (N_2O). NO_x is a precursor for photochemical smog, contributes to acid rain and ozone depletion. Thus, NO_x is a pollutant.

3.14 NOx Modeling in ANSYS Fluent

The ANSYS Fluent model provides the capability to model thermal, prompt, and fuel NO_x

formation, as well as NO_x consumption due to reburning in combustion systems. It uses rate models developed at the Department of Fuel and Energy at The University of Leeds in England, as well as from the open literature. NO_x reduction using reagent injection, such as selective non-catalytic reduction (SNCR), can be modeled in ANSYS Fluent, along with an N_2O intermediate model that has also been incorporated. To predict NO_x emissions, ANSYS Fluent solves a transport equation for nitric oxide (NO), concentration.

When fuel NO_x sources are present, ANSYS Fluent solves additional transport equations for intermediate species (HCN and/or NH_3). When the N_2O intermediate model is activated, an additional transport equation for N_2O will be solved. The NO_x transport equations are solved based on a given flow field and combustion solution. In other words, NO_x is postprocessed from a combustion simulation. It is therefore evident that an accurate combustion solution becomes a prerequisite of NO_x prediction. For example, thermal NO_x production doubles for every 90 K temperature increase when the flame temperature is about 2200 K. Great care must be exercised

to provide accurate thermophysical data and boundary condition inputs for the combustion model. Appropriate turbulence, chemistry, radiation, and other sub-models must be employed.

To be realistic, one can only expect results to be as accurate as the input data and the selected physical models. Under most circumstances, NO_x variation trends can be accurately predicted, but the NO_x quantity itself cannot be pinpointed. Accurate prediction of parametric trends can cut down on the number of laboratory tests, allow more design variations to be studied, shorten the design cycle, and reduce product development cost. That is truly the power of the ANSYS Fluent NO_x model and, in fact, the power of CFD in general.

3.14.1 NOx Formation and Reduction in Flames

In laminar flames and at the molecular level within turbulent flames, the formation of NO_x can be attributed to four distinct chemical kinetic processes: thermal NO_x formation, prompt formation, fuel NO_x formation, and intermediate N_2O . Thermal NO_x is formed by the oxidation of atmospheric nitrogen present in the combustion air. Prompt NO_x is produced by high-speed reactions at the flame front. Fuel NO_x is produced by oxidation of nitrogen contained in the fuel. At elevated pressures and oxygen-rich conditions, NO_x may also be formed from molecular nitrogen (N_2) via N_2O. The reburning and SNCR mechanisms reduce the total NO_x formation by accounting for the reaction of NO with hydrocarbons and ammonia, respectively.

3.14.2 Governing Equations for NOx Transport

ANSYS Fluent solves the mass transport equation for the NO species, considering convection, diffusion, production, and consumption of NO and related species. This approach is completely general, being derived from the fundamental principle of mass conservation. The effect of residence time in NO_x mechanisms (a Lagrangian reference frame concept) is included through the convection terms in the governing equations written in the Eulerian reference frame. For thermal and prompt NO_x mechanisms, only the NO species transport equation is needed:

$$\frac{\partial}{\partial t}(\rho Y_{NO}) + \nabla.\left(\rho \vec{V} Y_{NO}\right) = \nabla.(\rho D \nabla Y_{NO}) + S_{NO} \qquad Eq.10$$

The tracking of nitrogen-containing intermediate species is important. ANSYS Fluent solves a transport equation for the HCN or NH_3 species, in addition to the NO species.

$$\frac{\partial}{\partial t}(\rho Y_{HCN}) + \nabla.(\rho \vec{V} Y_{HCN}) = \nabla.(\rho D \nabla Y_{HCN}) + S_{HCN} \qquad Eq.10.1$$

$$\frac{\partial}{\partial t}(\rho Y_{NH_3}) + \nabla.(\rho \vec{V} Y_{NH_3}) = \nabla.(\rho D \nabla Y_{NH_3}) + S_{NH_3} \qquad Eq.10.2$$

$$\frac{\partial}{\partial t}(\rho Y_{N_2O}) + \nabla.(\rho \vec{V} Y_{N_2O}) = \nabla.(\rho D \nabla Y_{N_2O}) + S_{N_2O} \qquad Eq.10.3$$

Where Y_{HCN}, Y_{NH_3}, Y_{N_2O} and Y_{NO} are mass fractions of, HCN, NH_3, N_2O and NO in the gas phase, and D is the effective diffusion coefficient. The source terms are to be determined for different NO_x mechanisms such as thermal NO_x, prompt NO_x and fuel NO_x.

3.14.3 PT6A-27 Annular Combustor Geometry

In this type, an annular liner is mounted concentrically inside an annular casing. In many ways it is an ideal form of chamber, because of its clean aerodynamic layout results in a compact unit of lower pressure loss than other combustor types. The three main stages of the annular combustor are, the primary zone, secondary zone, and the dilution zone.

Lefebvre, in his book “Gas Turbine Combustion, Alternative fuels and emissions” describes the three zones of the annular combustor. The primary zone anchors the flame and provide sufficient time, temperature, and turbulence to achieve essentially complete combustion of the incoming fuel–air mixture. creation of a toroidal flow reversal that entrains and recirculates a portion of the hot combustion gases to provide continuous ignition to the incoming air and fuel. The intermediate zone or the secondary zone drops the temperature to an intermediate level by the addition of small amounts of air. This encourages the burnout of soot and allows the combustion of CO and any other unburned hydrocarbons (UHC) to proceed to completion.

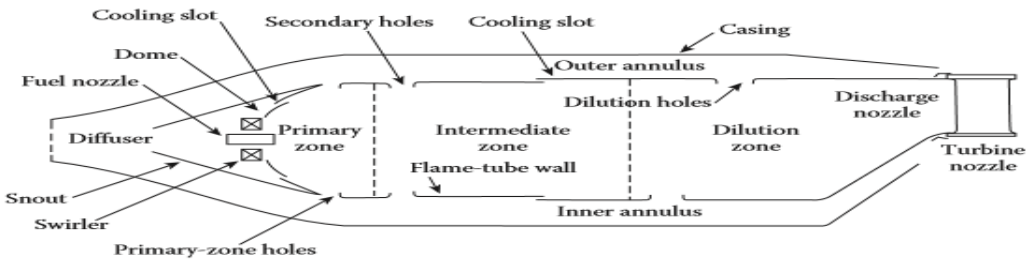

Figure 3. 6: Combustion Zones; source-"Gas Turbine Combustion and alternative fuels"

The role of the dilution zone is to admit the air remaining after the combustion and wall-cooling requirements have been met, and to provide an outlet stream with a temperature distribution that is acceptable to the turbine This temperature distribution is usually described in terms of "pattern factor" or "temperature traverse quality." The amount of air available for dilution is usually between 20 and 40% of the total combustor airflow (Lefebvre, 2010). Figure 3.6 shows a schematic diagram of combustion zones.

3.14.4 Brief description of PT-6A Turboprop Engine

The turboprop engine has played a major role in short haul commuter aircraft and military transport and patrol aircraft where speed is not critical (Saravanamuttoo, 1987). The PT6 power plant is a lightweight, free-turbine engine. Pressure ratio varies from 6.3:1 for early model engines to 10.0:1 for the second generation. Power ranges from 475 to 1700 SHP are achieved. The engine utilizes two independent turbine sections: one (compressor turbine) driving the compressor in the gas generator section, and the second (power turbine – two-stage in larger model engines) driving the output shaft through a reduction gearbox.

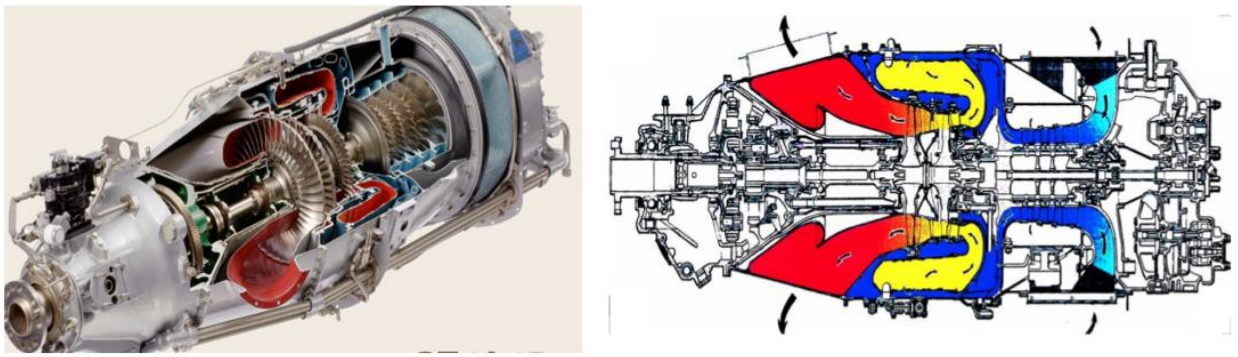

Figure 3. 7: PT6A series Turboprop Engine- Source, training manual for PT6 turboprop engine

Inlet air enters the rear of the engine through annular plenum chamber formed by the compressor inlet case where it is directed forward to the compressor. The compressor consists of three axial stages combined with a single centrifugal stage assembled as an integral unit. The rotating compressor blades and impeller add energy to the air passing through them by increasing its velocity (United Turbine Corp, 2016). Figures 3.7 and 3.8 shows a cross section of the PT62A-27 Turboprop engine and the annular combustor schematic drawing respectively.

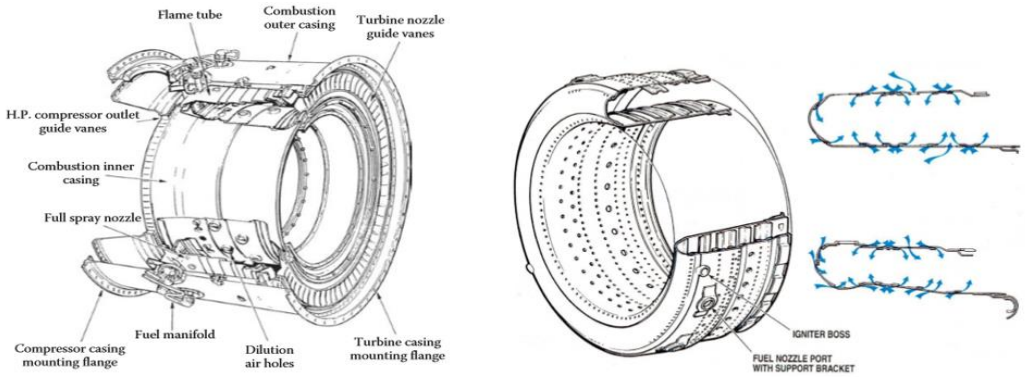

Figure 3. 8: Combustion chamber liner. Source training manual for PT6 turboprop engine.

CHAPTER 4: METHODOLOGY AND NUMERICAL EXPERIMENT SETUP

4.1 Introduction

The purpose of this chapter is to gain improved understanding of the complex physical flow and chemical processes in the PT6A-27 annular combustion chamber. This was achieved by simulating the combustion of kerosene-based jet fuel and was used as the baseline data for the subsequent simulations with biodiesel surrogates and bioethanol. The obtained flow regime was compared with the experimental data from literature sources. To validate the simulated results, surrogate fuels were used, and results compared with the kerosene-based jet fuel. It was on the established validation premise that the surrogate for biodiesel was used and mixed in varying proportions with bioethanol. To examine the combustion characteristics of alternative fuels in the annular combustor of the PT6A-27 engine, the operating parameters of the engine such as the bulk air mass flow rate, fuel injection pressure and simplex nozzle configuration were used. To have a substantial appreciation of the combustion thermal chemical processes Two combustion models were used. These included non-premixed combustion and the NOx sub model. The contour plots obtained are presented together with the associated resultant computational data in the ensuing figures of chapter 5.

The modelling and simulation of combustion of bioethanol and biodiesel blend in a PT6A-27 Turboprop annular combustor involved two general procedures of, modelling the annular combustor in SOLIDWORKS CAD Software and subsequently running simulations in a CFD software, ANSYS-FLUENT. The specific parameters to be assessed included:

- Thermal stability
- Adiabatic flame temperature
- Emissions

4.2 Overview of Geometry Modelling methodology

The annular combustor was modelled based on the design procedure proposed by Melconian and Modak (1985). The input equations and mass air flow distribution are as shown in the Appendix. Additionally, the available annular combustor design parameters from the PT6A-27 Turboprop

engine served as initial input data. The initial design parameters used where the compressor exit and turbine inlet constraint.

4.3 Overview of Simulation in ANSYS-FLUENT

The PT6A-27 Turboprop annular combustor simulation was done using a non-premixed model. The reaction was modeled using the species transport model and the non-premixed combustion model. The combustion simulation approach for bioethanol, biodiesel and their blends using the non-premixed combustion model for the reaction chemistry was as follows:

- Defining inputs for modeling non-premixed combustion chemistry.
- Preparation of the Probability Density Function table in ANSYS FLUENT software.
- Solving a bioethanol/biodiesel combustion simulation problem.
- The Discrete Ordinates (DO) radiation model for combustion was used to account for heat transfer.
- The $k-\varepsilon$ turbulence model was used to account for turbulence.

The non-premixed combustion model uses a modeling approach that solves transport equations for conserved scalars (mixture fractions) using the pressure-based solver in ANSYS FLUENT. Multiple chemical species, including radicals and inter mediate species, may be included in the problem definition. Their concentrations will be derived from the predicted mixture fraction distribution. Property data for the species are accessed through a chemical database and turbulence-chemistry interaction is modeled using a β function for the PDF (ANSYS, Inc, 2013).

4.4 Simulation Method

The six-step approach as outlined by Tu *et al* (2008), were used for the combustion analysis of the biodiesel, bioethanol, and their blends. The steps are as outlined.

4.4.1 **Step 1**: Creation of geometry

The first step was to create a 3-D geometry of the annular combustor in SOLISWORKS based on the equations as proposed by Melconian and Modak (1985). The other input data which included the gravimetric flow rate of air and fuel, the turbine inlet temperature and compressor exit

temperature was obtained from the operating parameters of the PT6A-27 engine. The created geometry was sectioned at 25^0, for the purpose of computational economy.

4.4.2 **Step 2**: Mesh Generation

The Mesh was created in ANSYS MESH with number of elements and nodes at 2.639487×10^6 and 5.00298×10^5 respectively. The Tetrahedral mesh method was used, with the element order being linear. The element size ranged between $5.0 \times 10^{-4}m$ to $8.0 \times 10^{-4}m$. The growth rate of the elements was set at 1.2. Mesh generation constitutes one of the most important steps during the pre-process stage after the definition of the domain geometry. CFD requires the subdivision of the domain into several smaller, non-overlapping subdomains to solve the flow physics within the domain geometry that has been created.

4.4.3 **Step 3**: Selection of physics and fluid properties

The selection of physics and fluid properties included the activation of different models to aid in running a non-premixed combustion simulation. The energy equation was activated as well as the standard $k - \varepsilon psilon$ $(2\ equetion)$ under the viscous model coupled with the enhanced wall treatment. Enhanced Wall Treatment is recommended for general single-phase fluid flow problems when using the k-epsilon model (ANSYS, Inc, 2013). Under the radiation model, the Discrete Ordinates (OD) radiation model was also activated to account for heat transfer. The DO radiation model was chosen because it provides a high degree of accuracy. The species model was also activated and subsequently the NOx model was used after creation of Probability Density Function in the Non-Premixed Combustion. The solution setup for NOx modelling is as indicated in the solution setup section of this chapter.

4.4.4 **Step 4**: Specification of boundary conditions

To obtain a unique solution to this combustion simulation, the boundary conditions were set. The gravimetric fuel flow rate, and air flow rate was set at 0.142 kg/s and 2.0 Kg/s respectively. The model back flow temperature for computational economy and to avoid the software shut down was set at 1000 K. The turbulent kinetic energy and turbulent dissipation rate were set at $1\ m^2/s^2$ and $1\ \mathrm{m}^2/\mathrm{s}^3$ respectively. The simulation was set to run at 1000 iterations and solution convergency was observed at 500 iterations.

4.4.5 **Step 5**: Initialization and solution control

The fifth step of the simulation involved two prerequisite processes within the solver, which are initialization and solution control. Firstly, the iterations were set at 1000 iterations with a backflow temperature of 1000 K to avoid shut down of the software during simulation. The relaxation factors were set at 0.2 and 0.8 for density and body forces respectively.

4.4.6 **Step 6**: Monitoring convergence

The iteration converged at 500 iterations from the commanded 1000 iterations. All the indicative lines including governing equations such as the continuity line, energy equation line converged at half the commanded iterations.

4.4.7 Summary of the Three actual main procedures used in the simulations.

- The annular combustor geometry was created using SOLIDWORKS software.
- The created model was imported into ANSYS Software.
- ANSYS Workbench software was launched to access the ANSYS Fluent platform for fluid flow analysis.
- The FLUENT fluid flow analysis system was created in ANSYS Workbench.
- The imported model was Meshed using ANSYS MESHING.
- The CFD simulation was set in ANSYS FLUENT, and it included:

  - Setting material properties and boundary conditions for a non-premixed combustion problem.

  - Initiating the calculation with residual plotting.

  - Calculating a solution using the pressure-based solver.

- Then finally visually examining the flow and temperature fields using the post-processing tools available in ANSYS FLUENT.

4.5 Solution Setup

4.5.1 Data sources and Collection techniques

The PT6A-27 engine combustion chamber operating parameters were obtained from a standard operating manual. With time, heat engines operating parameters do shift hence other data was also obtained in real time engine operation. The biodiesel and bioethanol data were obtained from literature.

4.5.2 Boundary Conditions

The suitable fluid flow boundary conditions were required to accommodate the fluid behavior entering and leaving the flow domain. Table 4.1 shows the input boundary conditions in the solution setup.

Table 4. 1: Initial parameters obtained from real-time data and used in the geometry design.

parameter	value	units
$\dot{m}_3$	2.0	Kg/s
T_3	315	K
P_3	1.0	Pa
$\dot{m}_f$	0.142	Kg/s

4.5.3 Geometry Creation in Solidworks

With all input data available for geometry creation. The geometry of an annular combustor was created in Solidworks software. The correct number of perforations for air intake in the recirculation, primary, secondary and dilution zones were critical, this was an iterative process to achieve results closest to actual conditions. Any variations would result in an otherwise unbalanced reactor. For computational costs to be maintained at manageable levels, the geometry was sectioned at 25 degrees as shown in the following figures 4.1, 4.2 and 4.3.

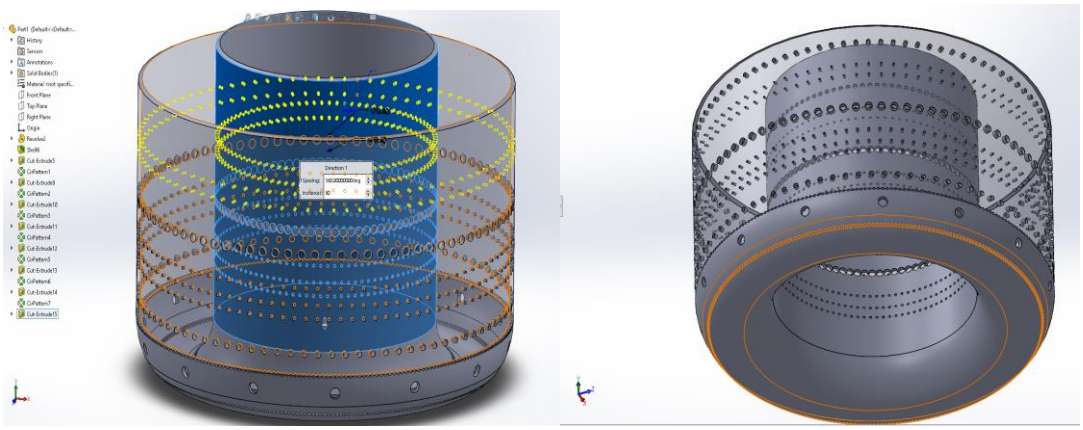

Figure 4. 1: Solidworks combustor geometry

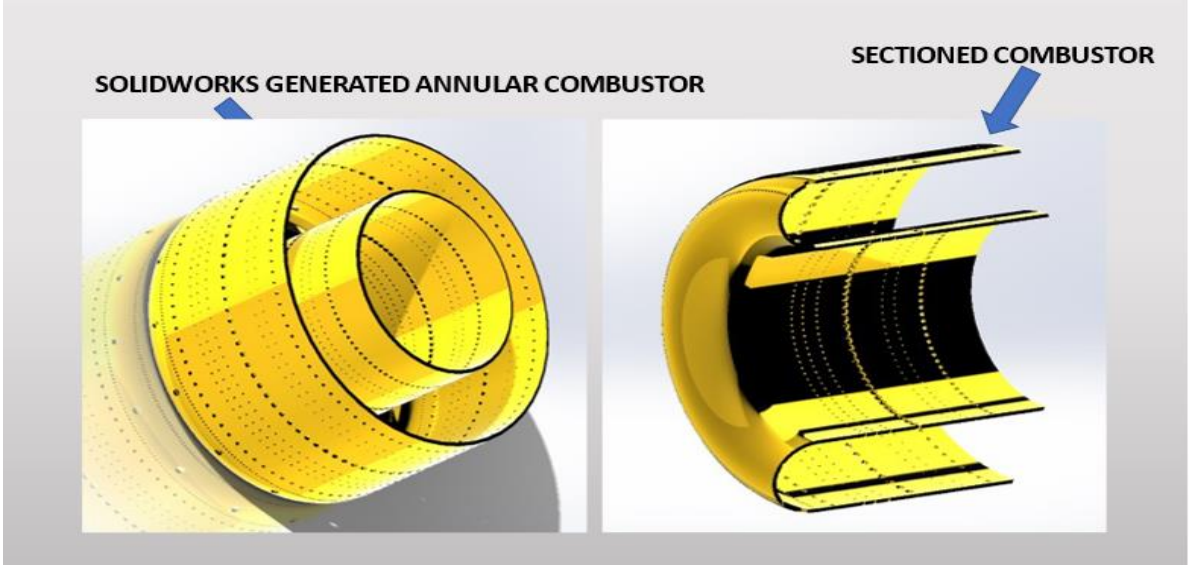

Figure 4. 2: Sectioned combustor geometry

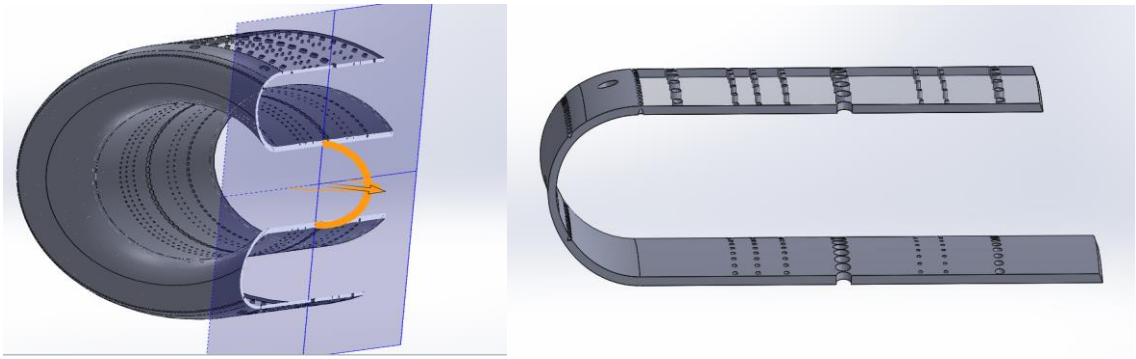

Figure 4. 3**:** 25degree Sectioned combustor geometry

4.5.4 Generated Mesh in ANSYS from imported SOLIDWORKS Geometry

The figure 4.4 shows the sectioned imported geometry into ANSYS and figure 4.5 shows the generated mesh and quality of the element order was about 90% as shown. The closer to unity (100%) the element order is, the more refined the mesh would be.

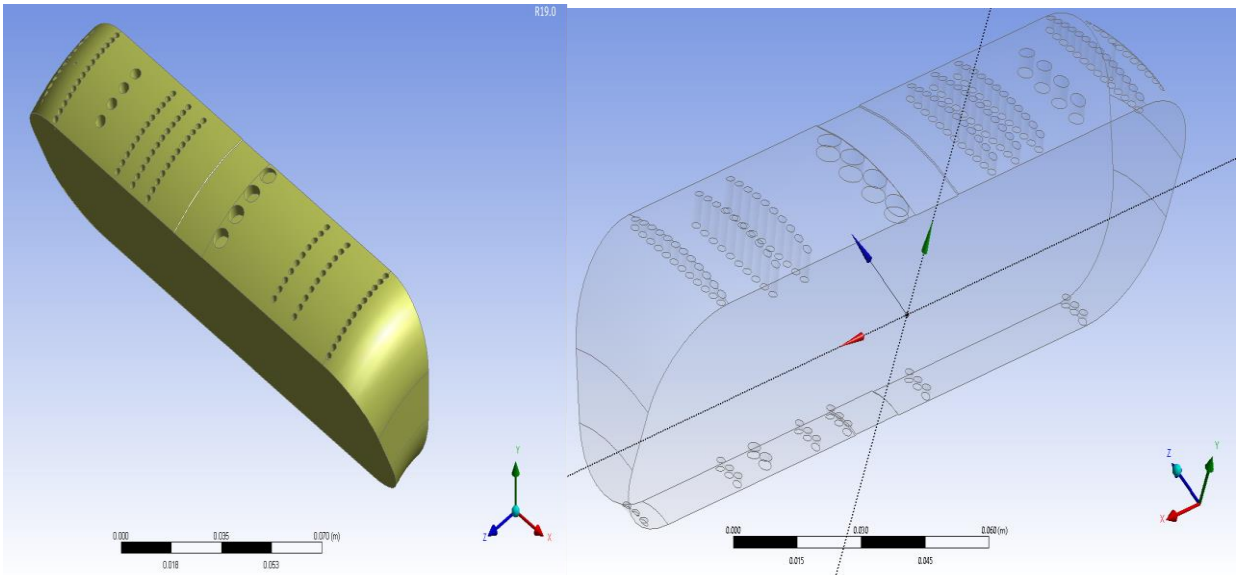

Figure 4. 4: Imported geometry from Solidworks.

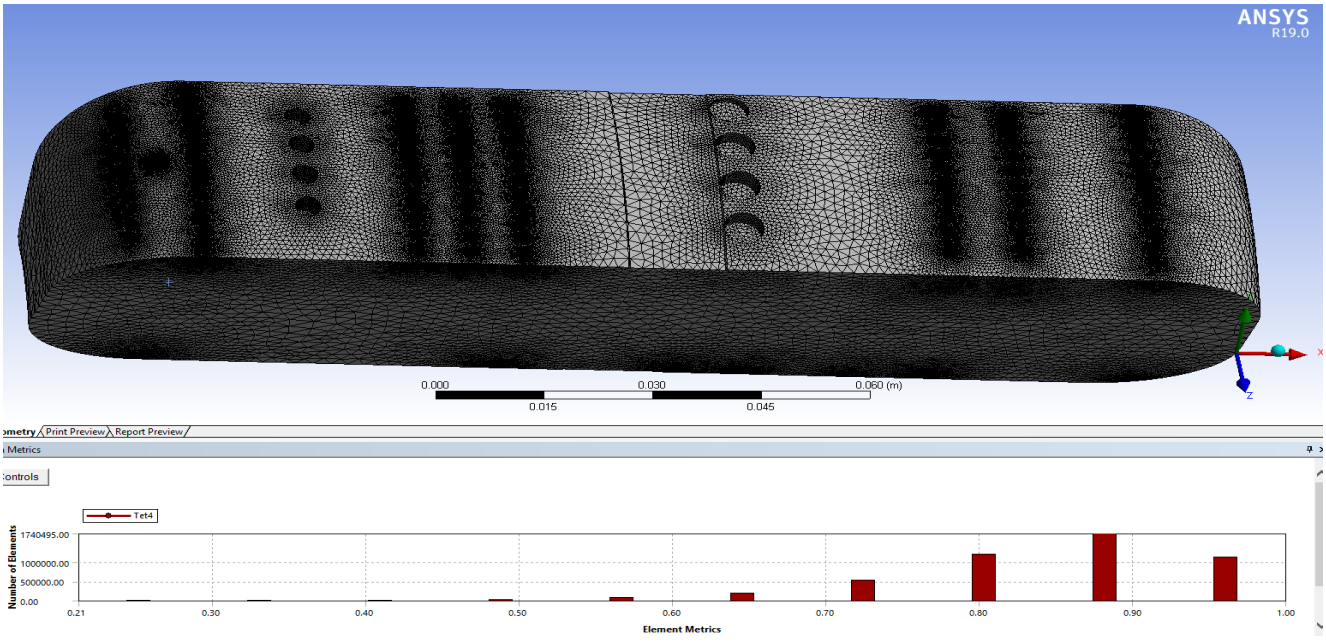

Figure 4. 5: Mesh generation in ANSYS MESH

4.5.5 Solution method and controls

Having used the density-based solver, the solution controls were used to specify various parameters associated with the solution to be used in the calculation of results. The tables 4.2, 4.3 and 4.4 show the solution controls for pressure velocity coupling, viscous model constants and the NOx model controls. Table 4.5 shows the boundary conditions for obtaining a unique solution in the simulation in the non-premixed and NOx models. These controls aid in under-relaxation factors which are required to ensure a robust and stable calculation.

Table 4. 2: Pressure-velocity coupling

Spatial discretization	**Method**
Gradient	Least square cell based
Pressure	Second order
momentum	Second order upwind
Turbulent kinetic energy	First order upwind
Turbulence dissipation rate	First order upwind
Temperature variance	Second order upwind
Energy	Second order upwind
$C_{12}H_{23}$,C_2H_5OH, O_2, H_2O	Second order upwind
Pollutant no	Second order upwind

Table 4. 3: Viscous model constants

Turbulence model	Model constants
Standard $k-\varepsilon$ (2 eq)	Cmu: 0.09
	C1: 1.92
	TKE Prandtl number: 1
	TDR Prandtl number: 1.3
	Energy Prandtl number: 0.85

	Wall Prandtl number: 0.85
	Turbulent Schmidt number: 0.7

Table 4. 4: NOx Formation Solution method

Formation	Formation model parameters	Turbulence interaction model
Thermal NOx Prompt NOx	$[O]$ partial equilibrium $[OH]$ Model-none	PDF mode-Temperature PDF type-beta PDF points 1 Temperature variance-transported T_{max} option- global T_{max} Fuel carbon number- 1 Equivalence ratio-0.76

Table 4. 5: Non-premixed Combustion and NOx Solution Setup Boundary conditions

Boundary	Mass flow rate (kg/s)	Initial gauge pressure (Pa)	Turbulence method	Turbulent Kinetic energy m^2/s^2	Turbulent Dissipation rate m^2/s^3	Inlet temperature (K)	Species	Backflow temperature
Fuel inlet	0.143	8.618	$k-\varepsilon$	1	1	300	$C_{12}H_{23}$ and C_2H_5OH	
Recirculation zone	0.67	1.0	$k-\varepsilon$	1	1	315	O_2	
Primary zone	0.67	1.0	$k-\varepsilon$	1	1	315	O_2	
Secondary zone	0.33	1.0	$k-\varepsilon$	1	1	315	O_2	
Dilution zone	0.33	1.0	$k-\varepsilon$	1	1	315	O_2	
Outlet								1,000

CHAPTER 5: NUMERICAL RESULTS AND DISCUSSION

5.1 Overview of non-premixed combustion performance results

The sectioned combustor at 25 degrees is presented and varying proportions of biofuels combustion simulations ranging from 100% bioethanol and 0% biodiesel to 100% biodiesel and 0% bioethanol. The biofuels were varied at 10% reduction intervals in bioethanol and 10% increment in the biodiesel. Figure 5.1 shows the simulated combustion of JetA-1 via surrogates. The recirculation and primary zones show a high-level activity of combustion with adiabatic flame temperature around 2300 K. This model's adiabatic flame temperature result can be considered a safe reference for the biofuel blends used in this study based on experimental studies undertaken by Xu et al (2015) for the National Jet Fuel Combustion Program where they tested 9 different Kerosene based Aviation fuels and reported the range of adiabatic flame temperature of 2280 K to 2300 K.

The combustion simulation for a non-blend of 100% bioethanol as shown in figure 5.3 with temperature contours in the recirculation zone, did not show higher temperature distribution as expected for the recirculation zone. This can be attributed to the low specific heat content of bioethanol. Similarly for the 80% bioethanol and 20% biodiesel blend, shown in figure 5.6, the temperature distribution was observed to be higher in the dilution zone and recirculation zone. The primary zone temperature distribution was not consistent with the annular combustor temperature distribution. Blending with biodiesel from range of 70% bioethanol and 30% biodiesel (70BE-30BD) to 30% bioethanol with 70% biodiesel (30BE-70BD) as shown in figures 5.9 to 5.23, the temperature contours distribution and the adiabatic flame temperatures showed a consistence in comparison with the combustion of JetA1 as shown in figure 5.1.

The levels of NOx emissions were determined through consideration of the different types of NOx emissions namely: Thermal NOx, Fuel NOx and Prompt NOx. From the fuel composition, Fuel NOx is evidently higher in the conversional Jet fuels. However, it was observed that an increase in the Adiabatic Flame Temperature directly increased the levels of Thermal NOx. The blend of 40% bioethanol to 60% biodiesel was observed to have a reduced Fuel NOx footprint, however, the rise in the calorific energy content of the fuel blend due to the presence of biodiesel in the

mixture contributed to the increase in Thermal NOx production, albeit still less than that obtained from a pure hydrocarbon fuel of JetA-1 as shown in figures 5.30 to 5.33.

A pure JetA-1 hydrocarbon fuel had a production rate of Thermal NOx ranging from $0.002699526\ \mathrm{Kgmol/m^3\ s}$ to $0.002705489\ \mathrm{Kgmol/m^3\ s}$. The Prompt NOx rate for Jet fuel was observed to be $1.789729 \times 10^{-6}\mathrm{Kgmol/m^3\ s}$. On the selected fuel blend of biofuels at the proportions of 40% bioethanol and 60% biodiesel, the observed production rate values of Thermal NOx and Prompt NOx were a range of $4.798448 \times 10^{-6}\mathrm{Kgmol/m^3\ s}$ to $5.01322 \times 10^{-6}\mathrm{Kgmol/m^3\ s}$ and $2.054488 \times 10^{-7}\mathrm{Kgmol/m^3\ s}$ respectively as shown in figures 5.32 and 5.33. This was indicative of a reduction in both Thermal and Prompt NOx when the two groups of fuels (Jet-A against 40BE & 60BD blend) were compared.

Kent Hoekman and Curtis Robbins (2011) in their research concluded that "literature contains a rich amount of information regarding the effects of biodiesel on NOx emissions. In most cases though certainly not all use of biodiesel or biodiesel blends increases NOx emissions in comparison with baseline petroleum diesel fuel. One reason for inconsistency in the literature is that no single factor is responsible for these NOx effects. Rather, numerous factors contribute, and their relative importance varies with engine technology and operating conditions" (Kent & Robbins,2011). This statement holds, considering the many contributing factors to the production rate of Thermal NOx. This research, however, did not attempt to evaluate the effects of combustor and fuel injection mechanisms to reduce NOx production but the introduction of a lower energy content bioethanol in the blend with biodiesel showed a reduction in the thermal NOx production rates.

In another study Silitonga *et al* (2018) published the findings of their study. They stated "the effect of bioethanol-diesel blends on engine performance characteristics had been studied, and it is found that these blends significantly reduce the exhaust emissions of compression ignition engines. It has been proven in previous studies that these blends improve the cetane number (and thus, ignition quality), which reduces the carbon monoxide (CO) and NOx emissions, as well as smoke opacity, (Silitonga et al 2018)." Despite this study by Silitonga *et al* (2018) not being a study on gas turbine engines, the combustion characteristics remain the same irrespective of the reacting chamber geometry. This study validates, the numerical simulations of this research on the NOx emissions.

5.2 Impact of NOx emissions and the types

Elevated levels of NOx are harmful to the environment especially vegetation. It damages the foliage decreasing growth or reducing crop yields. This research looked at the rate of NOx production for Thermal NOx and Prompt NOx. Fuel NOx is produced when the chemically bonded Nitrogen to fuel converts to NOx in the exhaust gases. Prompt NOx is produced when atmospheric nitrogen in the early stages of combustion reacts with fuel radicals atomic oxygen and hydroxides, it is also not temperature dependent. From the results, prompt NOx accounts for a smaller part of the overall NOx emissions. Thermal NOx is temperature dependent and is formed when nitrogen combines with atomic oxygen and hydroxides. The higher the temperature the more it is produced. The results showed also confirmed that it was temperature dependent.

5.3 Implications of results

The adiabatic flame temperature is an important combustion characteristic. Part of the objectives of this research was to determine the adiabatic flame temperature for different percentage compositions of the bioethanol and biodiesel blends. The implication of the reported adiabatic temperature value of 2260 K for 40% bioethanol and 60% biodiesel blend is key in conducting actual experimental tests. This result entails that.

- The quality of the fuel is good enough at the reported blend ratio of 40% bioethanol and 60% biodiesel.
- The blend is suitable for use in the PT6A-27 annular combustor.
- For any modifications and scaling up procedures, this blend ratio is still suitable for use in the PT6A-27 annular combustor.
- The fuel blend can be used as a replacement to the pure hydrocarbon Jet fuel in the PT6A-27 annular combustor.
- At this reported blend ratio, the level of thermal NOx production is lower than that produced by the pure hydrocarbon Jet fuel.

Jonathan *et al* (2013) simulated the use of alternative fuels in a turbofan engine. As the push to make the use of biofuels more pervasive in the airline industry continues, it is important to understand their broader impact, (Jonathan *et al*, 2013). A positive example of the engine performance simulations using C-MAPSS40k had demonstrated the thermodynamic compatibility

of biodiesel with existing engines. In this study the 100% biodiesel combustion simulation equally showed thermodynamic stability, however, due to the expected higher levels of NOx emissions from biodiesel. It is proposed that the blend ratio of 40%bioethanol and 40% biodiesel is suitable for application in the PT6A-27 turboprop annular combustor.

The experimental study by Saifuddin *et al* (2017) on the performance and emission characteristics of micro gas turbine engine fueled with bioethanol-diesel-biodiesel blends. The performance test in the micro gas turbine was limited up to 20% blend of biofuel, which showed improved thermal efficiency during the test. Subsequently, the emission test carried out in this work also showed significant enhancement in emissions, except nitrogen oxides (NOx) which contributed to the higher formation in comparison with the distillate diesel. Finally, B80E20 (80:20 of biodiesel-bioethanol) was proposed to be selected as an ideal blended fuel ratio to be applied in micro gas turbine engine due to its adaptability to replace diesel fuel, while showed better performance and emission properties as compared to the pure petroleum diesel. (Saifuddin *et al*, 2017). This study was aimed at substituting a pure petroleum diesel and their findings showed that the ratio of 20% bioethanol and 80% biodiesel was suitable. This research however proposes that the ratio of 40% bioethanol and 60% biodiesel blend is suitable for use in the PT6A-27 annular combustor.

The scope of this research did not take into account the phase separation in the proposed blends and any precipitation presence in the blend nor did the research attempt to modify fuel lines, nozzle configurations and perforations as proposed by Laranchi *et al* (2013), that a modified injector and the dilution air holes overall area were sufficient to achieve a comparable power and efficiency in relation to substituting Natural gas with bioethanol.

5.4 JetA-1 Combustion Performance

Figures 5.1 and 5.2 show the simulated combustion of JetA-1 via surrogates. The recirculation and primary zones show a high-level activity of combustion with adiabatic flame temperature around 2320 K. This model was used as a validation model for the other blends of bioethanol and biodiesel simulations. The profile is consistent with what is expected in the annular combustor, with the coolest temperatures in the dilution zone with the combustion products exiting at about maximum 600 K.

This particular result can be considered a safe reference for the biofuel blends used in this study based on experimental studies undertaken by Xu et al (2015) for the National Jet Fuel Combustion Program where they tested 9 different Kerosene based Aviation fuels and reported the range of adiabatic flame temperature of 2280 K to 2300 K.

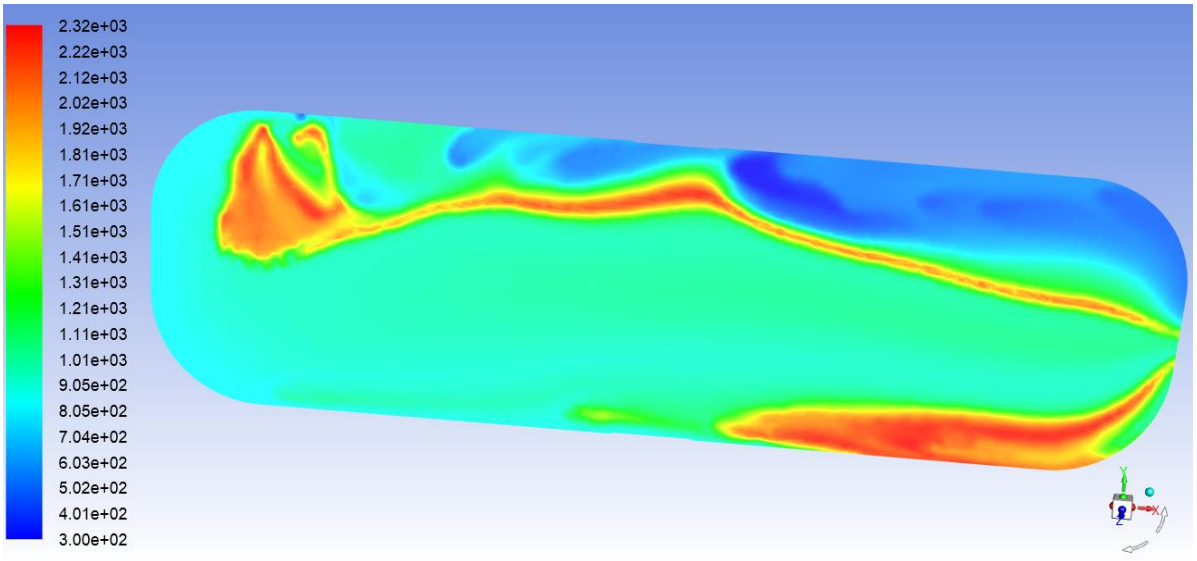

Figure 5. 1: Jet-A non-premixed temperature 2D contour

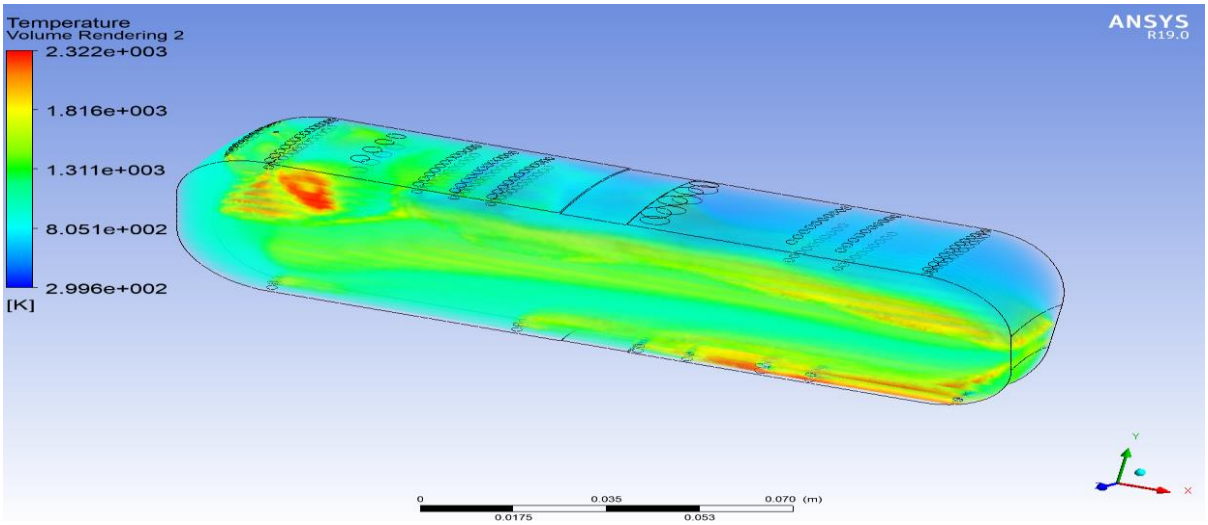

Figure 5. 2:Jet-A non-premixed temperature 3D Contour

Figures 5.3, 5.14 and 5.5 show the simulated combustion for a non-blend of 100% bioethanol. The temperature contours in the recirculation zone, did not show higher temperature distribution as expected for the recirculation zone. This can be attributed to bioethanol being an oxygenated fuel and the low specific heat content of bioethanol. The adiabatic flame temperature was at 2240 K.

This result means the use of non-blend bioethanol is not suitable for use as an alternative fuel for the PT6A-27 annular combustor.

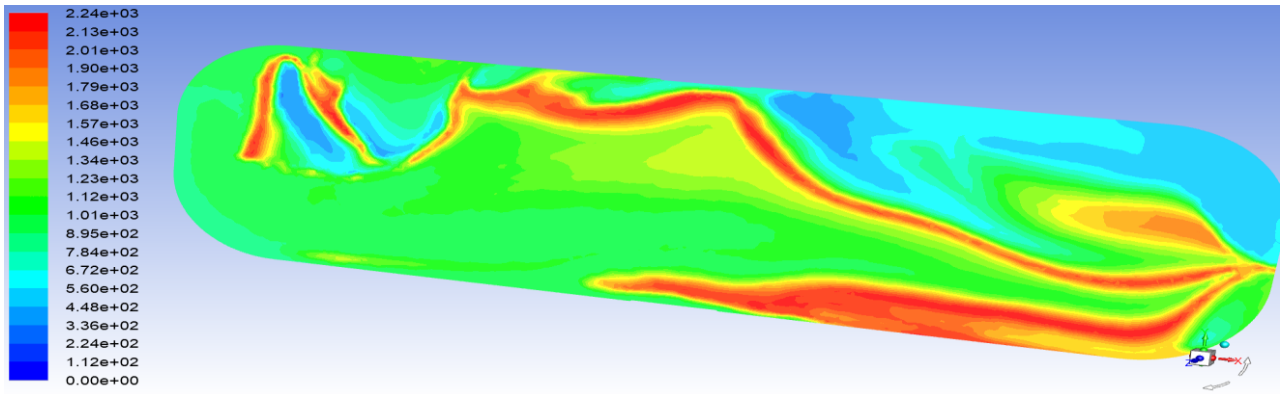

Figure 5. 3: 100% bioethanol 2D temperature contour non-premixed

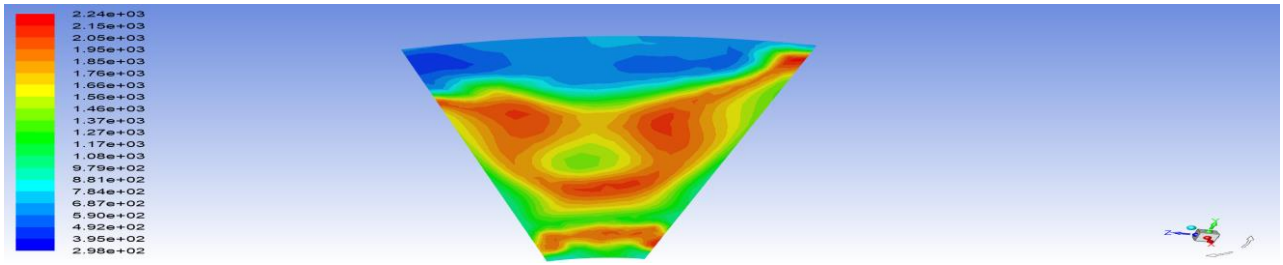

Figure 5. 4: 100% bioethanol 3D temperature contour non-premixed

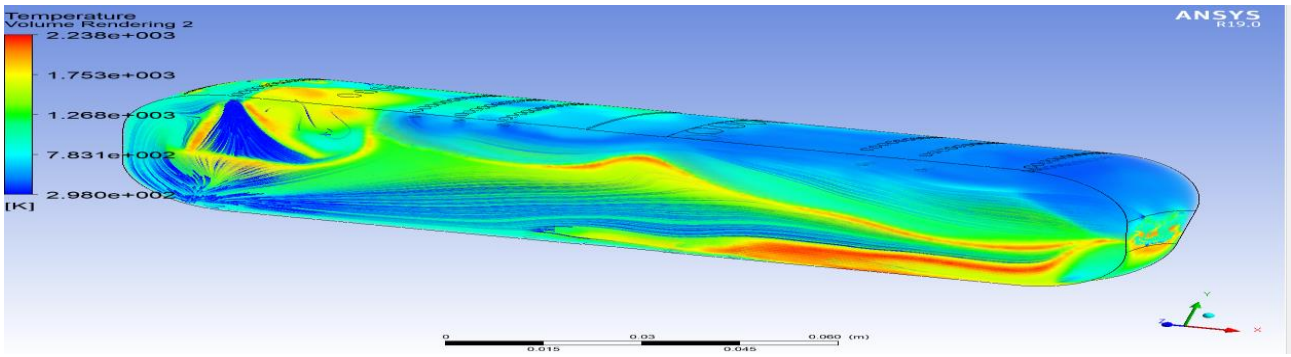

Figure 5. 5:100% bioethanol 3D temperature contour non-premixed

5.5 Bioethanol and Biodiesel blends Performance

For the 80% bioethanol and 20% biodiesel blend, shown in figures 5.6, 5.7 and 5.8, the temperature distribution was observed to be higher in the dilution zone than in the recirculation and primary zones. This could be because of near complete combustion in the dilution zone due to more air present. This temperature distribution was not consistent with the annular combustor temperature distribution profile. The adiabatic flame temperature was observed to be 2270 K.

This result of the 80% and 20% blend of bioethanol and biodiesel respectively would pose a problem for the turbine blades as the ensuing flow discharge would be at a higher temperature leading to more thermal loads on the blades.

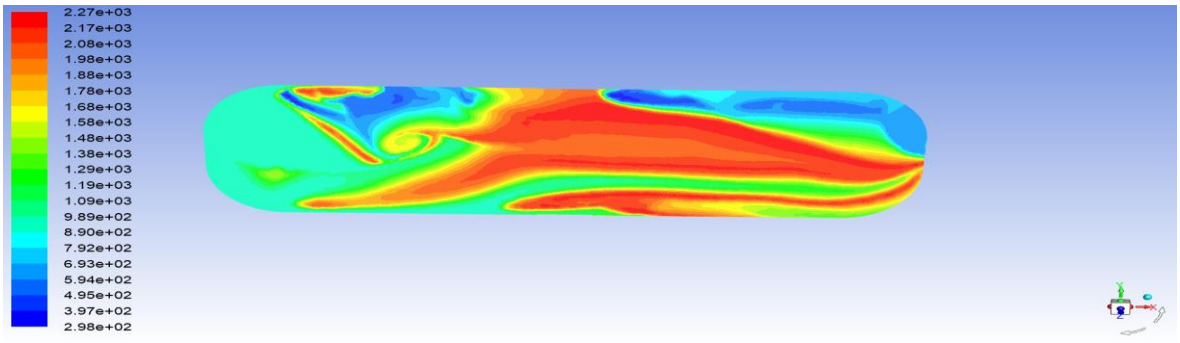

Figure 5. 6: 80% bioethanol, 20% biodiesel 2D temperature contour non-premixed

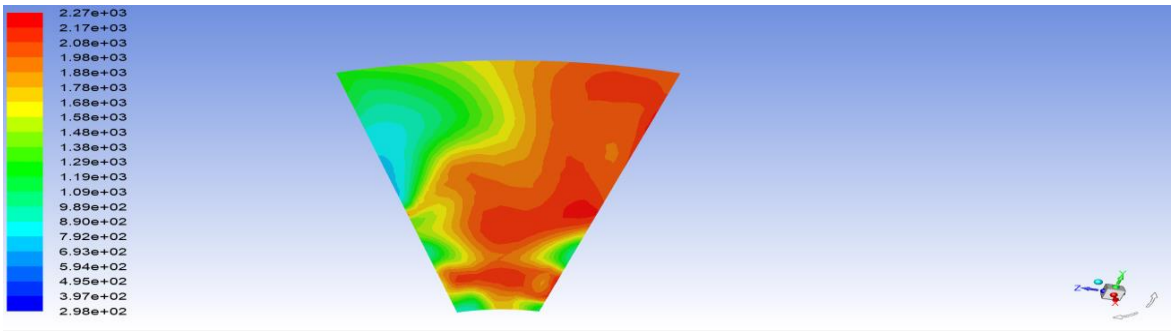

Figure 5. 7: 80% bioethanol, 20%biodiesel Side view temperature contour non-premixed

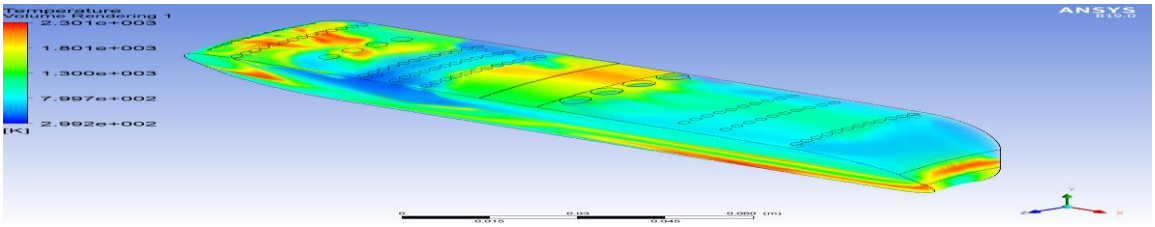

Figure 5. 8: 80% bioethanol, 20%biodiesel 3D temperature contour non-premixed

Figures 5.9, 5.10 and 5.11 show a blend of 70% bioethanol and 30% biodiesel (70BE-30BD). The temperature contours distribution and the adiabatic flame temperatures showed a consistence in comparison with the combustion of JetA1 as show in figures 5.1 and 5.2 with adiabatic flame temperature around 2280 K. The temperature contours in the recirculation and primary zones indicate a near complete combustion due to the presence of oxygen in the bioethanol. The secondary zone temperature distribution shows some stability of the combustion.

This particular result suggests that a blend of 70% bioethanol and 30% biodiesel can be used as an alternative fuel in place of Kerosene based hydrocarbon fuel.

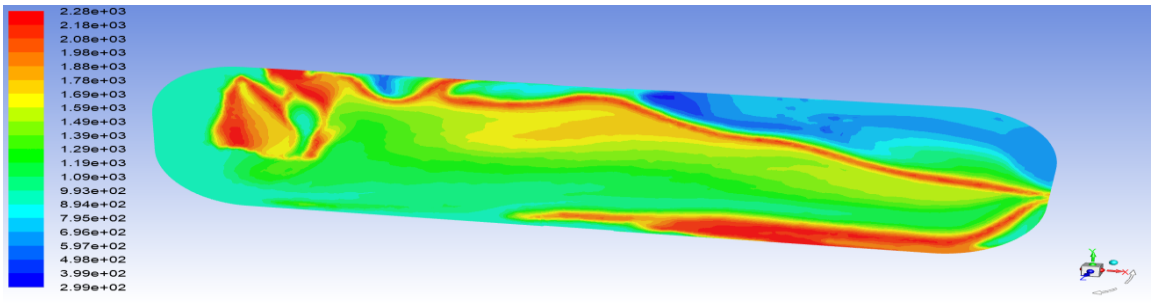

Figure 5. 9: 70% bioethanol, 30%biodiesel 2D temperature contour non-premixed

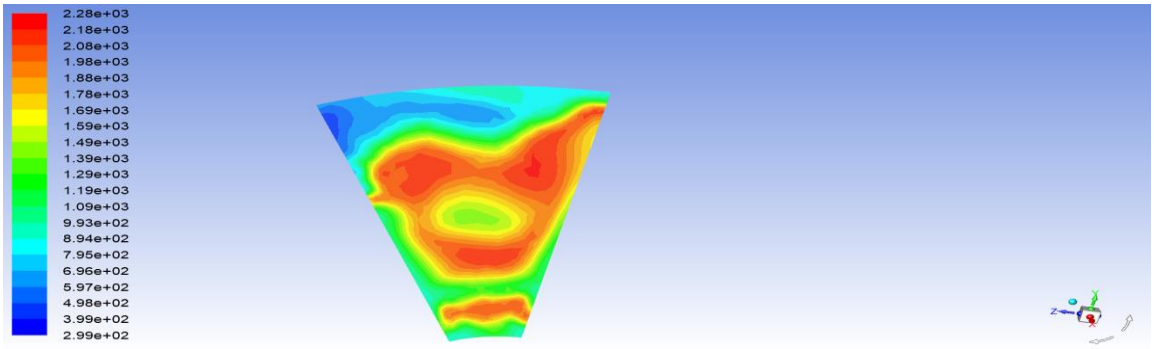

Figure 5. 10: 70% bioethanol, 30%biodiesel Side view temperature contour non-premixed

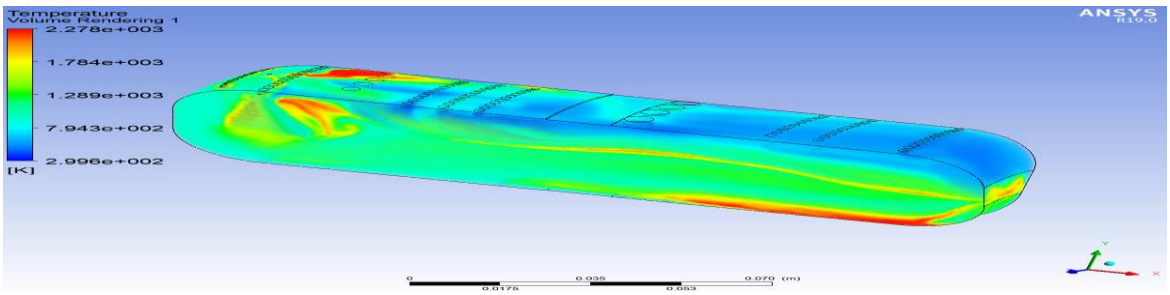

Figure 5. 11: 70% bioethanol, 30%biodiesel 3D temperature contour non-premixed

Figures 5.12, 5.13 and 5.14 show a blend of 60% bioethanol and 40% biodiesel (60BE-40BD). The temperature contours distribution showed more chemical interaction in the secondary zone. The adiabatic flame temperature was around 2290 K. The secondary zone temperature distribution shows some stability of the combustion. However, the chemical interaction was not higher in the recirculation and primary zones, hence more temperature concentration in the center (Secondary Zone). This distribution could be because of near complete combustion in the secondary zone.

This result indicates that for this blend, the expected combustion characteristics as that of using a pure hydrocarbon fuel would be achieved.

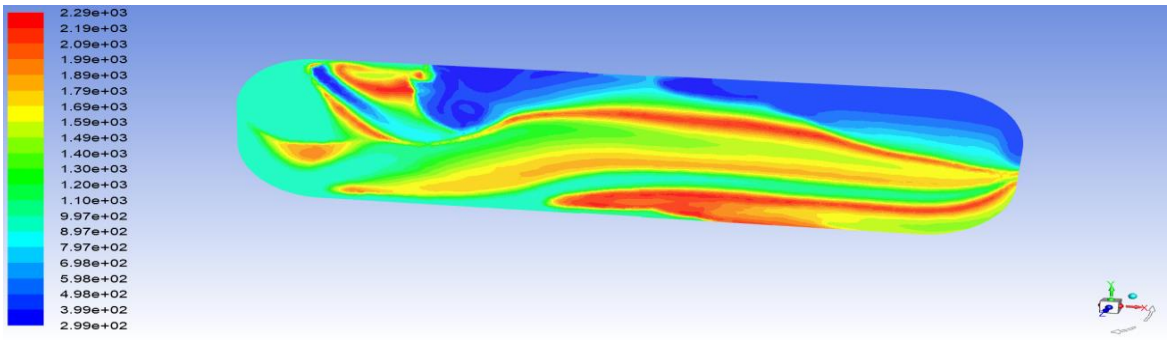

Figure 5. 12: 60% bioethanol, 40%biodiesel 2D temperature contour non-premixed

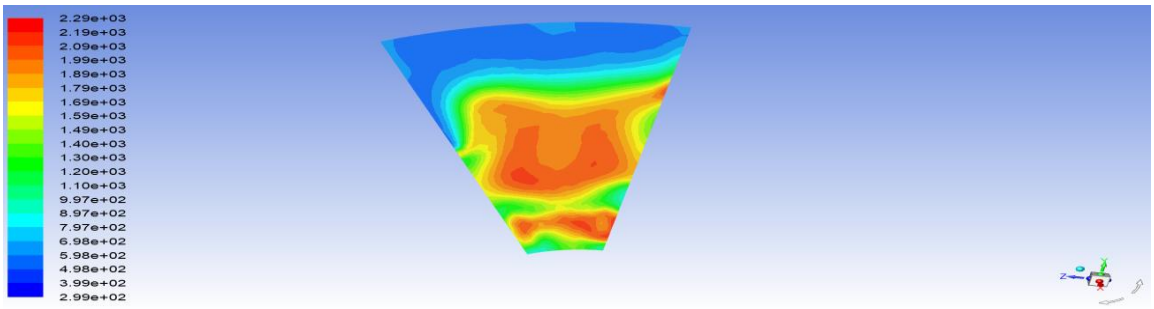

Figure 5. 13: 60% bioethanol,40%biodiesel Side View temperature contour non-premixed

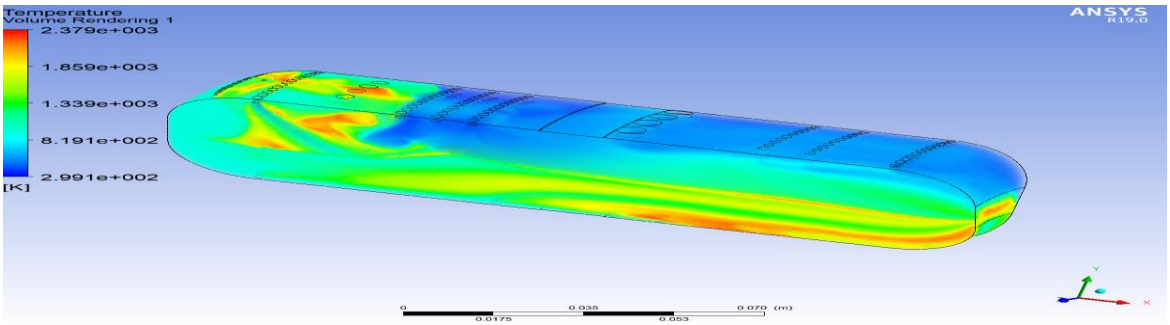

Figure 5. 14: 60% bioethanol, 40%biodiesel 3D temperature contour non-premixed

Figures 5.15, 5.16 and 5.17 show a blend of 50% bioethanol and 50% biodiesel (50BE-50BD). The temperature contours distribution showed more chemical interaction in the secondary zone. The adiabatic flame temperature was around 2350 K. The rest of the profile is like the 60BE-40BD (figures 5.12, 5.13 & 5.14) blend except for the recirculation and primary zones. There are higher temperatures in the primary zones contributing to the reported adiabatic flame temperature.

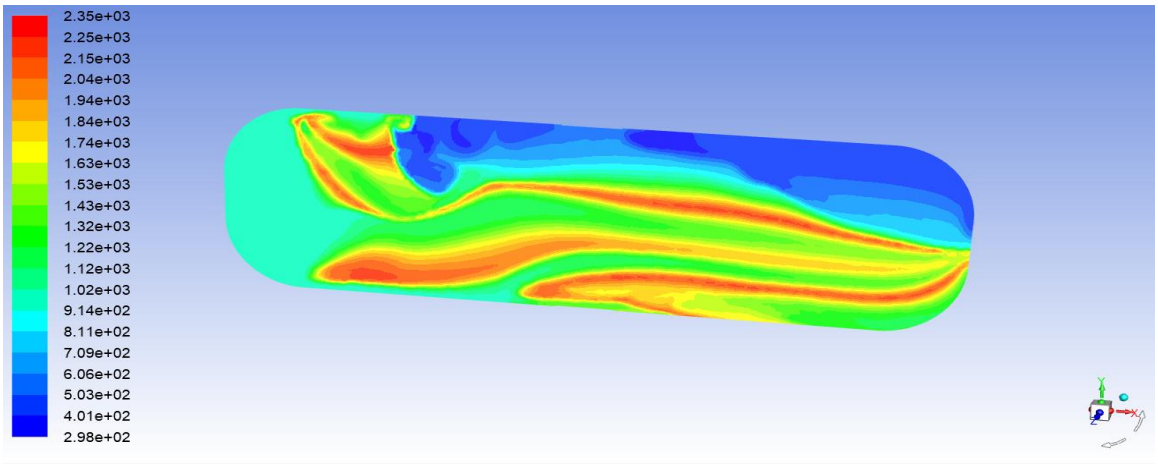

Figure 5. 15: 50% bioethanol, 50%biodiesel 2D temperature contour non-premixed

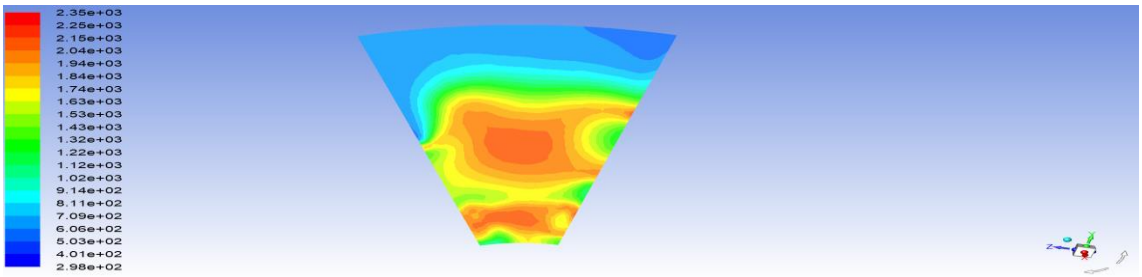

Figure 5. 16: 50% bioethanol, 50%biodiesel Side View temperature contour non-premixed

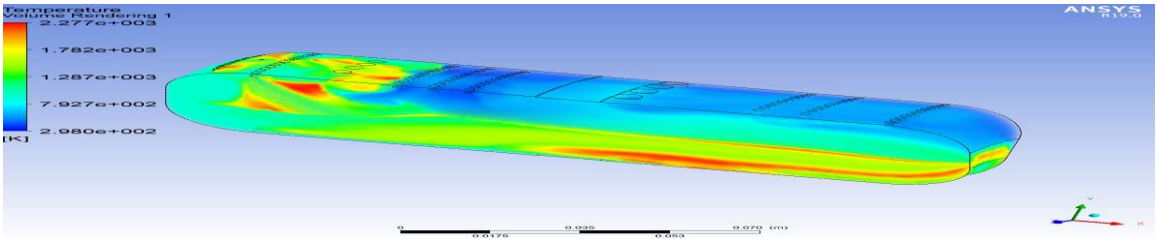

Figure 5. 17: 50% bioethanol, 50%biodiesel 3D temperature contour non-premixed

Figures 5.18, 5.19 and 5.20 show a blend of 40% bioethanol and 60% biodiesel (40BE-60BD). The temperature contour in the primary and recirculation zones showed consistency with the combustion in an annular combustor. There was more heat concentration in this region and the thermal stability across the sections including the secondary and dilution zones. The adiabatic flame temperature of about 2260 K was observed. This blend was further chosen in analyzing NOx emissions. The increase in biodiesel concentration contributed to this outcome.

The implication of this result is that the blend of 40% bioethanol and 60% biodiesel is the best combination among the other blends. This research recommends this blend for any future experimental trials on gas turbines by the Zambia Air Force (ZAF).

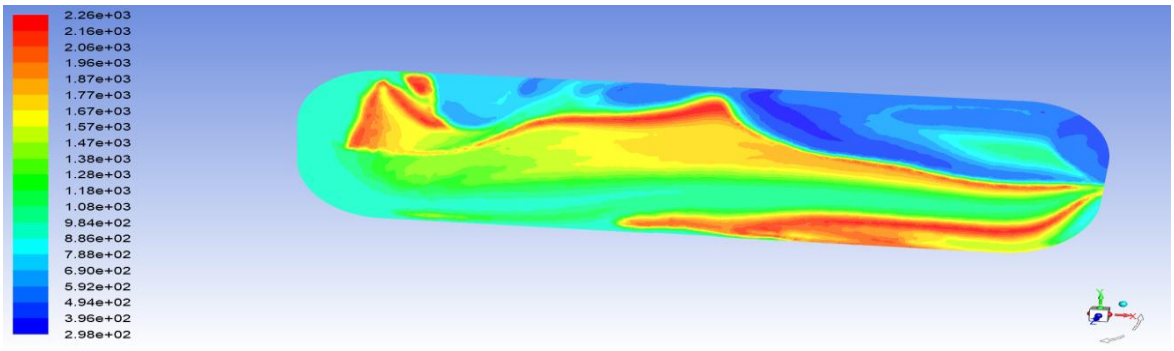

Figure 5. 18: 40% bioethanol, 60%biodiesel 2D temperature contour non-premixed

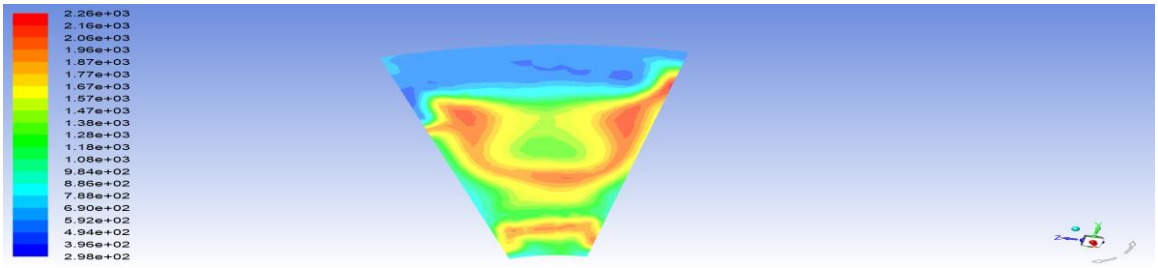

Figure 5. 19: 40% bioethanol, 60%biodiesel Side View temperature contour non-premixed

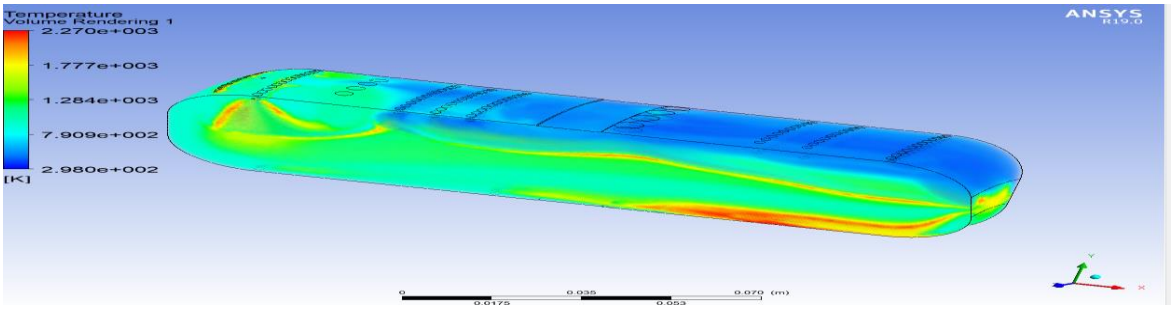

Figure 5. 20: 40% bioethanol, 60%biodiesel 3D temperature contour non-premixed

Figures 5.21, 5.22 and 5.23 show a blend of 30% bioethanol and 70% biodiesel (30BE-70BD). The temperature contour in the primary and recirculation zones showed consistency with the combustion in an annular combustor. There was more heat concentration in this region and the thermal stability across the sections including the secondary and dilution zones. The adiabatic flame temperature of about 2380 K was observed.

This result indicates that at this reported adiabatic flame temperature there would be more thermal NOx produced. However, this blend can be used as an alternative to the aviation pure hydrocarbon fuels.

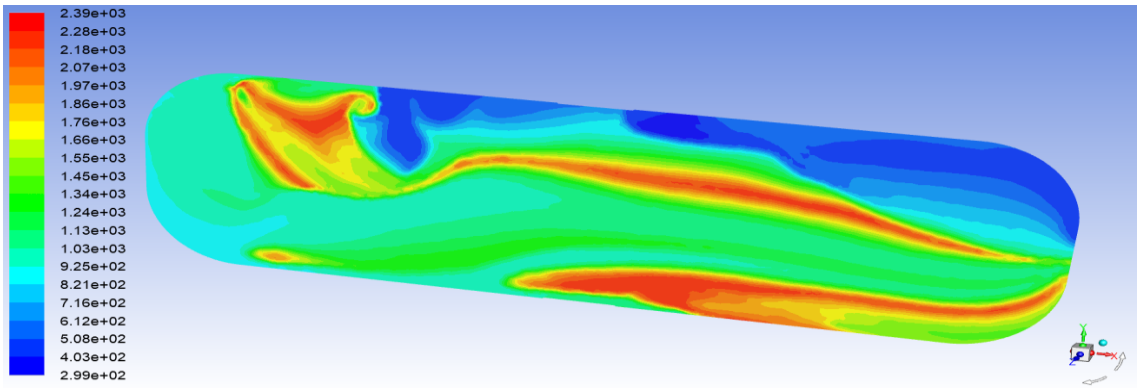

Figure 5. 21: 30% bioethanol, 70%biodiesel 2D temperature contour non-premixed

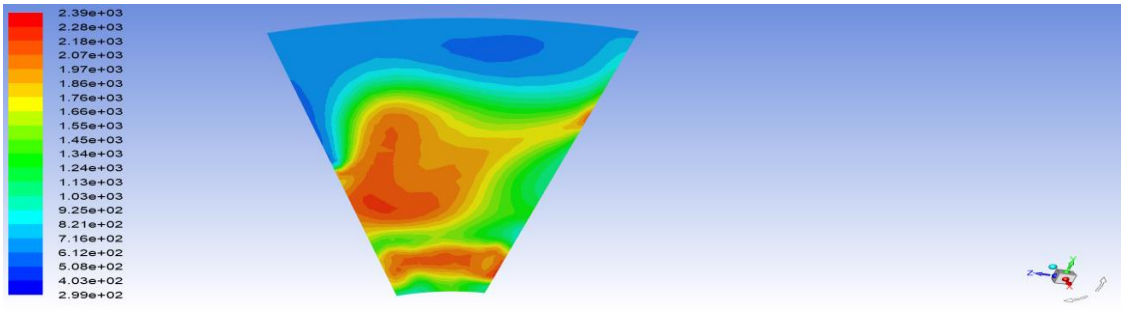

Figure 5. 22: 30% bioethanol, 70%biodiesel Side View temperature contour non-premixed

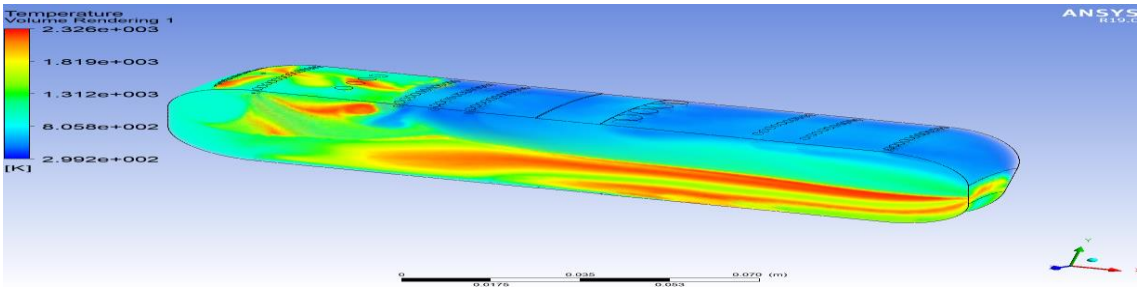

Figure 5. 23: 30% bioethanol, 70%biodiesel 3D temperature contour non-premixed

Figures 5.24, 5.25 and 5.26 show a blend of 20% bioethanol and 80% biodiesel (20BE-80BD). The temperature contour in the primary and recirculation zones did not show high combustion activity as indicated by presence of low temperature zone (bluish patch). There was more heat concentration in the secondary and dilution regions. The adiabatic flame temperature of about 2320K was observed.

This result indicates that the lack of combustion activity and a high temperature region in the dilution zones makes the blend of 20% bioethanol and 80% biodiesel not suitable for use in the PT6A-27 annular combustor.

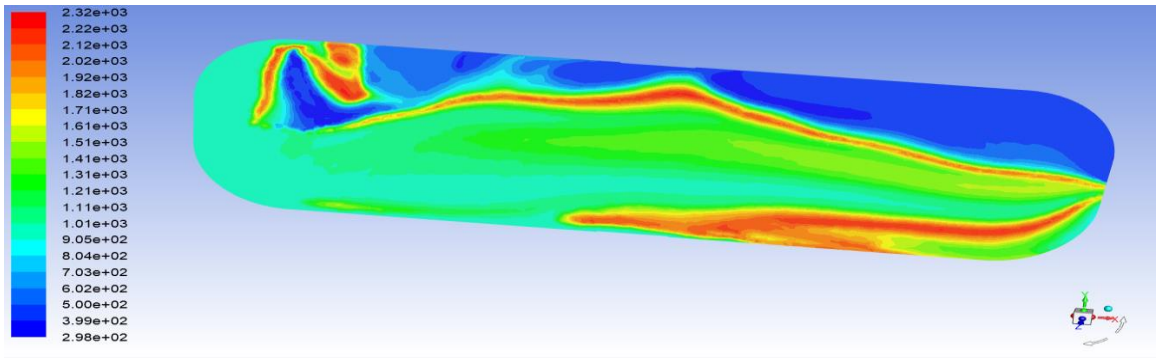

Figure 5. 24: 20% bioethanol, 80%biodiesel 2D temperature contour non-premixed

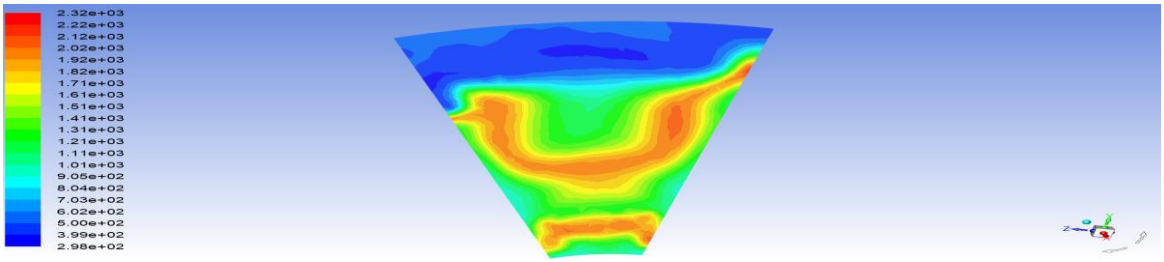

Figure 5. 25: 20% bioethanol, 80%biodiesel Side View temperature contour non-premixed

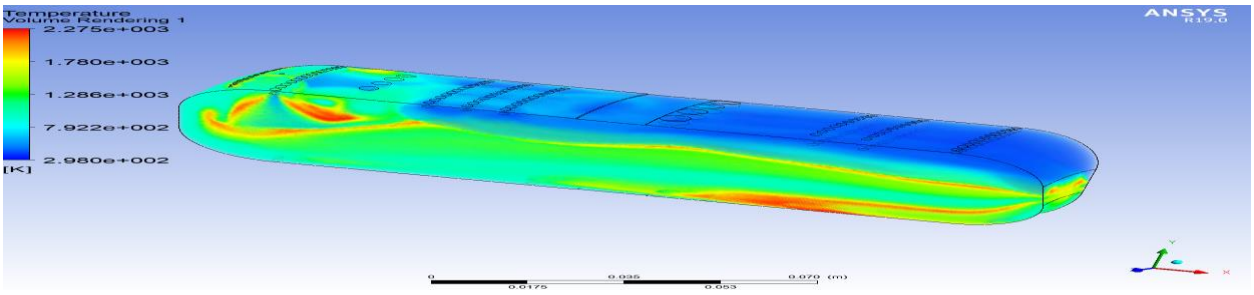

Figure 5. 26: 20% bioethanol, 80%biodiesel 3D temperature contour non-premixed

Figures 5.27, 5.28 and 5.29 show the simulated combustion of biodiesel only. The temperature contour in the primary and recirculation zones showed consistency with the combustion in an annular combustor. There was more heat concentration in this region and the thermal stability across the sections including the secondary and dilution zones. The adiabatic flame temperature of about 2310 K was observed.

This result suggests that biodiesel can be used as an alternative fuel in this combustor. The similarity in the temperature contour with the JetA-1 simulation further indicate that biodiesel as opposed to bioethanol non blend can be used for experimental tests.

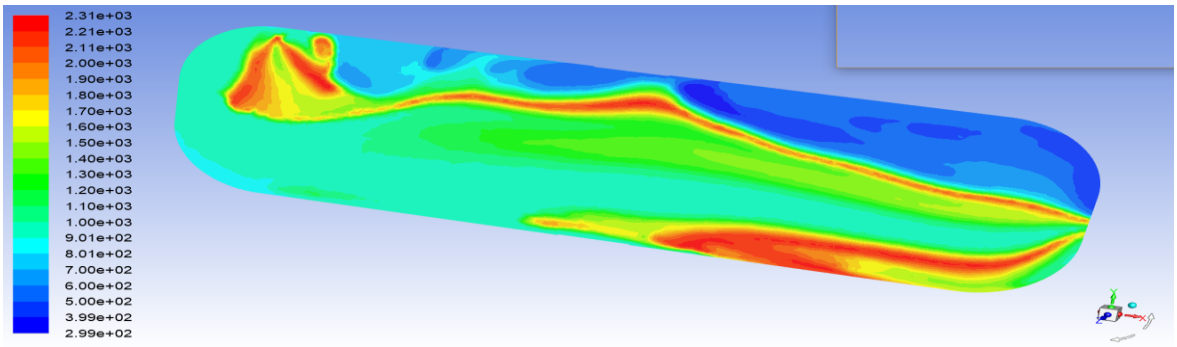

Figure 5. 27: 100% biodiesel 2D temperature contour non-premixed

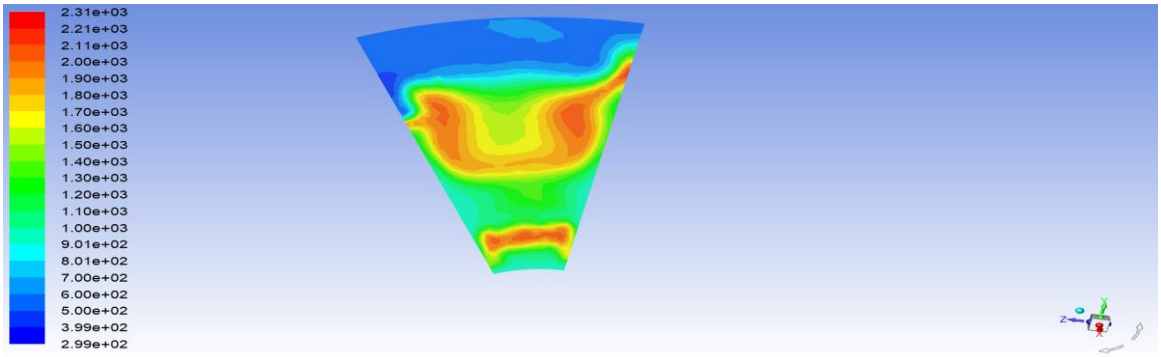

Figure 5. 28: 100% biodiesel Side View temperature contour non-premixed

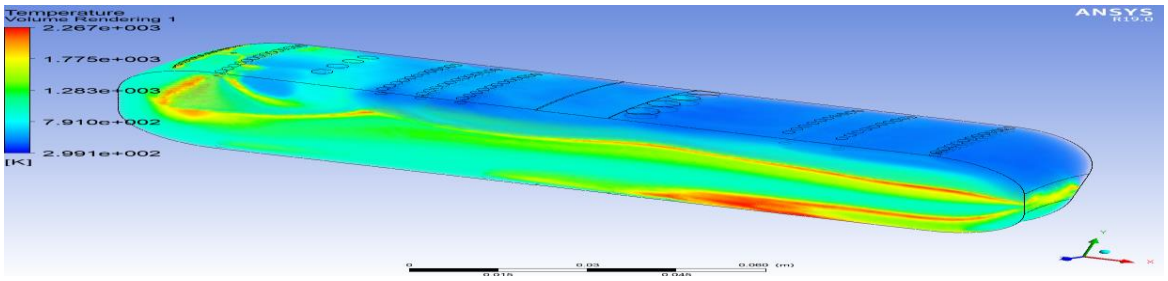

Figure 5. 29: 100% biodiesel 3D temperature contour non-premixed

5.6 NOx Production Rate

The levels of NOx emissions were determined through consideration of the different types of NOx emissions namely: Thermal NOx, Fuel NOx and Prompt NOx. From the fuel composition, Fuel NOx is evidently higher in the conversional Jet fuels. However, it was observed that an increase in the Adiabatic Flame Temperature directly increased the levels of Thermal NOx. The blend of 40% bioethanol to 60% biodiesel was observed to have a reduced Fuel NOx footprint, however, the rise in the calorific energy content of the fuel blend due to the presence of biodiesel in the mixture contributed to the increase in Thermal NOx production, albeit still less than that obtained from a pure hydrocarbon fuel of JetA-1 as shown in figures 5.30 to 5.33.

A pure JetA-1 hydrocarbon fuel had a production rate of Thermal NOx ranging from $0.002699526\ \text{Kgmol/m}^3\ \text{s}$ to $0.002705489\ \text{Kgmol/m}^3\ \text{s}$. The Prompt NOx rate for Jet fuel was observed to be $1.789729 \times 10^{-6}\text{Kgmol/m}^3\ \text{s}$.

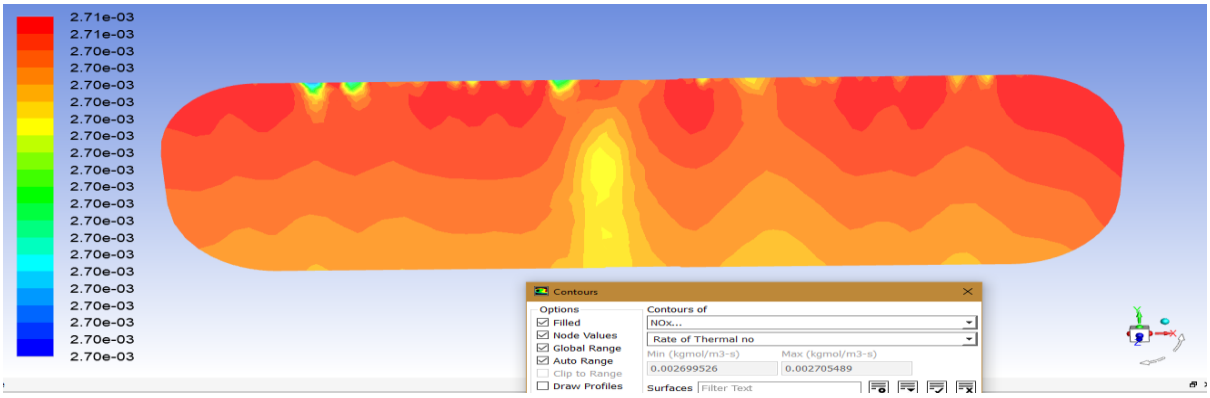

Figure 5. 30: Jet A Thermal NOx production rate $Kgmol/m^3\ s$

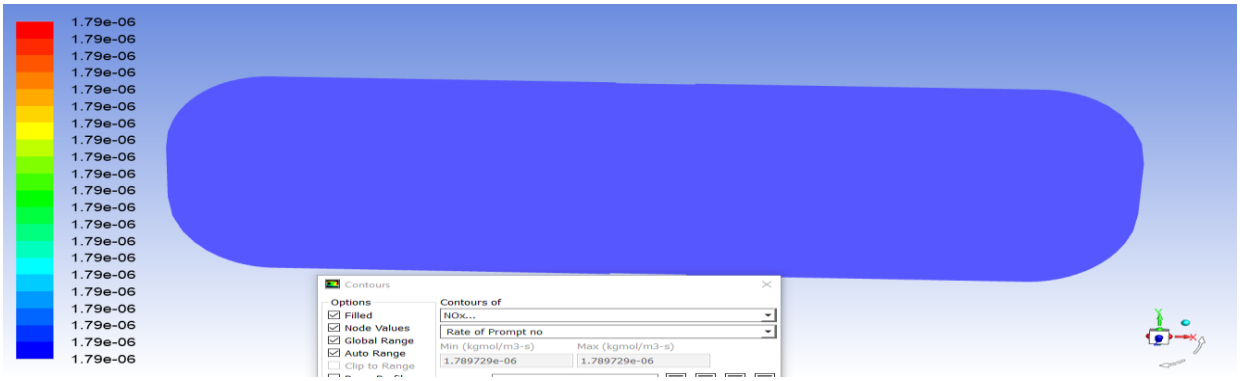

Figure 5. 31: Jet A Prompt NOx production rate $Kgmol/m^3\ s$

For 40% bioethanol and 60% biodiesel, the observed production rate values of Thermal NOx and Prompt NOx were a range of $4.798448 \times 10^{-6} Kgmol/m^3\ s$ to $5.01322 \times 10^{-6} Kgmol/m^3\ s$ and $2.054488 \times 10^{-7} Kgmol/m^3\ s$ respectively as shown in figures 5.32 and 5.33. This was indicative of a reduction in both Thermal and Prompt NOx when the two groups of fuels (Jet-A against 40BE & 60BD blend) were compared.

The implication of this result is that for the purpose of experimental tests and eventual use of the 40% bioethanol and 60% biodiesel blend there will be less thermal NOx emissions than that obtained using the pure hydrocarbon JetA-1 in the PT6A-27 annular combustor.

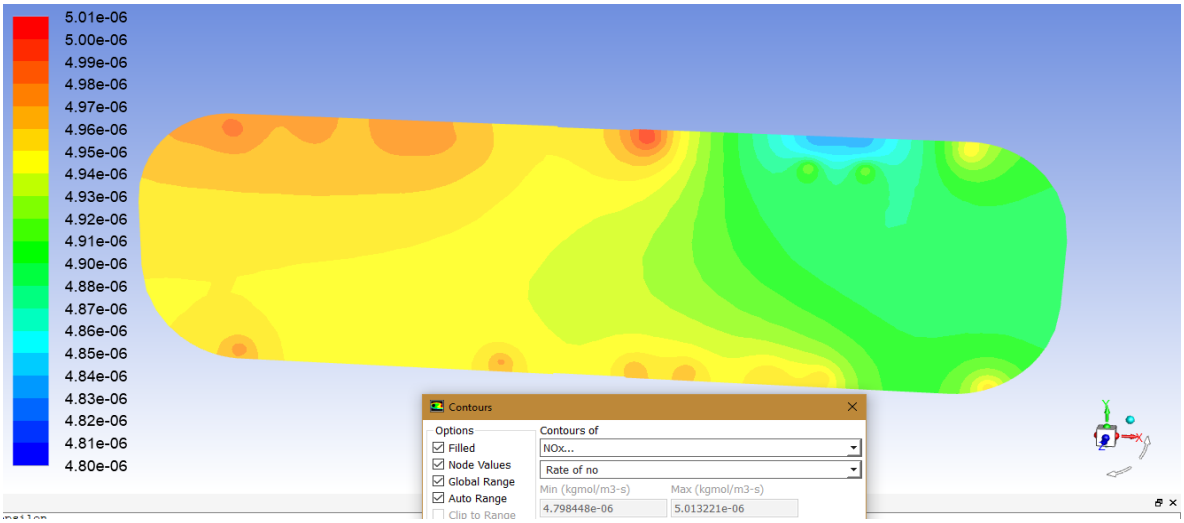

Figure 5. 32: Biofuels Blend Thermal NOx production rate $Kgmol/m^3\ s$

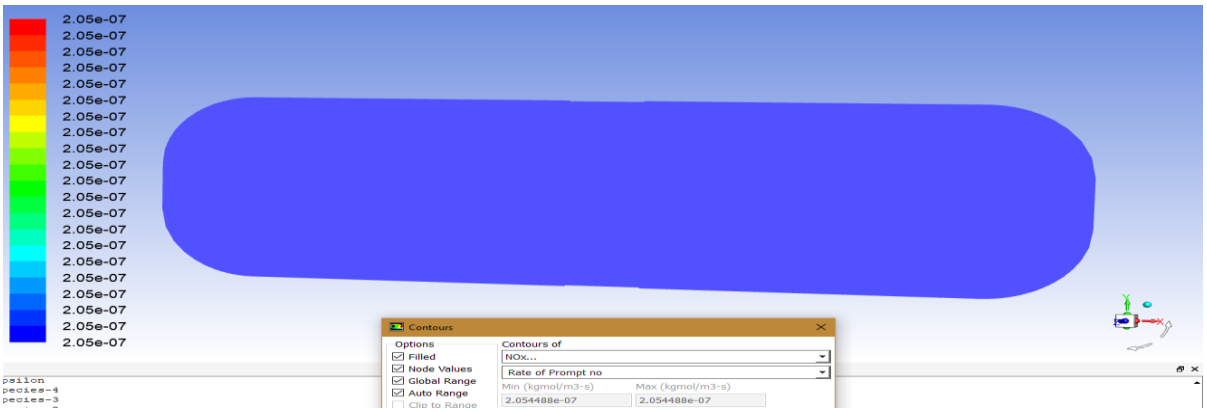

Figure 5. 33: Biofuel Blend Prompt NOx production rate $Kgmol/m^3\ s$

CHAPTER 6: CONCLUSION AND RECOMENDATIONS

6.1 Conclusion

6.1.1 Model Simulation Overview

This chapter summarises the results and presents the approach taken in obtaining the results. The PT6A-27 Turboprop Annular combustor was modelled and simulations on the combustion of biofuels using ANSYS Fluent CFD software. The levels of emissions particularly the NOx emissions were determined, and the profile of emissions was consistent with what is reported in literature sources and other experiments conducted. As pointed out by Navia (2010) that "For an accurate CFD analysis result of a gas turbine combustion chamber, it needs to simulate combustion and turbulence simultaneously. Thus, the design of the combustor was based on the combustion-turbulence interaction model. The equivalence ratio for the primary zone should be chosen assuming that the air and fuel injected in this region will form a flammable mixture before ignition; so, the equivalence ratio for the primary zone should be within the mixture flammable envelope for the reactants established" (Navia, 2010). The turbulence interaction model of k-e was adopted in this research.

6.1.2 Modelling and simulation of combustion of bio derived fuels using ANSYS software.

The geometry of the annular combustor was created using SOLIDWORKS and exported to ANSYS DESIGN MODELER for further conversion from a solid geometry into a fluid-based geometry. Creation of the computational mesh for the geometry using ANSYS MESHING was done in preparation for the setting up of the CFD simulation in ANSYS FLUENT. The simulation further included, setting material properties and boundary conditions for a non-premixed combustion problem, initiating the calculation with residual plotting, calculating the solution using the pressure-based solver and lastly visually examining the flow and temperature fields using the post-processing tools available in ANSYS FLUENT. The results are as presented in Chapter 5 of this Thesis. The different blends of biodiesel and bioethanol combustion were simulated, and the temperature distribution profiles with a specific combustion characteristic of adiabatic flame temperature reported at around 2300 K. The fuel blend from the range of 30% bioethanol and 70% biodiesel (BE30D70) to 70% bioethanol and 30% biodiesel (BE70BD30) indicated a combustion characteristic consistency with that obtained from the combustion of Jet-A1. Further, from the

comparisons of the blends and single biofuel combustion simulation the best blend combination was 40% bioethanol with 60% biodiesel (BE40-BD60) whose adiabatic flame temperature was about 2260 K. The single biofuel combustion simulation best pick was 100% biodiesel whose adiabatic flame temperature was about 2310 K.

6.1.3 Determining the levels of NOx emissions.

The levels of NOx emissions were determined through consideration of the different types of NOx emissions namely: Thermal NOx, Fuel NOx and Prompt NOx. From the fuel composition, Fuel NOx is evidently higher in the conversional Jet fuels. However, it was observed that an increase in the Adiabatic Flame Temperature directly increased the levels of Thermal NOx. The blend of 40% bioethanol to 60% biodiesel was observed to have a reduced Fuel NOx footprint. However, the rise in the calorific energy content of the fuel blend due to the presence of biodiesel in the mixture contributed to the increase in Thermal NOx production, albeit still less than that obtained from a pure hydrocarbon fuel of JetA-1. A pure JetA-1 hydrocarbon fuel had a production rate of Thermal NOx ranging from $0.002699526\ \mathrm{Kgmol/m^3\ s}$ to $0.002705489\ \mathrm{Kgmol/m^3\ s}$. The Prompt NOx rate for Jet fuel was observed to be $1.789729 \times 10^{-6}\mathrm{Kgmol/m^3\ s}$. On the selected fuel blend of biofuels at the proportions of 40% bioethanol and 60% biodiesel, the observed production rate values of Thermal NOx and Prompt NOx were a range of $4.798448 \times 10^{-6}\mathrm{Kgmol/m^3\ s}$ to $5.01322 \times 10^{-6}\mathrm{Kgmol/m^3\ s}$ and $2.054488 \times 10^{-7}\mathrm{Kgmol/m^3\ s}$ respectively. This was indicative of a reduction in both Thermal and Prompt NOx when the two groups of fuels (Jet-A against 40BE & 60BD blend) were compared.

These results showed that reduction of NOx emissions is achievable for a blend of 40% bioethanol and 60% biodiesel in a combustion reaction as a substitute for the hydrocarbon JetA in the PT6A-27 turboprop engine.

6.1.4 Implications of results

The adiabatic flame temperature is an important combustion characteristic. Part of the objectives of this research was to determine the adiabatic flame temperature for different percentage compositions of the bioethanol and biodiesel blends. The implication of the reported adiabatic temperature value of 2260 K for 40% bioethanol and 60% biodiesel blend is key in conducting actual experimental tests. This result entails that.

- The quality of the fuel is good enough at the reported blend ratio of 40% bioethanol and 60% biodiesel.
- The blend is suitable for use in the PT6A-27 annular combustor.
- For any modifications and scaling up procedures, this blend ratio is still suitable for use in the PT6A-27 annular combustor.
- The fuel blend can be used as a replacement to the pure hydrocarbon Jet fuel in the PT6A-27 annular combustor.
- At this reported blend ratio, the level of NOx production is lower than that produced by the pure hydrocarbon Jet fuel.

6.2 Recommendations

The following are the recommendations:

- The simulations to be carried out using the Large Eddy Simulation (LES) model to have a thorough visualization of the combustion and fluid interaction. This research could not carryout this LES due to the huge computational costs.
- There is need to carry out the actual tests on a gas turbine engine and measure the emissions including observation of the effects of bioethanol and biodiesel on the spray pattern of both the simplex and duplex nozzles in the annular combustor.

REFERENCES

AIAA, 2005. Combustion Instabilities in Gas Turbine Engines: Operational Experience, Fundamental Mechanisms, and Modeling. *PROGRESS IN ASTRONAUTICS AND AERONAUTICS,* Volume 210.

Altaher M. A, Andrews G.E , Li H. 2014. Study of Biodiesel Emissions and Carbon Mitigation in Gas Turbine Combustor. *American Journal of Engineering Research (AJER),* 03(11), pp. 290-29.

ANSYS, Inc, 2013. *ANSYS Fluent Theory Tutorial guide.* Southpointe : 275 Technology Drive.

ASTM International, 2011. *Evaluation of Bio-Derived Synthetic Parafinic Kerosenes (Bio-SPKs),* West Conshohocken: ASTM International.

ASTM International, 2012. *Standard Specification for Aviation Turbine Fuels,* West Conshohocken: ASTM International.

Azami M.H and Savill.M, 2017. Pulse Detonation Assessment for Alternative Fuels. *Energies,* 10(369).

Bicen, A. F, Tse D., Whitelaw J.H, 1988. Flow and Combustion Characteristics of an Annular Combustor. *COMBUSTION AND FLAME ,* Volume 72, pp. 175-192 .

Cengel A.Y and Cimbala J.M., 2014. *Fluid Mechanics Fundamentals and Applications.* 3rd ed. New York: McGraw Hill.

Chong C.T and Hotchgreb S, 2016. Flame Structure, Spectroscopy and Emissions Quantification of Rapeseed Biodi esel under Model Gas Turbine Conditions. *Applied Energy,* 8(2), p. 1383–1392.

Chuck, C. J., 2016. *Biofuels for Aviation, feedstocks technology and implementation.* London: Elsevier Inc..

Dagget, D. L ,Hendricks R.C, Walther R, Corporan E, 2007. *Alternate fuels for use in commercial aircraft,* s.l.: s.n.

Ellis, W. William E.L, Singh B., Srinivassan A.,2008. Flameless Combustion of Biofuels in a Semi-Closed Cycle Gas Turbine. *46th AIAA Aerospace Sciences Meeting and Exhibit 7.*

Goodger, E.M, Allen, John E., 2000. *Transport fuels thechnology*, Norwich, UK: Landfall Fall Press.

Hemighaus G, Batcha J, Boval T., 2006. *Alternative Jet Fuels, Addendum 1 to Aviation Fuels Technical Review (FTR-3/A1),* California San Ramon: Chevron Corporation.

Hilleman, J I, Ortiz S.D., Bartis, J.T., 2008. *alternative jet fuels,* Boston: s.n.

IATA, 2015. *IATA report on alternative fuels,* Ottawa: s.n.

Johnson, J. A., 2012 . *Measuring Conventional and Alternative Exhaust Emissions from a Gas Turbine Engine.* Kansas: s.n.

Jonathan S.L, Chin J.C, Liu Y, 2013. *Simulating the Use of Alternative Fuels in a Turbofan Engine,* Cleveland, Ohio : National Aeronautics and Space Administration-NASA.

Khalil, E.E, 1982. Modelling of Furnaces and Combustors. *Abacus Press,* pp. 1-3, 13.

Kohse, K. Obwald P, Cool T.A, 2010. Biofuel Combustion Chemistry: From Ethanol to Biodiesel. *Angew. Chem. Int. ,* Volume Ed. 49, p. 3572–3597.

Kumaran P, Gopinathan M, Kantharrajan M, 2014 . Combustion Characteristics of Improved Biodiesel in Diffusion Burner. *International Journal of Automotive and Mechanical Engineering (IJAME) ,* Volume 10, pp. 2112-2121.

Laranchi P, Bidini G, Desideri U, Fantozzi F. 2013. CFD analysis of an annular micro gas turbine combustion chamber fueled with liquid biofuels: preliminary results with bioethanol. *Proceedings of ASME Turbo Expo 2013: Power for Land, Sea and Air GT2013* , 3-7 June.

Law, C. K., 2006. *Combustion Physics.* 1st ed. New York: Cambridge University Press.

Lefebvre, A. H., 2010. *Gas Turbine Combustion "Alternative fuels and emissions".* 3rd ed. s.l.:CRS Press.

Li C.H, 2011. Experimental Study of Nanoadditives for Biofuel Combustion. *Proceedings of the ASME 2011 International Mechanical Engineering Congress and Exposition,* 11-17 November.

Maiorov A.I, Vasil'ev A.Y, Sviridenkov A.A, Chelebyan O.G, 2017. The atomization and burning of biofuels in the combustion chambers of gas turbine engines. *Journal of Physics: Conference Series 891 012221.*

Melconian, J.O; Modak, A.T., 1985. Combustor design. In: SAWYER, JAW. (Ed.) Sawyer's gas turbine engineering handbook design. Volume 1, Theory & design. 3. ed. Connecticut: Turbo machinery International Publications, v.1, Chapter. 5, p 5-1-5-62Navia, J. A. N., 2010. *Preliminary design methodology for multy fuel gas turbine combustor.* Sao Paulo-Brazil: Aeronautics Institute of Technology.

Panchasara H.V, 2010. *Spray Characteristics and Combustion of Unheated and Preheated Liquid Biofuels.* Tuscaloosa, Alabama: The University of Alabama.

Pierre-Alexandre G, Bounaceur R, Moliere M, 2009. Adiabatic Flame Temperature from biofuels and fossil fuels and derived effect on NOx emissions. *Fuel Processing Technology,* Issue 91, p. 229–235.

Priyant Mark & Selwyn A, 2016. Design and analysis of annular combustion chamber of a low bypass Turbofan engine in a jet trainer aircraft. *Propulsion and Power research,* 2(5), pp. 97-107.

Hoekman S.K & Robbins C, 2011. Review of the effects of Biodiesel in NOx emissions. *Fuel Processing Technology,* Issue 2012.

Rodionova M.V, Poudyal R.S, Tiwari R.A, 2016. Biofuel Production. *Journal of Hydrogen Energy.*

Saifuddin, N, Refal H, Kumaran P, 2017. performance and emission characteristics of micro gas turbine engine fuelled with bioethanol-diesel-biodiesel blends. *Journal of Automotive and Mechanical Engineering,* 14(1), pp. 4030-4049.

Saravanamuttoo H.I.H, 1987. Modern Turboprop Engines. *Prog. Aerospace Sci. Vol 24,* pp. 225-248.

Silitonga, A. S Masjuki H.H, Dharma S. 2018. Evaluation of the engine performance and exhaust emissions of biodiesel-bioethanol-diesel blends using Kernel based extreme learning machine.. *Energy.*

Toop, G., 2014. *Accounting methods for biojet fuels,* Berlin: s.n.

Tu, J, Yeoh G, Liu C, 2008. *computational fluid dynamics a practical approach.* 1st ed. london,UK: Elsevier Inc.

United Turbine Corp, 2016. *PT6 Descriptive Course and Guide to Troubleshooting.* Miami: s.n.

Uryga-Bugajska I, Pourkashanian M, Borman D, 2008. Assessment of the performance of alternative aviation fuel in a modern air-spray combustor (MAC).. *ASME 2008 International Mechanical Engineering Congress and Exposition* , pp. 61 - 69.

Wilson G R, Edwards T. Corporan E, Freerks L.R, 2013. Certification of Alternative Fuels and Blended Components. *Energy and Fuels 27(2),* pp. 962-966.

Xu R., Wang H., Colket M & Edwards T, 2015. National Jet Fuel Combustion Programme (NJFCP).

Zingg W.D, Gudler L.O., 2016. *Technology Developments and Renewable Fuels for Sustainable Aviation.* Quebec: McGill.

APPENDIXES

APENDIX I: Annular Combustor Design Theory and Mass Air Flow Distribution

Melconian and Modak (1985) proposed the design of an annular combustor using equations presented in the table below.

Nomenclature used in Annular design.

Parameter	Parameter	unit
D_{out}	Outer diameter	m
$\dot{m}_3$	Inlet air mass flow rate	Kg/s
$\dot{m}_{DZ}$	Dilution zone air mass flow rate	Kg/s
$\dot{m}_{DCool}$	Dome cooling air mass flow rate	Kg/s
$\dot{m}_{PZ}$	Primary zone air mass flow rate	Kg/s
$\dot{m}_{RZ}$	Recirculation zone air mass flow rate	Kg/s
$\dot{m}_{SW}$	Swirler air mass flow rate	Kg/s
$\dot{m}_{SZ}$	Secondary zone air mass flow rate	Kg/s
$\dot{m}_{an}$	Annulus air mass flow rate	Kg/s
$\dot{m}_{cool}$	Cooling air mass flow rate	Kg/s
$\dot{m}_f$	Fuel mass flow rate	Kg/s
$\frac{\Delta P_{3-4}}{q_{ref}}$	Combustor pressure drop factor	-
$\frac{\Delta P_{3-4}}{P_3}$	Combustor pressure loss	-
$\frac{\Delta P_{\mathrm{L}}}{q_{ref}}$	Liner pressure drop factor	-
$\frac{\Delta P_{\mathrm{SW}}}{q_{ref}}$	Swirler pressure drop factor	-
$\frac{\Delta P_{\mathrm{dif}}}{P_3}$	Diffuser pressure loss	-
A_3	Inlet (compressor exit) area	m^2
A_{L}	Liner area	m^2
A_{S}	Snout area	m^2
A_{SW}	Swirler flow area	m^2
A_{an}	Annulus area	m^2
A_{ref}	Reference area	m^2
C_{ds}	Snout discharge coefficient	m
D_3	Inlet diameter	m
D_{hub}	Injector hub diameter	m
D_{L}	Liner diameter	m
D_{SW}	Swirler diameter	m
D_{in}	Inner diameter	m
D_{o}	Snout outer diameter	m
D_{ref}	Reference diameter	m
K_{SW}	Swirler concordance factor	
L_{DZ}	Dilution zone length	m
L_{L}	Liner length	m
L_{PZ}	Primary zone length	m
L_{RZ}	Recirculation zone length	m
L_{SZ}	Secondary zone length	m
L_{Dome}	Dome length	m

$\boldsymbol{M_W}$	Molecular weight	Kg/mol
$\boldsymbol{P_3}$	Inlet pressure	Pa
$\hat{R}$	Arrhenius molar rate of creation/destruction	-
$\boldsymbol{R_3}$	Inlet radius	M
$\boldsymbol{R_o}$	Snout outer radius	M
$\boldsymbol{T_3}$	Inlet temperature	K
$\boldsymbol{T_4}$	Exit temperature	K
$\boldsymbol{T_{in}}$	Zone inlet temperature	K
$\boldsymbol{T_{max}}$	Maximum outlet temperature	K
$\boldsymbol{T_{out}}$	Zone exit temperature	K
$\boldsymbol{K_b}$	Backward rate constant	
$\boldsymbol{K_f}$	Forward rate constant	
$\boldsymbol{n_B}$	Number of Swirler blades	
$\boldsymbol{q_{ref}}$	Reference dynamic pressure	
ΔT	Temperature rise	K
CAD	Computer Aided Design	
CFD	Computational Fluid Dynamics	
CPF	Circumferential Pattern factor	
FAR	Fuel air ratio	
HP	High Pressure	
R	Reactant	
RPF	Radial Pattern Factor	
SFC	Specific Fuel Consumption	
A	Empirical Constant A=4.0	
B	Empirical Constant B=0.5	
C	Molar Concentration	Mol/m^3
N	Number of reactions	
P	Product	
PF	Pattern Factor	
R	Universal gas Constant	N.m(Kg.K)
R	Net rate of production	
Y	Mass fraction	
ij	Species	
r	reaction	
β_{SW}	Turning angle of the airflow	Degree
η'	Rate exponent for reactant	
η''	Rate exponent for product	
η_{CC}	Combustor efficiency	%
θ_{RZ}	Recirculation zone angle	Degree
ϑ'	Stoichiometric coefficient for reactant	
ϑ''	Stoichiometric coefficient for product	
Γ	Net effect of third bodies on reaction rate	
ρ	density	Kg/m^3
φ	Diffuser angle	degree

Table 0.1: Basic Equations for combustor modelling

Parameter	Equation
Casing Area	$\boldsymbol{A_{ref}} = \left[\frac{R}{2}\left(\frac{\dot{m}_3 T_3^{0.5}}{P_3}\right)\frac{\Delta P_{3-4}}{q_{ref}}\left(\frac{\Delta P_{3-4}}{P_3}\right)^{-1}\right]^{\mathbf{0.5}}$

Combustor sectional area: Liner area	$A_L = 0.66A_{ref}$
Difference between the casing area and liner area: Annulus area	$A_{an} = A_{ref} - A_L$
Pattern factor	$PF = \frac{T_{max} - T_4}{T_4 - T_3}$
Liner length	$L_L = \frac{-D_L}{0.05 \frac{\Delta P_L}{q_{ref}} ln(1 - PF)}$
Primary zone length	$L_{PZ=\frac{3}{4}D_L}$
Dilution zone length	$L_{DZ} = D_L(3.38 - 11.83PF + 13.4PF^2)$
<u>Diffuser dimensions</u> Snout outer area Diffuser angle Diffuser length <u>Swirler dimensions</u> Snout area Swirler flow area Swirler diameter Recirculation zone length: $2D_{SW}$ Recirculation zone angle	$A_0 = \frac{\dot{m}_3}{\dot{m}_{an}} A_{an}$ $\varphi = \tan^{-1}\left[\frac{\frac{\Delta P_{dif}}{P_3} A_3^2 P_3^2}{502.4\left(1 - \frac{A_3}{A_0}\right)^2 \dot{m}_3^2 T_3}\right]^{\frac{1}{1.22}}$ $L_{dif} = \frac{(R_0 - R_3)}{tan\varphi}$ $A_s = A_0 \frac{\dot{m}_{RZ}}{\dot{m}_3} \frac{1}{C_{ds}}$ $A_{SW} = \sqrt{\frac{A_{ref}^2}{\left[\frac{\Delta P_{SW}}{q_{ref}} K_{SW}^{-1} \left(\frac{\dot{m}_3}{\dot{m}_{SW}}\right)^2 + \left(\frac{A_{ref}}{A_L}\right)^2\right] cos^2 \beta_{SW}}}$ $D_{SW} = \sqrt{\left[\frac{A_{SW}}{n_B} + \left(\frac{\pi}{4} D_{hub}^2\right)\frac{4}{\pi}\right]}$ $\theta_{RZ} = \cos^{-1}\left[\frac{-D_L(D_L - 2D_{SW}) - (D_L - 4L_{RZ})\sqrt{(D_L^2 - 4D_L D_{SW} + 4D_{SW}^2 - 8D_L L_{RZ} + 16L_{RZ}^2)}}{2D_L^2 - 4D_L D_{SW} + 4D_{SW}^2 - 8D_L L_{RZ} + 16L_{RZ}^2}\right]$
Dome length	$L_{Dome} = \frac{D_L - D_{SW}}{2\tan\theta_{RZ}}$

Mass Air Flow Distribution

For conventional design about half of the primary zone air mass flow rate would be admitted through the Swirler.

Mass Air Flow Distribution

Parameter	Air mass flow rates	Percentage %
$\dot{m}_3$	Inlet air mass flow rate	100
$\dot{m}_{RZ}$	Recirculation zone/snout air mass flow rate	20
$\dot{m}_{SW}$	Swirler air mass flow rate	12
$\dot{m}_{DCool}$	Dome cooling air mass flow rate	8
$\dot{m}_{an}$	Annulus air mass flow rate	80
$\dot{m}_{PZ}$	Primary zone air mass flow rate	20
$\dot{m}_{SZ}$	Secondary zone air mass flow rate	10
$\dot{m}_{DZ}$	Dilution zone air mass flow rate	10
$\dot{m}_{cool}$	Cooling air mass flow rate	40

APPENDIX II: Ethical Clearance Certificate Approval

THE UNIVERSITY OF ZAMBIA
DIRECTORATE OF RESEARCH AND GRADUATE STUDIES

Great East Road Campus | P.O. Box 32379 | Lusaka10101 | Tel: +260-211-290 258/291 777
Fax: (+260)-211-290 258/253 952 | E-**mail**: director.drgs@unza.zm | Website: www.unza.zm

APPROVAL OF STUDY

IORG No. 0005376
NASRECREC IRB No. 00006465

26th April, 2023

REF NO. NASREC-2023- APRI – 009

Mr. Rodgers Bwalya
Chisenga,
The University of Zambia,
School of Engineering,
P.O. Box 32379,
LUSAKA.

Dear, Mr. Rodgers Bwalya
Chisenga,

RE: "MODELLING AND SIMULATION OF THE COMBUSTION OF BIO-DERIVED FUELS IN A PT6A-27TURBOPROP ENGINE"

Reference is made to your protocol dated as captioned above. NASREC resolved to approve this study and your participation as Principal Investigator for a period of one year.

REVIEW TYPE	ORDINARY REVIEW	APPROVAL NO. NASREC-2023 - APR - 009
Approval and Expiry Date	Approval Date: 26th April, 2023	Expiry Date: 25th April, 2024
Protocol Version and Date	Version - Nil.	25th April, 2024
Information Sheet, Consent Forms and Dates	• English.	To be provided
Consent form ID and Date	Version - Nil	To be provided
Recruitment Materials	Nil	Nil
Other Study Documents	Questionnaire.	

Specific conditions will apply to this approval. As Principal Investigator it is your responsibility to ensure that the contents of this letter are adhered to. If these are not adhered to, the approval may be suspended. Should the study be suspended, study sponsors and other regulatory authorities will be informed.

CONDITIONS OF APPROVAL

- No participant may be involved in any study procedure prior to the study approval or after the expiration date.

- All unanticipated or Serious Adverse Events (SAEs) must be reported to NASREC within 5 days.

- All protocol modifications must be approved by NASREC prior to implementation unless they are intended to reduce risk (but must still be reported for approval). Modifications will include any change of investigator/s or site address.

- All protocol deviations must be reported to NASREC within 5 working days.
- All recruitment materials must be approved by NASREC prior to being used.

- Principal investigators are responsible for initiating Continuing Review proceedings. NASREC will only approve a study for a period of 12 months.

- It is the responsibility of the PI to renew his/her ethics approval through a renewal application to NASREC.

- Where the PI desires to extend the study after expiry of the study period, documents for study extension must be received by NASREC at least 30 days before the expiry date. This is for the purpose of facilitating the review process. Documents received within 30 days after expiry will be labelled "late submissions" and will incur a penalty fee of K500.00. No study shall be renewed whose documents are submitted for renewal 30 days after expiry of the certificate.

- Every 6 (six) months a progress report form supplied by The University of Zambia Natural and Applied Sciences Research Ethics Committee as an IRB must be filled in and submitted to us. There is a penalty of K500.00 for failure to submit the report.

- When closing a project, the PI is responsible for notifying, in writing or using the Research Ethics and Management Online (REMO),both NASREC

- and the National Health Research Authority (NHRA) when ethics certification is no longer required for a project.

- In order to close an approved study, a Closing Report must be submitted in writing or through the REMO system. A Closing Report should be filed when data collection has ended and the study team will no longer be using human participants or animals or secondary data or have any direct or indirect contact with the research participants or animals for the study.

- Filing a closing report (rather than just letting your approval lapse) is important as it assists NASREC in efficiently tracking and reporting on projects. Note that some funding agencies and sponsors require a notice of closure from the IRB which had approved the study and can only be

generated after the Closing Report has been filed.

- A reprint of this letter shall be done at a fee.

- All protocol modifications must be approved by NASREC by way of an application for an amendment prior to implementation unless they are intended to reduce risk (but must still be reported for approval). Modifications will include any change of investigator/s or site address or methodology and methods. Many modifications entail minimal risk adjustments to a protocol and/or consent form and can be made on an Expedited basis (via the IRB Chair). Some examples are: format changes, correcting spelling errors, adding key personnel, minor changes to questionnaires, recruiting and changes, and so forth. Other, more substantive changes, especially those that may alter the risk-benefit ratio, may require Full Board review. In all cases, except where noted above regarding subject safety, any changes to any protocol document or procedure must first be approved by NASREC before they can be implemented.

Should you have any questions regarding anything indicated in this letter, please do not hesitate to get in touch with us at the above indicated address.

On behalf of NASREC, we would like to wish you all the success as you carry out your study.

Yours faithfully,

Dr. Mususu Kaonda

VICE-CHAIRPERSON
THE UNIVERSITY OF ZAMBIA NATURAL AND APPLIED SCIENCES RESEARCH ETHICS COMMITTEE - IRB

CC: Director, Directorate of Research and Graduate Studies
Assistant Director (Research), Directorate of Research and Graduate Studies
Assistant Registrar (Research), Directorate of Research and Graduate Studies

APPENDIX III: Certificate of Journal Publication

e- certificate

EPRA JOURNALS

www.eprajournals.com

Certificate of Acceptance

This is to certify that our editorial board accepted the paper of

Author's Name : Rodgers Bwalya Chisenga

Paper Title : MODELLING AND SIMULATION OF THE COMBUSTION OF BIODERIVED FUELS IN A PT6A-27 TURBOPROP ENGINE

Paper Index : 202305-05-013077

Date of Acceptance : 03-May-23

Journal Name : EPRA International Journal of Climate and Resource Economic Review (CRER)

ISSN : 2347-7431

EPRA JOURNALS TRICHIRAPALLI

Dr. A. Singaraj
Chief Editor